Assessing maize water requirements in the context of climate change uncertainties over southern Africa

Sepo Hachigonta

Dept. of Enviromental and Geographical Sciences

University of Cape Town

Thesis

Presented to the Faculty of Science

for the Fulfillment of the Requirements for the Degree of

Doctor of Philosophy

June, 2011

Declaration

I declare that this thesis is my own work and has not been submitted in any form for another degree or diploma at any university or other institute of tertiary education. Information derived from the published and unpublished work of others has been acknowledged in the text and a list of references is given.

Signed by candidate

Signature Removed

Sepo Hachigonta

June, 2011

Assessing maize water requirements in the context of climate change uncertainties over southern Africa

Abstract

Climate change studies are subject to high uncertainties partly resulting from data reliability. This study investigates the challenges of using statistical downscaled climate data to examine the likely impacts of climate change on maize growth in southern Africa in the context of these uncertainties. Daily downscaled data from five General Circulation Models (GCMs) were used to investigate changes (between the future and recent past) in rainfall totals, evapotranspiration, crop sowing dates, as well as the number and length of dry spells during critical periods for growing maize. A crop model is used together with the downscaled climate data to simulate maize water requirement satisfaction index at 176 stations in southern Africa. A new sensitivity approach that investigates the contribution of sowing decisions to the variation in the maize water requirement satisfaction index is used to develop adaptation options.

The projected climate change results show that there is a strong likelihood for increased precipitation over south eastern South Africa. This is characterised by an increase in specific humidity as well as anticyclonic wind anomalies centred along the border between South Africa and Mozambique during the summer rainfall season. In addition, late sowing dates are projected over Botswana, Zimbabwe, central parts of Zambia, the Limpopo region of South Africa and the region bordering Mozambique and South Africa, while earlier sowing are projected over the central and eastern parts of South Africa.

The maize water requirement satisfaction index simulations across the five GCMs are more consistent in projecting future changes than the rainfall totals. It suggests that consistent responses may be better detected in crop model outputs as opposed to changes in seasonal or monthly rainfall characteristics. Expected rainfall in the first sowing dekad is the most significant factor to the yield variation in most regions over southern Africa, and as such is an important component of future adaptation in maize growth.

Acknowledgments

I acknowledge the support, encouragement and guidance rendered by my supervisor Bruce Hewitson and my co-supervisor Mark Tadross. Their wide knowledge, guidance and thoughtful suggestions were exceptionally valuable. I thank my colleagues, especially Olivier Crespo, Daithi Stone, Chris Lennard, Lawrence Ngorora, Hayley Mcintosh, Ruth Cerezo and Alice Favre for their willingness to help whenever it was necessary. I am also grateful to all those I have not mentioned, who helped me in whatever way to reach this stage in my career.

I give credit to the SysTem for Analysis, Research, and Training (START), Water Research Commission and National Research Foundation, for generously supporting this work financially. Special thanks to the Climate Systems Analysis Group at the University of Cape Town for the exceptional and delightful working environment. I also thank Sharon Barnard for organizing my finances whenever I needed help.

I am thankful to my family and my friends for their moral support and confidence in me. Most importantly, I sincerely thank my wife, Chioniso, for her invaluable love, patience and encouragement. Finally, I dedicate this thesis to my wife and our beautiful baby girl Luyando.

God is Good

Table of Contents

Chapter 1
Introduction

At present, there is a growing drive for the development of regional tools to be used in the evaluation of climate change and responses to it (*Wilby and Fowler, 2010*). In addition, stakeholders (e.g. decision makers, farmers) require regional climate change information for adaptation purposes. In this context, adaptation means short-term and long-term structural changes to improve a system's resilience/sustainability for a changing climate (*Eriksen, 2005*). As a result of this drive, there is a great opportunity for scientists to explore ways to translate climate data, which is robustly predicted across a range of climate models, into information that can easily be interpreted by various stakeholders at a regional level.

This thesis explores the complexities of assessing the impacts of climate change on maize growth over southern Africa by using downscaled climate data. For definition and techniques of downscaling, refer to section 1.3 and section 2.3 respectively. This downscaled data is useful as farming systems, soil types and vegetation also vary on fine spatial scales. A case study is used to elucidate the issues involved.

1.1 Background

A number of studies have investigated the impact of climate change on global and regional agricultural production (*Fischer et al., 2002; Gbetibouo and Hassan, 2005; Walker and Schulze, 2008; Thorton et al., 2008; Brown and Funk, 2008; Lobell et al., 2008; Nelson et al., 2009).* A common message emerging from these studies is that climate change could intensify existing problems in developing countries, where communities have a high dependence on the natural environment.

Lobell et al. (2008) projected that by 2030, southern Africa, without sufficient adaptation measures, could suffer negative climate change impacts on crops, although these impacts would vary widely by crop. The study showed that adaptation priorities will, among other factors, depend on the financial capabilities of small scale farmers. Using two General

Circulation Models (GCMs) (developed by Commonwealth Scientific and Industrial Research Organisation (CSIRO) and National Center for Atmospheric Research (NCAR)), *Nelson et al. (2009)* showed pronounced negative effects of climate change on crop production around the globe including sub-Saharan Africa by 2050. They concluded that climate change could result in additional price increases for most crops (maize, rice, wheat and soybeans) resulting in a substantial fall in cereals consumption. *Gbetibouo and Hassan (2005)* measured the economic impact of climate change on major crops in South Africa. They highlighted the sensitivity of yield to temperature and rainfall change based on the last 30 years of the 20th century. Though they concluded that net revenue might either increase (e.g. Free State, Northern Cape) or decrease (e.g. Gauteng, Kwazulu Natal), they noted that both major crops and the cropping calendar may be affected by climate change. Similarly, *Walker and Schulze (2008)* simulated the variability of yield, risk and soil organic nitrogen levels over three South African climate regions (Christana, Bothaville and Piet Retief). They focussed on maize production and simulated the potential outcome of nine different carbon dioxide concentration scenarios, concluding that climate scenarios show negative impacts mainly in the drier western part of the country.

While previous studies have focused on reporting the impacts that climate change might pose to human well being, little work has been done to explore ways to better understand and represent the uncertainties that arise when conducting such studies. Additionally, several studies in southern Africa have largely investigated climate change impacts using data obtained directly from GCMs, or used a small sample of GCMs thus not encompassing a wider range of uncertainties. In cases where downscaled GCM data that is at a locally relevant scale (e.g. station level) has been used, it has been limited to very small domains (e.g. *Walker and Schulze, 2008*).

In the following sections, a short overview is presented of the southern African's agricultural system, including factors currently affecting small scale farmers. In particular, the role of crop and climate modeling studies in exploring the range of options for agriculture development is discussed.

1.2 Agriculture in southern Africa

Agriculture remains the primary source of employment and income in most of Southern Africa Developing Community's (SADC) rural population with small-scale farmers contributing a large part of the annual yield. It is also the major source of government revenue for most countries in the region. For instance, the Food and Agriculture Organisation (FAO) notes that about 39% of Malawi's Gross Domestic Product (GDP) is from agriculture (*FAO, 2005*). In Zimbabwe, an estimated 80% of the population directly depend on agriculture, of this over 60% are small scale farmers (*Raes et al., 2004; Rukuni and Eicher, 1994; N.O.A.A., 2002*). In Zambia, agriculture contributes about 18% of the GDP. Small-scale farmers contribute about 60% of the farming outputs with a large share of production being maize crop (*IDL, 2002*). South Africa has a dual agricultural system, with both well-developed commercial farming and more subsistence-based production in the deep rural areas. Agriculture contributes about 3% to the South Africa's GDP (*GCIS, 2009*). Southern Africa as a whole has more than 50% of its agricultural land allocated to cereals, with maize (the main staple crop) accounting for more than 40% of the total harvested area (*Pratt and Diao, 2006*). South Africa is the largest maize producer in the region mainly due to the contribution of irrigated farm lands.

This thesis focuses on eight countries in southern Africa: Botswana, Malawi, Mozambique, South Africa, Namibia, Lesotho, Zambia and Zimbabwe (Figure 1.1) mainly due to availability of climate data in these countries. With the exception of Western Cape in South Africa, the western parts of the study region (referred to as closed grasslands) are mostly arid with little crop farming activities. The largest crop lands (yellow shading in Figure 1.1) are observed over the Free State province of South Africa. Southern Zambia, Zimbabwe and the Limpopo province of South Africa indicate patches of crop land spread across these areas. Some countries in the region have relatively small agricultural sectors due to unfavourable climatic conditions, as is the case with Botswana and Namibia.

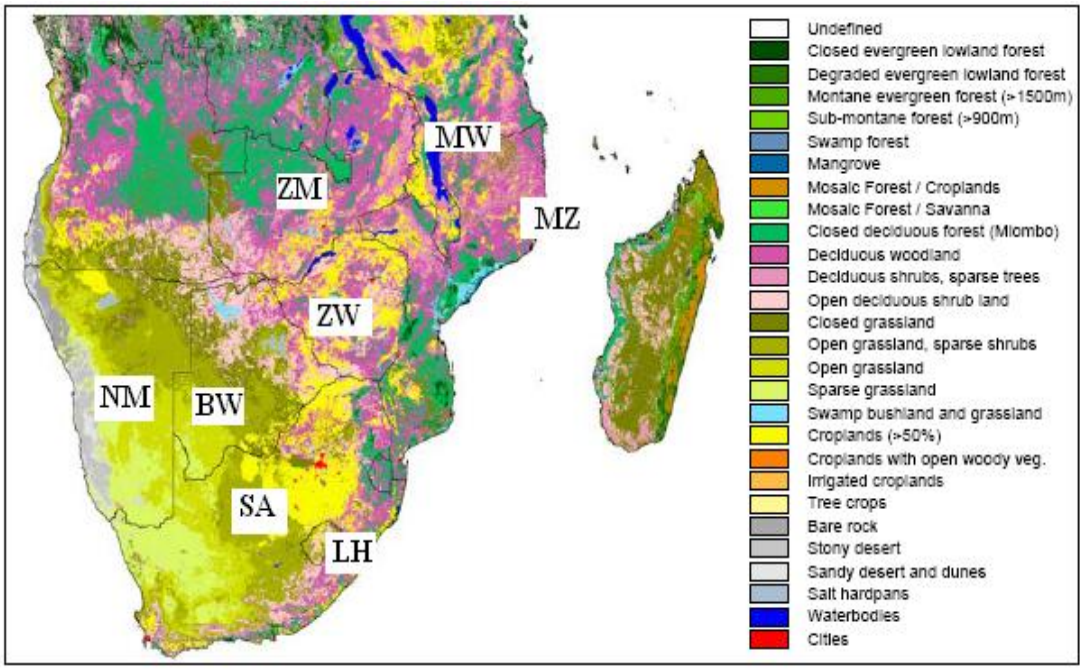

Figure 1.1: *Study region and classification of vegetation types based on the Global Land Cover-2000 data (Bartholomeacute and Belward, 2005), for Botswana (BT); Malawi (MW); Mozambique (MZ); South Africa (SA); Namibia (NM); Lesotho (LH); Zambia (ZM) and Zimbabwe (ZW).*

1.3 Climatic factors affecting small-scale agricultural production

Both climate variability and climate change affect crop production, though on different time scales. Whilst climate variability affects inter-annual (year to year) production, changes in climate influence the ratio of good (cropping success) and bad (cropping failure) years, and therefore the economic sustainability of crop production.

1.3.1 Climate variability

Southern Africa is a region characterised by substantial climate variability on intraseasonal, interannual and longer scales (*e.g. Matarira and Jury, 1992; Levey and Jury, 1996; Mason and Jury, 1997; Reason and Mulenga, 1999; Cook et al., 2004; Reason et al., 2005*). Most often, periodic extreme climatic events (e.g. droughts, floods, changes in the frequency and intensity of dry spells) negatively impact agriculture over southern Africa. Small scale farmers are particularly vulnerable to bad climate conditions as most households depend on rain-fed crops, livestock and other climate-dependent

resources for their survival (*Gay and Hall, 2000; Ziervogel, 2004*). During drought years, crop loss over the region can approach 60% in individual seasons (*Rosen and Scott, 1992*). *Tadross et al. (2010)* showed that rainfall characteristics such as dry spells over southern Africa may have an impact on maize growth. On the other hand, in many cases in Africa, too many or too intense wet spells may lead to flooding in areas causing crop failure (*FAO, 1998*). In some instances high temperatures might lead to reduced crop quality and yield as a result of reduced soil moisture content (*Hargurdeep and Lalonde, 2003*).

Southern Africa is also prone to high variability in rainfall onset dates (*Reason et al., 2005*). Having prior information about when the first rains are likely to occur has strong implications for most small scale farmers and hence on crop yields later in the season. *Omotosho et al. (2000)* noted that during the first few weeks of sowing, enough soil moisture is required to meet the needs of a particular crop at a particular time. Information on sowing dates of the rainy season becomes critical for planning for the majority of the farmers, especially if it is made available before the growing season starts. This can greatly assist on-time preparation of farmlands, mobilisation of seeds and also reduce the risks involved in planting too early or too late. This thesis partly addresses these questions through the evaluation of aspects of rainfall frequency, rainfall variability and the crop sowing dates.

1.3.2 Climate change

At present, southern Africa faces tremendous challenges in the agricultural sector associated with water supply variability, soil degradation, and recurring extreme climate events. There is a growing concern that climate change is expected to intensify existing agriculture problems in developing countries where communities are directly dependent on the natural environment and are under-resourced to adequately adapt to extreme changes in climate (*Meinke et al., 2006; Ziervogel et al., 2008a*). Based on various climate model projections and scenarios, the Intergovernmental Panel on Climate Change (*IPCC, 2007)* has projected that global mean temperature will increase by ~0.6°C between 2020 and 2029 when compared to the recent past. Over Southern Africa the

estimates are slightly higher, ranging from 0.5-1.5°C depending on location, with coastal projections lower than over interior. Sea level rise is estimated at 18-59 cm from the lowest to highest ranges (*Meehl et al., 2007*). Considering that approximately 30% of population growth by 2050 is expected to be in developing countries (*Wiebe, 2009*), climate change presents both challenges (e.g. developing more resilient food crops) and opportunities (e.g. increasing food production). An in depth review of the existing literature on climate change projections in southern Africa is presented in Chapter 4.

GCMs are currently the main tools used for impact, change and scenario studies on global or continental scales (*Gaslikova, 2006*). These models provide a critical link between increasing greenhouse gas concentrations and the resulting changes in climate. By simulating plausible climate scenarios, GCMs help identify climate outcomes consistent with physical laws and understood changes taking place in atmospheric composition (*Williams et al., 1998*). However, several uncertainties limit the accuracy of these models. Uncertainties result from:

- Limitations in modeling processes that take place at scales smaller than the GCM resolution. For example, clouds are very important in the energy budget of the model, but are sub-grid scale and therefore difficult to represent realistically (e.g. *Beaumont et al., 2008*);
- Limitation in current understanding of the physical process controlling regional climate systems;
- Scenario uncertainty (e.g. the extent to which the doubling of atmospheric carbon dioxide affects increase in temperature);
- The contribution of natural variability to climate change not well understood;
- Difficulty in modeling climate responses to changes in radiative forcing;
- Wide range of possible future world trends in population, economy, technology, energy, agriculture and land use.

The problem of predicting the future course of agriculture in a changing world is further compounded by both the fundamental complexity of natural agricultural systems as well

as the social economic systems governing world food supply and demand (*Rosenzweig and Hillel, 1995*).

Uncertainties associated with GCM projections at a smaller scale has led to the development of techniques, such as downscaling, specifically tailored for the study of regional and local-scale climate change. The term "downscaling" refers to methods by which local to regional-scale (10 to 100 km) climate information is derived from coarse resolution GCM variables. These procedures adjust for systematic biases arising from atmospheric processes or land-surface features that are too small to be resolved by large-scale climate models (*Wilby and Fowler, 2007*). (For further details on downscaling techniques, refer to chapter 2.)

1.4 Adapting agriculture to projected changes in climate

Adaptation has been and will continue to be a strong component of human survival as the effects of natural variability and climate change manifest themselves. Agricultural adaptation to climate change depends on the technological potential (e.g. irrigation technologies), water, biological response, and the capability of farmers to detect climate change and undertake any necessary actions (*Schimmelpfennig et al., 1996*). *Shah et al. (2008)* noted that agriculture in sub Saharan Africa faces two inter-linked climate change/variability adaptation challenges. The first relates to increasing the resilience of crops and adapting farming methods to the region's highly variable climate (at seasonal and decadal scales) and the occurrence of extreme events. The second concerns the development and incorporation of long-term climate change adaptation strategies in agricultural development planning, management and governance. Effective adaptation strategies and actions should aim to enhance the well-being of communities in the face of climate variability, climate change and a wide variety of difficult-to-predict biophysical and social contingencies (*Ziervogel et al., 2008b)*.

1.5 Thesis goal

Given the need for adaptation to both natural variability as well as climate change in the agricultural context, the goal of this thesis is to determine the response of maize water

requirement satisfaction index (see section 2.5.1 for definition) to future changes in rainfall, temperature and evapotranspiration, given the uncertainties in the data and modeling methods. This goal seeks to explicitly underpin the challenge of decision making in agricultural systems in the context of incomplete or limited climate data and tools.

The focus in this thesis is on using a suite of downscaled climate projections from multiple GCMs, for the periods 1979 to 1999 and 2046 to 2065, to investigate how these data may be used within a crop model and, to investigate how uncertainties in the climate data affect an evaluation of the potential impacts and mitigating adaptation options. A new sensitivity approach is presented and tested as a general tool to help analyse the potential effectiveness of changes in management decisions to mitigate the impacts of climate change on crop production.

To achieve the above mentioned goal, this thesis addressed the following questions:

1. Given the limited data of evapotranspiration over southern Africa, which evapotranspiration estimation method is suitable for use in the crop models and how sensitive is the calculation of reference evapotranspiration to different climate variables?
2. Which changes in crop-relevant rainfall characteristics are consistently simulated across multiple downscaled GCMs and are these changes supported by large scale atmospheric circulation dynamics?
3. What is the response of maize water requirement index to simulated change in downscaled rainfall, temperature and evapotranspiration?
4. How can changes in the sowing date decision rule (changes in maize planting dates) be used to mitigate negative climate change impacts?

1.6 Thesis outline

An overview of the thesis chapters is given below.

Chapter 2 describes the sources of different data sets used in the study and the sensitivity analysis method of maize growth to sowing dates. Techniques used to generate maize water requirement outputs, including methods for estimation of solar radiation and reference evapotranspiration, are also discussed.

Chapter 3 presents results on the evaluation of GCM simulations of the recent past, and the crop model performance. The GCMs and crop model outputs are tested using observed climate data as well as observed crop yield data. In addition, this chapter evaluates the sensitivity of reference evapotranspiration to different input variables and identifies a suitable evapotranspiration method for the study.

Chapter 4 presents the results of projected changes in local climate features using downscaled GCM data and the associated circulation patterns. Projected regional changes in climate variables, including rainfall totals, sowing dates, number/duration of dry spells and evapotranspiration are evaluated. Results in this chapter address the second and third thesis research questions.

Chapter 5 discusses experiments in which the crop model is used together with downscaled data derived from five GCMs to simulate changes in the water requirement of maize over southern Africa. A new sensitivity approach intended to provide sowing date adaptation strategies over southern Africa is also presented. This chapter addresses the fourth research question.

Chapter 6 summarizes the findings, concludes the thesis and proposes future work in this area of study.

This page is intentionally left blank

Chapter 2
Data and methodology

2.1 Introduction

Considering the research questions stated in chapter 1, key tasks for this study include identifying regions showing significant changes (between the future and recent past) in climate characteristics from a set of downscaled GCM simulations and the impacts these changes could have on maize development over southern Africa. This chapter presents a description of climate data and a water balance crop model used in the study. Methods for deriving solar radiation and evapotranspiration required for crop simulation experiments in later chapters are also reviewed.

Section 2.2 describes the source of observational climate data used in this study, followed by a description of climate models and the downscaling techniques in section 2.3. Data estimation techniques used for computing solar radiation and evapotranspiration are reviewed in section 2.4 while section 2.5 presents the crop model as well as tools for evaluating adaptation options.

2.2 Observation data

The observation data analysed in the study includes daily meteorological station data, monthly climatology dataset of the Climatic Research Unit (CRU) (*New et al., 1999*) and National Centre for Environmental Prediction/National Centre for Atmospheric Research (NCEP/NCAR) reanalysis data (*Kalnay et al., 1996)*. With the exception of CRU, all datasets are at a station level thus they were interpolated to a common 0.5 by 0.5 resolutions using *Cressman (1959)* technique in order to have a spatial representation of climate characteristics. A 20 year period (1979 to 1999) is used for all the experiments as the control period to match with available crop yield and observation weather station data.

2.2.1 Meteorological Station data

Daily values of precipitation, minimum and maximum temperature are available for the period 1979 to 1999. These parameters allow for the computation of dry spells, sowing dates and daily evapotranspiration values needed for evaluating the crop growth model. In addition,

this data is used to analyse the baseline climate characteristics over selected regions (see section 2.6.2 and section 2.6.3).

In total, 170 observation weather stations obtained from National Weather Services (NWS) are used in the study. Figure 2.1 shows the location of stations considered for the study. Some regions have few stations to cover the 20 years analysed in the thesis thus not included in the experiments (e.g. the western parts of Zambia and central Botswana). It should be pointed out here that observational data has its own limitations and associated uncertainties (e.g. instrumentation errors, human errors) (*Huffman et al., 1997*). Quality control is performed on the data by visual inspection of precipitation and temperature time series for the 170 stations. Daily precipitation records that fall outside four standard deviations of climatology (1979 to 1999) and those that showed negative precipitation are set to missing values (see *da Silva et al., 1994; New et al., 2006*).

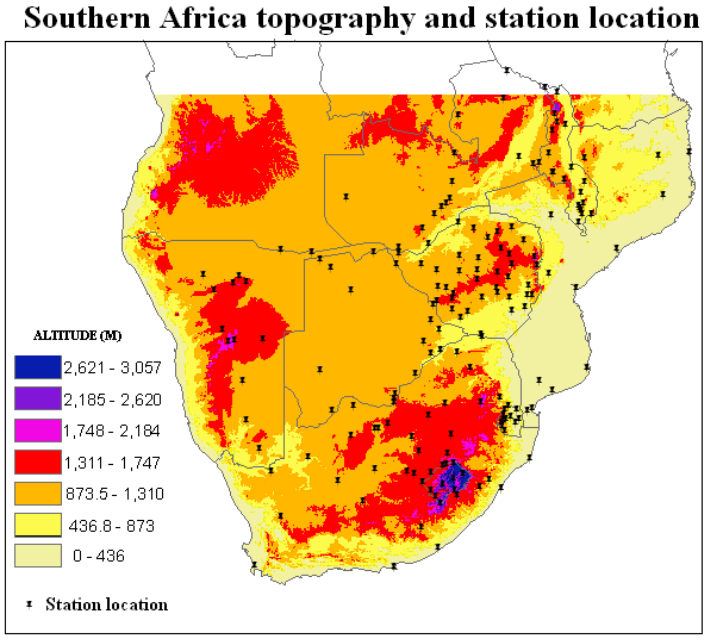

Figure 2.1: *Topography and geographical distribution of the stations used (black dots)*

2.2.2 Climate Research Unit data

The CRU CL1.0 data (*New et al., 1999*) is used for the evaluation of solar radiation and evapotranspiration (ET) estimates. This version of CRU comprises monthly climatology values (1961 to1990) of precipitation and wet-day frequency; mean, maximum and minimum temperature; vapour pressure; solar radiation and cloud cover; frost frequency; and wind

speed. CRU offers a good source for data when estimating variables that have a high 'input data' requirement as is the case with evapotranspiration.

The CRU mean climate surfaces have been constructed from a dataset of stations obtained from national meteorological agencies, the World Meteorological Organization (WMO) and CRU global datasets of station time series. This dataset has a 0.5° ×0.5° spatial resolution. The station data were interpolated as a function of latitude, longitude and elevation using thin-plate splines (*New et al., 1999*). The accuracy of the interpolations were assessed using cross-validation and by comparison with other climatologies (*New et al., 1999*).

The drawback with CRU data is that it is only available at a monthly time step thus could not be used in the evaluation of the crop model which requires data at a daily or 10 day time scale (see section 2.5.1). In this case, daily evapotranspiration values used to drive the crop model are computed using data from meteorological weather stations and downscaled GCMs data.

2.2.3 NCEP reanalysis data

NCEP reanalysis atmospheric fields are used to generate high resolution (downscaled) precipitation and temperature data representative of present day climate. The downscaled NCEP reanalysis data is used to evaluate comparable downscaled data from GCM simulations of the present day.

Kalnay (2000) defines "reanalysis data" as a state-of-the-art data integration system used to reprocess all past environmental observations, combining them with short forecasts in order to derive the best estimate of the state and evolution of the environment. The NCEP reanalysis dataset includes data obtained through land surface, ship, rawinsonde, pibal, aircraft, satellite, and other data (*Kalnay et al., 1996).* The database is enhanced with many sources of observations provided by different countries and organizations. The NCEP reanalysis has a horizontal resolution of 222km with 28 vertical levels (*Kanamitsu et al., 2002*).

In reality, NCEP reanalysis is not classified as observation as it is a model run in a coarse resolution that is 'forced' to converge to some true observations. This data has its own inherent errors and limitation (see *Poccard et al., 2000*). However, a number of studies have shown that NCEP reanalysis is a good proxy for observation over the region (*e.g. Kalnay et al.,*

1996, Widmann and Bretherton, 2000; Hewitson and Crane, 2006) thus it is used in this study.

2.3 General Circulation Models (GCMs) and downscaling techniques

2.3.1 GCMs

GCMs represent the physical processes in the atmosphere, ocean, cryosphere and land surface (*IPCC, 2007*). In addition, they provide a critical link between increasing greenhouse gas concentrations and resulting changes in climate. GCMs depict the climate using a three dimensional grid over the globe and typically have a coarse horizontal resolution of about 300 km and 10 to 30 vertical layers in the atmosphere and the oceans (*IPCC, 2007*). Recent advancements in GCMs used by the IPCC fourth assessment report (AR4) include improvements in modeling dynamics of systems that influence climate over particular regions (e.g. advection, increase in horizontal and vertical resolutions in some GCMs). Additionally, recent GCMs have integrated more processes, in particular the modelling of aerosols, and land surface and sea ice processes. There have also been improvements in the parameterizations of physical processes (*Randall et al., 2007*).

In order to project changes in future climate characteristics and maize water requirement over the study domain, downscaled data from five GCMs covering the period 1979 to 1999 and 2046 to 2065 are used. The five models were selected largely on the basis of availability, but they represent the latest state-of-the-art downscaled temperature and precipitation data for southern Africa. In addition, these models have been shown to reasonably capture and reproduce past climatic features over South Africa *(Hewitson and Crane, 2006)*.

The five GCMs are part of the Coupled Model Intercomparison Project phase 3 (CMIP 3) in the IPCC, AR4. Their simulations are based on the SRES A2 (*Special Report on Emission Scenarios, Nakicenovic et al., 2000*) emissions scenario. The A2 emissions scenario storyline is characterised by a very heterogeneous world with continuously increasing global population and regionally oriented economic growth that is more fragmented and slower than in other storylines (*Nakicenovic et al., 2000*). Table 2.1 lists the GCM names (first column) followed by the horizontal resolution in the second column. The third column shows the acronyms for the GCMs used in this thesis while the last column lists the institution sponsoring the model.

Table 2.1: *List of GCMs used in downscaling process forced by the SRESA2 emission scenario. Further details are available at http://www-pcmdi.llnl.gov/ipcc/model_documentation/ipcc_model_documentation.php*

CMIP3 Name	Horizontal Resolution	Name Used	Institution
cccma_cgcm3_1	***~2.8° x 2.8°***	***CCCM***	Canadian Centre for Climate Modeling and Analysis, the third generation coupled global climate model (CGCM3.1 Model, T47)
cnrm_cm3	***~1.9° x 1.9°***	***CNRM***	Météo-France, Centre National de Recherches Météorologiques, the third version of the ocean-atmosphere coupled model (CM3 Model)
gfdl_cm2_0	***2.0° x 2.5°***	***GFDL***	NOAA Geophysical Fluid Dynamics Laboratory, CM2.0 coupled climate model
giss_model_e_r	***4.0° x 5.0°***	***GISS***	NASA Goddard Institute for Space Studies, ModelE20/Russell
mpi_echam5	***~1.9° x 1.9°***	***ECHAM***	Max Planck Institute for Meteorology, Germany, ECHAM5 / MPI OM

Although GCMs provide realistic representations of large-scale aspects of the climate, they generally do not give good descriptions of local and regional scales (*Benestad, 2004*). *Mearns (2003)* notes that GCMs are unable to explicitly capture the fine scale structure that characterizes climatic variables in many regions of the world (refer to section 1.3.2 of chapter 1 on GCM limitations). In order to capture these finer scale features, there is a need to run GCMs at much higher resolutions (Figure 2.2).

The high resolution (downscaled) data is vital for climate impact studies such as farming systems where rainfall, soil types, vegetation (among other variables) vary over small spatial scales. Most downscaling techniques have their conceptual roots in the experimental, objective weather forecasting of the mid 20th century (*Mearns, 2003*).

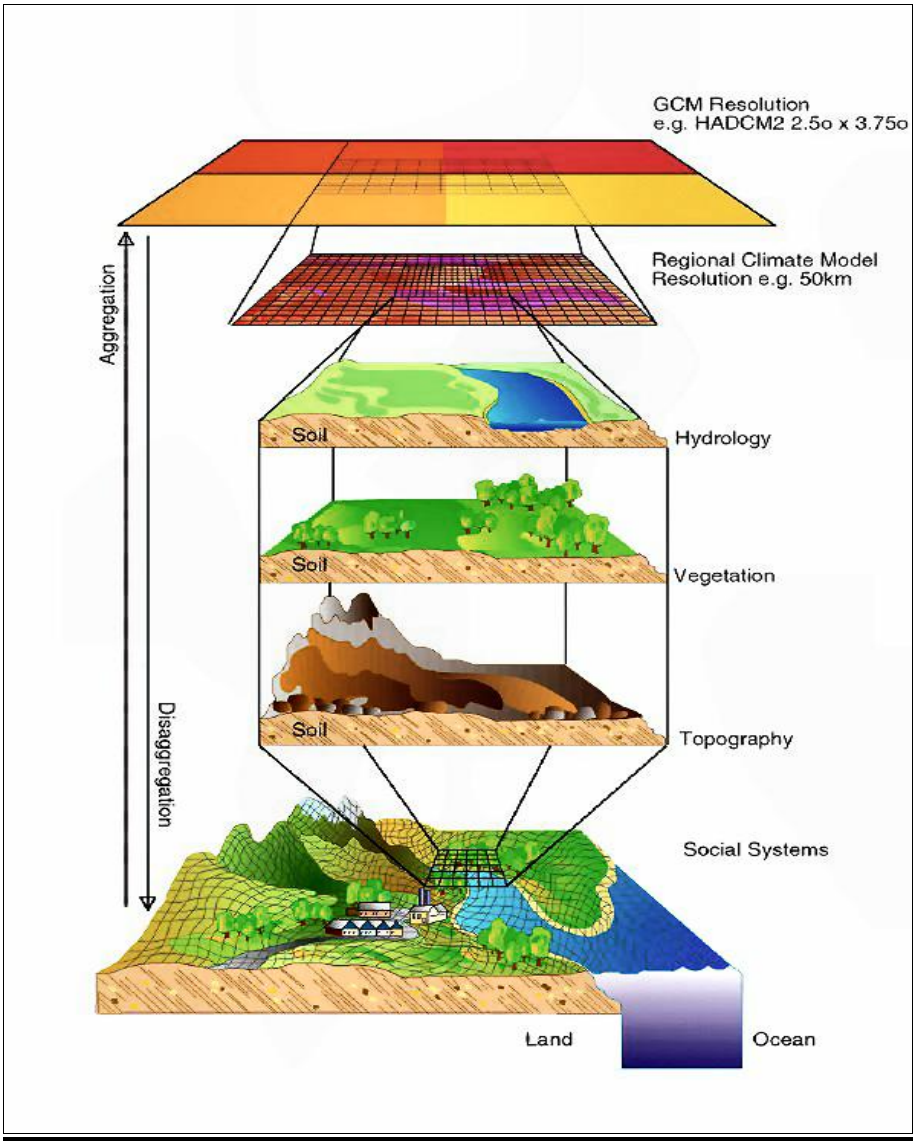

Figure 2.2: *Schematic representation of the downscaling principle. The process takes into account hydrology, vegetation responses, topography, land/sea processes and social systems at the higher resolution. Image courtesy of the UK Met. Office (http://www.metoffice.gov.uk).*

During the last two decades, downscaling methods to assess the effect of large-scale circulations on local parameters have received much attention (*e.g. Giorgi and Mearns, 1991; Hewitson and Crane, 1996; Mearns et al., 2003; Wilby et al., 2004*). Recently the World Climate Research Program (WCRP) formed a task Force on Regional Climate Downscaling

(TFRCD) whose mandate is to: (i) develop a framework to evaluate and possibly improve regional climate downscaling (RCD) techniques for use in downscaling global climate projections; (ii) promote an international coordinated effort to produce improved multi-model RCD-based high resolution climate change information over regions worldwide; (iii) promote greater interaction and communication between global climate experts, the downscaling community and end-users to better support impact/adaptation activities (*CORDEX, 2010*). If successful, such a project would see the development of improved multiple downscaled datasets on a broader scale thus providing input to impact/adaptation work at a local scale. In the following sections, two widely used downscaling procedures (dynamic and statistical) are discussed.

2.3.2 Dynamic downscaling

Dynamic downscaling (DD) involves the use of Regional Climate Models (RCMs) nested within GCMs that covers the regional domain of interest. RCMs are physically based models, like GCMs, that simulate climate within specified boundary conditions (e.g. Southern Africa and the surround oceans). RCMs are often used to gain information on regional scales that GCMs could only give at a much coarser resolution (*Feser, 2005*). In the DD process, the GCM is used to simulate the response of the global circulation to carbon dioxide emissions at a large-scale while the RCM is used to account for sub-GCM grid scale features (e.g. complex topographical features) in a physically-based way and enhance the simulation of atmospheric circulations (*IPCC, 2001*). DD can achieve high spatial resolutions of approximately 20 by 20km and can capture most local scale features (e.g. variation in landscape). In some instances (e.g. Weather Research and Forecasting model) DD can achieve resolution of up to 1 km.

One of the major set backs in using RCMs has been the high computational requirements needed to run the models (see Table 2.2). This is of particular concern when downscaling, multiple GCMs over longer time scales. However, recent studies have shown the potential of using multiple RCMs. In a study over Europe, *Van der Linden and Mitchell (2009)* showed that for near-surface temperature, the signal of the multi-model RCMs ensemble (sixteen) is positive (i.e. increase in temperature) and much larger than the standard deviation implying a robust signal over Europe. The study also showed that the RCMs are consistent in projecting increased precipitation over northern Europe during winter periods.

2.3.3 Statistical downscaling (SD)

Statistical downscaling (also known as empirical downscaling) involves the development of quantitative relationships between large scale atmospheric variables (predictors) and local surface variables (predictands). According to *Hewitson and Crane (2006),* SD is based on the idea that local climate is conditioned by large-scale atmospheric forcing. SD can be further subdivided into weather classification schemes, transfer functions and weather generators. Weather classification schemes relate the occurrence of particular "weather patterns" to a local climate. Analogue approaches are examples of a weather method in which predictands are chosen by matching previous (i.e., analogous) situations to the current weather-state (*Wilby and Fowler, 2007*). Transfer functions directly quantify relationships between predictands and a set of predictors (*Giorgi and Hewitson, 2001*). Examples of transfer function based statistical downscaling methods include those which use linear and nonlinear regression, artificial neural networks (ANN), canonical correlation analysis (CCA) and principal component analysis (PCA) (*Anandhi et al., 2007*). A weather generator is a statistical model used to generate realistic daily sequences of weather variables. They are adapted for statistical downscaling by conditioning their parameters on large-scale atmospheric predictors, weather states or rainfall properties (*see Wilby and Fowler, 2007*). Table 2.2 highlights the advantages and disadvantages of statistical downscaling.

For this study, the data used was downscaled by the Climate Systems Analysis Group (CSAG) based at the University of Cape Town using a Self Organising Map (SOM) statistical downscaling approach (referred here to as SOMD). A SOM is a type of ANN developed by *Kohonen (1995)* which can recognise commonly occurring patterns within multi-dimensional data sets (see *Hewitson and Crane, 2002* for detailed description on SOMs). The SOMD based downscaling approach was introduced by *Hewitson and Crane (2006).* In this approach, a SOM is used to identify commonly occurring weather patterns over a particular region.

Hewitson and Crane (2006) showed that SOMs were able to capture and reproduce most of past climatic features over the region thus they were used to downscale the data from the five GCMs and produce data suitable for regional analysis. The concept behind this approach is to identify modes of circulation over a particular region, with each circulation mode being associated with an observed precipitation probability density function (PDF). For each day in the GCM time series, the method samples from the PDF associated with the GCM

atmospheric circulation on that day. The training is performed using observed (NCEP reanalysis) circulation fields and GCM biases are reflected in both the control and future simulations.

The resulting downscaled GCM variables include daily values of precipitation, minimum and maximum temperature obtained at each of the 170 stations. The following sections present and discuss methods for estimating solar radiation and evapotranspiration, the two necessary variables needed as input in crop growth models. These two variables were not available in the downscaled GCM data used for the study thus the need to compute them via empirical methods.

Table 2.2: *Illustrates some advantages and disadvantages of dynamic downscaling (DD) and statistical downscaling (SD).*

Method	**Advantages**	**Disadvantages**
DD	(i) Accounts for sub-GCM grid scale forcing (e.g. topography) (ii) Information is derived from physically based models (iii) Better representation of some weather extremes as compared to GCMs	(i) Effects of systematic errors in the driving fields provided by global models. (ii) Lack of two-way interactions between regional and global climate. (iii) Expensive to run RCMs as compared to statistical downscaling over a large region. (iv) Its dependence on GCM predictors. (v) Parameterization vulnerable to stationarity issues and choices between equally defensible parameterization schemes and other options can significantly alter the results. (vi) Grid resolution is lower as compared to SD.

SD	(i) Its efficient and cheap computation requirements makes statistical downscaling an easier approach when looking at larger regional domain (e.g. southern Africa) (ii) Its ability to provide point resolution climatic variables from GCM outputs (iii) Its ability to directly incorporate observations. (iv) The method can easily be transferred to other regions.	(i) Its high dependence on the predictors (ii) Its non inclusion of climate system Feedbacks (iii) Vulnerability to non-stationarity of the cross scale relationships

2.4 Methods for estimating solar radiation and evapotranspiration

Apart from daily values of precipitation, minimum and maximum temperature, climate change impact studies on crop development often require additional variables such as solar radiation and evapotranspiration. Solar radiation is the visible and near visible (ultraviolet and near-infrared) radiation emitted from the sun. Evapotranspiration (ET) is a combined process of evaporation from soil, plant surfaces and transpiration through plant canopies. Solar radiation and evapotranspiration measurements are rarely recorded at weather stations largely because of technical and economical limitations associated with direct measurements (*Samani et al., 2007*).

The following section discusses empirical methods for estimating solar radiation and evapotranspiration. *Hargreaves and Samani (1982)* solar radiation method (referred here as HS method) is evaluated using monthly solar radiation values obtained from CRU1.0 dataset (refer to chapter 3 for the evaluation results). Three evapotranspiration techniques are evaluated and they include the FAO-56 Penman-Monteith (referred to as PM which has a high input data requirement), Priestly Taylor (referred to as PT which has moderate input data relative to PM) and Hargreaves (referred to as HG and has a low input data relative to PT and PM) methods. The PM equation was used as a standard method while the other two methods are alternatives in the absence of sufficient input data as was the case in this thesis. The PT and HG methods are evaluated against the PM technique and the closest method matching PM is picked and used with the GCM scenarios.

2.4.1 Solar radiation estimation

Solar radiation is the main driver for the energy and moisture budget of the soil and atmosphere (*Allen, 1997*). All atmospheric movement and change result from variations in the amount of solar radiation in time and space. Ultimately, solar radiation is the generator of all weather and climate (*Schulze, 2007a*). It acts as a source for sensible heat (i.e. the loss of energy from the surface by movement of air) for crops as most of the energy retained by the ground is disposed of as flux through the soil. The amount of solar radiation reaching the surface of the earth depends on a number of factors such as time of day, location, cloud cover (amount of cloudiness, thickness/type of cloud), altitude (the higher the altitude, the lower the atmospheric pressure and consequently the more intense the radiation), dust and water vapour

content (the higher the water vapour content, the less solar energy passes through the atmosphere) (*Schulze, 2007a*).

Over the years, various empirical methods for estimating solar radiation from minimum and maximum temperature have been developed (*e.g. Thornthwaite, 1948; Hargreaves and Samani, 1982; Bristow and Campbell, 1984*). Some techniques have proved to produce good estimations when compared to measured values in many parts of the globe. However, for accurate estimation, most of these methods have to be calibrated if used in regions other than those for which they were developed and validated. For instance, a study by *Meza and Varas (2000)* showed that literature values of the Hargreaves and Samani (HS) coefficients do not estimate solar radiation correctly when applied at various locations in Chile.

Allen (1997) proposed a self calibrating model for estimating monthly solar radiation as a function of temperature and extraterrestrial radiation (i.e. radiation incident at the top of the atmosphere) using a modified Hargreaves and Samani model. He recommended empirical coefficient values of 0.17 and 0.20 for the interior and coastal regions respectively. Extraterrestrial radiation can be calculated using standard geometric methods as a function of latitude, mean earth-sun distance, solar constant and day of the year (see, Appendix A). Using long-term daily measurements of maximum and minimum temperature, precipitation and extraterrestrial radiation, *Bristow and Campbell (1984)* developed a simple algorithm for estimating site-specific solar radiation. They found that they could account for 70% to 90% of the variation in daily incoming solar radiation from three sites located in North America (Tacoma, Pullman-WA, and Great Falls). *Schulze and Chapman (2007a)* used a modified Bristow and Campbell (BC) model to calculate solar radiation by means of optimised site coefficients in selected parts of South Africa. Using temperature as a substitute for atmospheric water vapour content, they devised a method that accounted for clear sky extinction of solar radiation by water vapour.

The modified Hargreaves and Samani model is used here because of its low data requirement, its reduced number of coefficients, its general acceptable performance over the region (see chapter 3) and because it has been observed to perform well under diverse climatic conditions (*Allen, 1997; Ball et al., 2004*). The structure of the HS model generally reduces the amount of extraterrestrial radiation by a fraction lost due to scattering and absorption of radiation in

the presence of clouds and atmospheric particles (*Winslow et al., 2001*). In the HS method, solar radiation is a function of transmissivity coefficient (K_s) (computed from temperature) and extraterrestrial radiation as shown in Equation 2.1. The coefficient (K_s) in the HS equation allows for the calculation of solar radiation using temperature. The modified version of the HS model, takes account of altitude (*h* in Equation 2.2 and 2.3), which was introduced in the calculations as suggested by *Ball et al. (2004).*

$$R_s = k_s \times R_a \qquad (2.1)$$

where R_s and R_a are the solar and extraterrestrial radiations respectively and k_s is the daily total atmospheric transmissivity to solar radiation (Equation 2.2).The empirical coefficient a, as derived from Equation 2.3 is the ratio of CRU monthly solar radiation climatology R_{CRU}, altitude (h), extraterrestrial radiation and temperature difference.

$$k_s = a(1 + 2.01 \times 10^{-5} h)\sqrt{T_{max} - T_{min}} \qquad (2.2)$$

$$a = 0.16 + 0.018(1 + 2.01 \times 10^{-5} h)\sqrt{T_{max} - T_{min}} \qquad (2.3)$$

Net solar radiation (R_n), required as an input in the Penman-Monteith evapotranspiration method, is the difference between the downward and upward radiation fluxes. Equation 2.4, expresses net solar radiation as a function of downward and upward radiation fluxes.

$$R_n = R_{ns} - R_{nl} \qquad (2.4)$$

Where :

R_{ns} ($MJ.m^{-2}.day^{-2}$) is the incoming short-wave irradiance; $R_{ns} = (1-\alpha)R_s$; ά is the albedo = 0.23; R_{nl} ($MJ.m^{-2}.day^{-2}$) is the outgoing net long-wave irradiance, $R_{nl} = f_c f_h \sigma \left(\frac{T^4_{max} + T^4_{min}}{2} \right)$, Where σ = Stefan-Boltzman constant ($4.903x10^{-9}$ $MJ\ m^{-2}\ .K^{-1}\ .day^{-1}$); f_c = cloudiness factor (function of solar and extraterrestrial radiation);

$f_c = \left(\frac{1.35}{R_{so}} - 0.35 \right) R_{so}$ *is the clear sky solar irradiance;* $R_{so} = (0.75 + 2x10^{-5} Altitude) R_a$

f_h is the air humidity correction factor; $f_h = 0.34 - 0.14\sqrt{e_a}$, *where e_a is the actual vapour*

pressure; $e_a = 0.6108 \exp\left(\frac{17.27 T_{dew}}{T_{dew} + 237.3}\right)$ *T_{dew} is the dew point temperature estimated as a function of maximum and minimum temperature (T_{max} and T_{min}) according to Linacre (1992);* $T_{dew} = 0.25T_{\min} + 0.6\mathrm{T}_{\max} - 0.009T^2{}_{\max} - 2.$

2.4.2 FAO-56 Penman-Monteith evapotranspiration method

Evapotranspiration is a standard measure for quantifying water consumption needed for suitable crop growth. This makes ET one of the major components in most water balance calculations used in crop models and in the monitoring of water stress for irrigation planning. As a result, accurate estimations of ET are important particularly in arid and semiarid environments where the lack of precipitation limits crop growth and yield.

Two commonly used evapotranspiration concepts are reference evapotranspiration and potential evapotranspiration. *Allen et al. (1998*) defines reference evapotranspiration as "the rate of evapotranspiration from a hypothetical reference crop with an assumed crop height of 0.12 m, a fixed surface resistance of 70 sec m^{-1} and an albedo of 0.23, closely resembling the evapotranspiration from an extensive surface of green grass of uniform height, actively growing, well-watered, and completely shading the ground". On the other hand, potential evapotranspiration is not related to a specific crop and only described as the amount of water transpired in a given time by a "short green crop, completely shading the ground, of uniform height and with adequate water status in the soil profile" (*http://edis.ifas.ufl.edu)*.

Pioneering work in estimating ET is largely attributed to *Penman (1948),* who used a combination of energy balance and mass transfer methods to derive an equation for computing evaporation from an open water surface using standard climatological records. *Monteith (1965),* built on the principle of Penman to form the much used energy balance and an aerodynamic formula combination of Penman-Monteith (PM) equation. The PM equation is widely recommended because of its detailed theoretical base and its accommodation of small time periods (*Samani, 2000*).

A number of studies have done further developments on the PM equation and it has been used and validated in parts of southern Africa using ground based measurements. For instance,

Schulze et al. (2007b) produced ET maps for South Africa using the PM equation. They showed that monthly averages of accumulated daily ET during the summer season are closely related to measured values in parts of South Africa. However ET values increased by about 80mm in the arid western region of the country when compared to lysimeters (instruments used to measure ET) measured values. *Persaud et al. (2007)* used the Penman method, to evaluate the accuracy of measured ET coefficient values when compared to two observation ET stations in Botswana. The results showed that the coefficients currently used by the Department of Meteorological Services (DMS) in Gaborone, Botswana, best matched the lysimeter field measurements. However, they suggested further work would be appropriate to cover various regions and to verify the correctness of Penman-derived long-term values.

Annandele et al. (2001) studied the response of PM evapotranspiration method when incomplete data is used. The study was done over three regions of South Africa, all with different climatic conditions, namely stations located in Stellenbosch (Mediterranean climate), Pietermaritzburg (sub-tropical with hot, humid conditions in summer) and Kakamas (dry and hot conditions). Using error analysis methods to determine estimated variables that influence reference ET calculation, they showed that solar radiation could be omitted at Stellenbosch during winter periods without large errors arising in predicting reference ET. In Pietermaritzburg, they concluded that the wind variable is less sensitive while the in arid climates (Kakamas), all weather parameters (see next section for PM input data requirements) strongly influence ET calculations significantly.

According to the Food and Agriculture Organization Irrigation and Drainage Paper No. 56 (*Allen et al., 1998*), the modified PM evapotranspiration method (referred to as reference evapotranspiration) is considered to offer the best ET estimates with minimum possible error in relation to a living grass reference crop. The reference Penman-Monteith (PM_o) approach requires minimum and maximum temperature, solar radiation, wind speed, and humidity as primary input climate dataset. The PM_o method is expressed as shown in Equation 2.5.

$$PM_o(mm/day) = \frac{\text{Slope}_{vpf}.(R_n - SHF) + (DF \cdot VPD \cdot C_{va}/ra)}{\text{Slope}_{vpf} + \gamma.\left(1 + \frac{r_c}{r_a}\right)} \quad (2.5)$$

Where:

SHF	*($MJ.m^{-2}.day^{-2}$)*	*is the Soil Heat Flux.*
DF	*(0-1)*	*is the fraction of the day that is in daylight.*
C_{va}	*($(MJ.m^{-3})/°C$)*	*is the volumetric heat capacity of air taken as $1.2x10^{-3}$.*
γ	*(kPa/°C)*	*is the psychometric constant.*
$Slope_{vpf}$	*(kPa/°C)*	*is the slope of saturation vapour pressure, a function of temperature.*
VPD	*(kPa)*	*is the Vapour Pressure Deficit*
R_n	*($(MJ.m^{-2})/day$)*	*is the net radiation calculated from solar radiation.*

($day.m^{-2}$) are the aerodynamic and canopy resistances to vapour transfer of the reference crop. For a short clipped grass (0.12m height).

r_c = 0.000787034 (this may be adjusted in the case of CO_2 simulation); ws (m/s) is the wind speed, hs (m) is the screening height (Screening height is the height of the wind measurement device at the weather station), hp (m) is the plant height (the reference plant height). According to (Allen et al., 1998) saturated vapor pressure VPD can be estimated using equation (2.6).

$$VPD = e_s - e_a \quad (2.6)$$

Where e_s is the mean saturation vapour pressure (kPa); $e_s = (e_o(T_{max}) + e_o(T_{min}))/2$;

$e_o(T_{max})$ and $e_o(T_{max})$ are the saturation vapor pressure at maximum and minimum air temperature respectively. e_a is the actual vapour pressure.

2.4.3 Priestly-Taylor evapotranspiration method

The *Priestly-Taylor (1972)* method is a widely used technique to estimate evapotranspiration because of its simplicity and less input data requirements (*Hoogenboom, 2001*) as compared to the PM equation. The PT method has previously been shown to provide reasonable ET values for different humid locations (*Jensen et al., 1990*). The PT method requires net solar radiation and air temperature as input data. The PT method replaces the aerodynamic term (r_a and r_c) of PM equation by a dimensionless empirical multiplier (Priestley-Taylor coefficient) and is useful in conditions where weather inputs for the aerodynamic term are not available (e.g. relative humidity and wind speed), as the case with this study. The PT equation calculates ET as expressed shown in Equation 2.7.

$$\mathrm{PT} = \frac{\mathrm{Slope}_{\mathrm{vpf}}.\mathrm{PT}_c.(R_n - \mathrm{SHF})}{\mathrm{Slope}_{\mathrm{vpf}} + g} \qquad (2.7)$$

PT_c	*(unitless)*	*is the Priestley-Taylor constant location parameter*
R_n	*(MJ.m^{-2}.day^{-2})*	*is the net radiation*
$Slope_{vpf}$	*(kPa/°C)*	*is the slope of saturation vapor pressure function of temperature*
g	*(kPa/°C)*	*is the psychometric constant*
SHF	*(MJ.m^{-2}.day^{-2})*	*is the psychometric constant*

2.4.4 Hargreaves evapotranspiration method

Hargreaves et al. (1985) derived a function that requires only measured minimum air temperature *Tmin (°C) and* maximum air temperature *Tmax (°C)* data to estimate evapotranspiration. The Hargreaves method (HG) is one of the simple but widely used empirical techniques for calculating potential ET (Equation 2.8). Despite its weak theoretical basis as compared to PM method, the Hargreaves method has been shown to produce values close to those from PM in parts of the Globe (*Di Stefano and Ferro, 1997).*

$$\mathrm{HG} = 0.0023 \times R_a \times (TC + 17.78) \times (TR)^{0.5} \qquad (2.8)$$

Where: TR is the temperature range (Tmax- Tmin) and it implicitly accounts for the effects of cloudiness, TC= is the mean temperature in degree Celsius, R_a is extraterrestrial radiation.

2.5 Crop models

Crop models are tools used to simulate growth and yield of field crops. They provide an opportunity to translate shifts in climate, soil and ecological data (among other variables) into meaningful information tailored for decision makers. A crop growth simulation model not only predicts the final state of harvestable yield, but also contains quantitative information about major processes involved in the growth and development of a plant (*Jame and Cutforth, 1996*). In practice, crop yield is a result of the interaction between ecological, technological and social economic factors. However most crop models are only able to simulate a portion of these factors as some factors or linkages between them are either not well understood or are too complicated (e.g. pest, weeds) to implement in crop models (*Boogaard et al., 1998*). In addition, these models are influenced by various factors including the quality and availability of input data.

The two basic groups of crop models that exist are mechanistic models and water balance crop models (*Sakamoto et al., 2006*). Mechanistic models describe crop growth based on the underlying processes, such as photosynthesis, organic formation, carbon dioxide, water and nitrogen dynamics in the soil and plant and how these processes are affected by environmental conditions. Examples of Mechanistic crop models are WOFOST (*Supit et al., 1994*) and APSIM *(Keating et al., 2003)*. On the other hand, water balance crop models are more descriptive of the crop water stress and usually include crop phenology development, water balance dynamics in the soil and in the plant. These models are more useful in cropping areas where water is a limiting factor for plant growth and subsequently yield (*Gommes, 1998*). An example of a water balance crop model is the Agrometshell (*Mukhala and Hoefsloot, 2004*).

2.5.1 Agrometshell model

In the recent past, a number of crop simulation models have been used to study the impact of climate change on agricultural production and food security. In this thesis, the Agrometshell crop model is used to simulate maize water requirements under present and future climate conditions. The Agrometshell model was developed by the Food and Agriculture Organization (FAO), Environment and Natural Resources Service. It is based on crop specific water balance methods (*see Doorenbos and Kassam, 1979*). This crop model was specifically used in this study mainly because: (1) it has low data requirement (i.e. considering the limited

data from the climate models) as compared to other complex models (e.g. APSIM), (2) it has been used by the Regional Remote Sensing Unit (RRSU) for food security assessment (*Mukhala and Hoefsloot, 2004*).

At the core of Agrometshell is a water balance model which is described as difference between the effective amounts of rainfall received and the amounts of water lost by the crop (see Equation 2.9). The inputs (on a 10-day time scale) to Agrometshell crop model include precipitation, evapotranspiration and soil water holding capacity. Among the water balance output variables that are produced are actual evapotranspiration, water deficit, water access and a Water Requirement Satisfaction Index (WRSI).

(2.9)

Where PPT is precipitation, Gi is ground water, Q is stream discharge, ET is evapotranspiration losses and Go is ground water. The first part of the equation (PPT + Qi) is referred to as inflow (i.e. the water coming in) while the second part is the outflow.

In this study, only the WRSI output is assessed due to its high correlation with maize yield over the region (*Agrometshell, 2004*). The WRSI expresses the percentage of the crop's water requirements that are actually met, excess soil water and soil water deficit over the initial, vegetative, flowering and ripening phases (see Table 2.3).

Table 2.3: *Illustrates the crop water requirement coefficients (maize) for each stage of the plant cycle. The development stage is estimated by daily interpolation between initial and middle phases.*

Phase	Initial	Vegetative	Flowering	Ripening
Length (days)	25	35	40	30
k_c(t) Maize	0.45	0.8	1.1	0.55

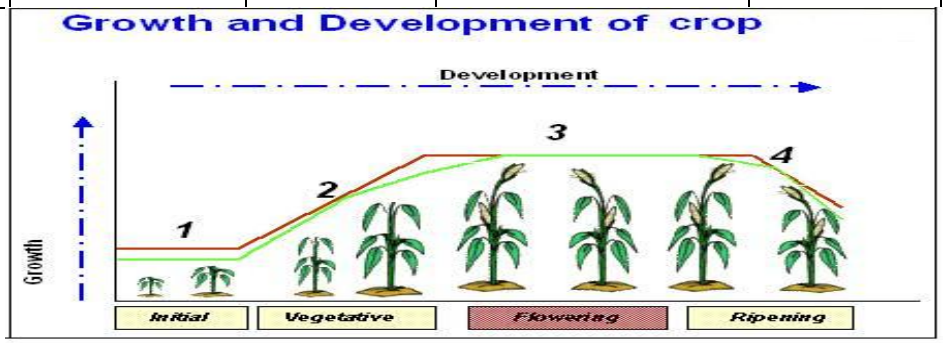

Within the crop model, the WRSI is calculated as illustrated in Equation 2.10. When water supply is limited, actual evapotranspiration (ETa) is less than maximum evapotranspiration (ETm) (see Equation 2.11), resulting in the crop suffering water-stress. Maximum evapotranspiration varies with the phase of the crop and with the climate characteristics of the region (*Martin et al., 1998*). Table 2.4 shows how WRSI relates to maize yield.

(2.10)

Where, WRSI is water requirements satisfaction index

ET_a *is actual evapotranspiration* = ET_m *if soil water (SW)* > ET_m

= *SW if soil water* < ET_m

ET_m *is maximum evapotranspiration*

$$ET_m = k_c(t) * ET \qquad (2.11)$$

Where: ET_m *is maximum evapotranspiration,* $k_c(t)$ *is time-varying crop water coefficient and ET is reference evapotranspiration.*

Table 2.4: *Classification of water-limited performance (see Martin et al., 1998)*

Expected percentage of maximum (potential) yield	**Classification of Crop Performance**	**WRSI**
> 100	Very good	100
90 - 100	Good	95-99
50-90	Average	80-94
20-50	Mediocre	60-79
10-20	Poor	50-59
<10	Complete failure	< 50

2.5.2 Method for calculating crop sowing dates

During the first few weeks of sowing, enough soil moisture is required to meet the needs of a particular crop at a particular time. Information on sowing dates of the rainy season becomes critical for planning for the majority of farmers, especially if it is made available before the onset of rainfall.

The definition of sowing date used in this study is purely derived from rainfall amount needed in a certain period for successful crop germination. Based on the definition by Famine Early Warning System (FEWS); *AGRHYMET, (1996)* and *Tadross et al. (2005),* the sowing date or dekad is defined according to the fulfilment of the following conditions after the 1st of August: At least 25 mm of rainfall amount in the first dekad followed by at least 20 mm of rainfalls in the following 2 dekads. The variability of sowing dates is calculated using standard deviation, (Equation 2.12).

$$std = \sqrt{\frac{\sum (X - Y)^2}{N}} \qquad (2.12)$$

Where std is standard deviation, X is sowing date for each year, Y is the mean sowing dates for the period 1979 to 1999, N is the number of years.

2.5.3 Method for evaluating sensitivity of WRSI to sowing dates

A sensitivity tool was developed to explore sowing date adaptation options over the region. The sensitivity of WRSI to the definition of the sowing date (i.e. the date or window period to plant a seed) for both the present and future climates were performed. The WRSI sensitivity method used in this study is based on the Fourier amplitude sensitivity test (FAST). It allows the computation of the total contribution of each input factor to the output's variance (in our case, WSRI). *Saltelli and Tarantola (1999)* initially introduced this method and the R statistical package (*http://cran.r-project.org*) was used for this study. Two parameters are used to define the sowing dekad (10-day period) namely; *x1* (rainfall amount in the first dekad after 1st August) and *x2* (rainfall amounts in following two dekads) such that X = {*x1, x2*}. The crop model simulations provide outputs (i.e. the WRSI) that are dependent on the input parameters and the climate. The combinations of x1 and x2 affects the WRSI, which was assigned to a function y1 (i.e. Y = {y1}) was evaluated. Sensitivity analysis of Y as a

response to X allows the computation of the total contribution of each input factor to the output's variance.

The first step involves building an input matrix of all combinations to be simulated by the crop model. The second stage performs a wide range of crop model simulations dependant on *x1* and *x2* combination for each year. A decision space consisting of 1000 simulations was performed for each year. It was assumed that 1000 simulations enclosed most of the possible combinations. The last stage associates the contribution of each parameter to WRSI using FAST analysis. Figure 2.3 shows a simplified representation of the results computed for one station and a single climate representation. In this example, the variance of outcome *Y* is due mostly to the single decision parameter *x1*, then by the combination of both *x1* and *x2*, and to the least extent due to the single decision *x2*. According to the decision sowing rule which involves *x1* and *x2*, this specific case depicts a station where more than half of the crop yield variability (when *x1* and *x2* are varied under this particular climate) is due to the variation of the rainfall amount in the first dekad. Rainfall that occurs in the following 2 dekads explains only slightly more than 10% of the yield variability. This kind of information is useful from an adaptation point of view as it allows the decision maker to identify the sowing decision that should be adapted in order to have a noticeable effect on the desired outcome i.e. crop yield.

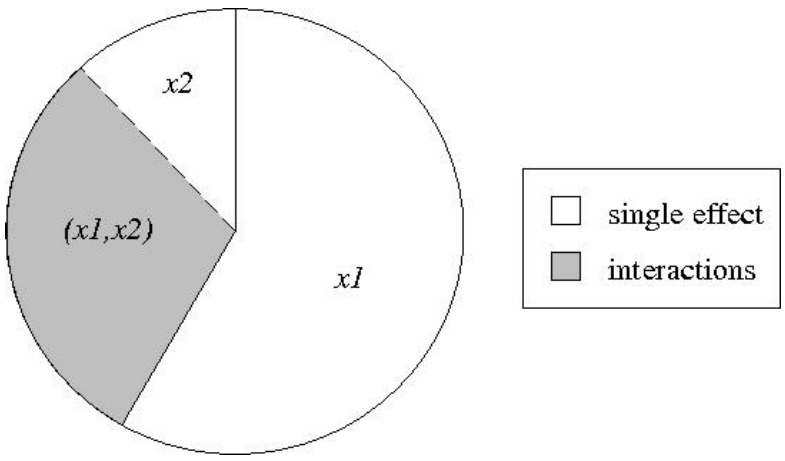

Figure 2.3: *FAST method output: example showing the contribution percentage of single and coupled effects of x1 and x2 on the Y outcome variance*

In order to explore both actual and potential combinations of sowing dekad parameters, a wider range of possible sowing dekads was explored. All possible combination of *(x1, x2)* with the range of *x1* and *x2* being *{0,50},* were considered. Though neither of the four extreme possible combinations *(x1,x2)={(0,0),(0,50),(50,0),(50,50)}* will occur in a practical crop sowing process.

2.5.4 Method for calculating dry spell distribution

The length of an agricultural dry spell for grain cultivation in semi-arid tropical conditions in sub-Sahara Africa generally ranges between 5 and 15 days (*Barron et al., 2003; Fox and Rockstrom, 2000*). The definition of a dry spell used in this study is based on daily rainfall data described by *Usman et al. (2004)* and *Hachigonta and Reason, (2006*). A dry spell is said to have occurred when the rainfall amount in five consecutive days is less than 5mm. The DJF season is assessed because of its relevance as the peak of the growing season within the major cropping areas. A mean duration of a dry spell is defined by the average length (in days) of dry episodes between rainfall events during the DJF season.

2.6 Summary

This chapter has described the source and nature of data, as well as the methods used in this thesis. Literature on the estimation of solar radiation and evapotranspiration has also been reviewed. For the simulation of maize water requirement satisfaction index and identification of regions vulnerable to the impacts of climate change, a water balance based crop model was presented. In addition, a sensitivity approach that distinguishes efficient decision in sowing dates to be adapted was also introduced and is applied in chapter 5.

The methodologies used in this thesis can be summed up in six steps: 1) Evaluate downscaled GCM outputs against downscaled climate observations, 2) Compute and compare outputs from different evapotranspiration methods using observed climate data and identify the best method for the region, 3) Evaluate crop model by comparing model outputs with historical crop yield, 4) Asses projected changes in local climate features using downscaled GCM outputs and associate changes to regional circulation patterns, 5) Simulate crop growth using downscaled GCM variables and investigate changes of maize water requirement by 2050, 6) Perform sensitivity analysis aimed at providing sowing date adaptation strategies over southern Africa.

In the next chapter, the ability of the downscaled GCM data to adequately represent the climate of the southern African region is evaluated with downscaled NCEP-NCAR reanalyses data. The above observations of the recorded data may not necessarily be simulated by the downscaled GCM variables. However, the downscaled GCM data are expected to successfully simulate trends and mean state of the atmosphere although they are not expected to simulate the year to year variability in the observed climate. In addition solar radiation and evapotranspiration methods discussed in section 2.4 are evaluated in chapter 3.

Chapter 3
Model evaluation

3.1 Introduction

Numerical models attempt to simulate geophysical processes through the mathematical description of these processes and the interaction between them. As a result of computational and knowledge restraints, modeling is a simplification of reality. Therefore some processes within a complex system might not be fully represented thus introducing elements of uncertainty into the modeled output. Furthermore, in the context of crop models, uncertainties arise when simulating crop yield as a result of transfer of error (e.g. uncertainty caused by the errors of the measured weather data being transferred to crop model outputs). Uncertainties become even more pronounced when dealing with future scenarios as model evaluation can only be done on the present day climate and assumptions have to be made that these models would also yield the most reliable representation of future climate (*IPCC, 2007*).

In order to have confidence in a model, it is essential to first establish that the model reasonably simulates the observed system (e.g. crop yield) over a region of interest on both spatial and temporal scales of relevance. Model evaluation is therefore a central necessity in any model analysis and includes quantification of uncertainty. *Randall et al. (2007)* noted that testing the climate model's ability to simulate past and present climate is an important part of model evaluation. *Forest et al. (2003)* also note that an accurate description and understanding of the uncertainty inherent in the system being modeled can help improve on the decisions made.

The objectives of this chapter are: (i) to evaluate downscaled GCM data during a control (or historical) period (1979 to 1999) in order to identify regions and models showing a strong bias relative to observational NCEP reanalysis data, and (ii) to evaluate and select best regional empirical methods used for computing solar radiation and evapotranspiration needed for crop simulations over southern Africa. This is done in order to fulfil the first research question of this thesis.

This chapter begins by giving a general description of regional baseline climate. A comparing statistically downscaled precipitation and temperature variables from five GCMs with high

resolution data downscaled from NCEP reanalysis atmospheric fields for the period 1979 to 1999 is also done. Following this is an estimation and evaluation of solar radiation and evapotranspiration (refer to chapter 2 for definitions). These variables are unavailable in the downscaled GCM data, yet they are crucial for crop modeling purposes. The last section involves a general evaluation of the Agrometshell crop model at selected locations.

3.2 Temporal and Spatial distribution of baseline climate characteristics

In climate change studies, it is important to evaluate the baseline (recent past) climate conditions as they serve as reference on which the future scenarios are based. For this study, it is assumed that the impacts of climate change on crop yield will vary on space-time scales as each localized area has its own specific and unique environmental conditions. In the case of agriculture, the difference between the future and the present climatic conditions could shift in such a way that the impact of climate change is more noticeable in the semi dry agriculture regions as compared to the humid regions. This could be the case with other variables than seasonal precipitation totals like onset of rainfall, length of growing period and frequency of dry spells during the summer season which usually affect rain-fed agriculture systems.

3.2.1 Precipitation distribution

Figure 3.1a shows the annual cycle of area averaged precipitation over southern Africa (12°E-40°E; 35°S-8°S) constructed using CRU climatology data set (1961 to 1990). Precipitation over the ocean is masked out thus has no influence on the seasonal cycle. The peak of the rainfall season over southern Africa is from December to February. The humid (or semi humid) areas over northern parts of; Angola, Zambia, Mozambique, and Malawi receive the highest rainfall (averaging above 10 mm/day) during the peak summer season (Figure 3.1b). The high precipitation over these areas is understood to be associated with the southward migration of rainfall systems from the north such as the Intertropical Convergence Zone (ITCZ). In addition, the location of the Tropical-Temperate-Trough (TTT) systems is known to induce rainfall over much of southern Africa large scale systems (*Crimp et al., 1997; Todd and Washington, 1999*). It should also be noted that the western Indian Ocean is the major source of moisture for summer rainfall over southern Africa (*Hansingo, 2008*).

A decrease in precipitation is observed south of the region and is well pronounced over the southwest arid regions of southern Africa. The distribution of rainfall within the season (intraseasonal) or over the years is subjected to high variability with some seasons and regions often having their peak season extended or reduced (*Reason et al., 2005*).

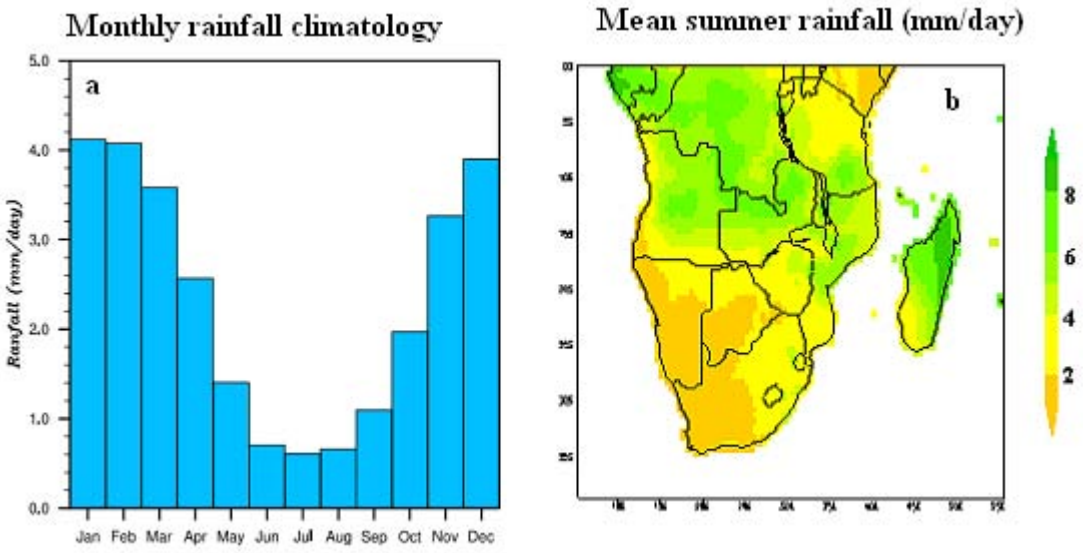

Figure 3.1: *(a) Annual Precipitation cycle averaged over southern Africa (12°E-40°E; 35°S-8°), (b) December to February climatology precipitation over southern Africa in mm/day for the period 1961-1990. (Note: Plots above use CRU 1.0 data)*

During the last decades, several studies have investigated climate variability over southern Africa and around the globe, especially for precipitation and temperature (*Mason and Jury, 1997; Hulme et al., 2001; New et al., 2006; IPCC, 2007; Tadross et al., 2010*). In a study over South Africa, *Kruger (2009)* noted that while there has been no significant change in annual rainfall totals during the past century, there is evidence of significant increases in extremes and interannual variability of precipitation over southern Africa. In a similarly study, the *IPCC, (2007)* work group 1, reported some downward trend and strong multi-decadal variability in precipitation over southern Africa during the period 1901 to 2005. It was noted that, in most cases, the change in rainfall events over the region occurs fairly abruptly.

In addition to the evidence of the observed change in the extreme precipitation characteristics, there is also a growing body of literature that indicates that as the global

temperature increases as a result of the increase in greenhouse gas concentrations in the atmosphere, further changes in the characteristics of heavy precipitation are likely (*Semenov and Bengtsson, 2002; Tebaldi et al., 2006*). Over southern Africa, *Mason and Joubert (1997)* showed the frequency and intensity of extreme daily and prolonged (five-day) rainfall events generally increased under doubled atmospheric carbon dioxide conditions in the future, even in some areas where decreases in mean annual rainfall were simulated.

Apart from seasonal means in precipitation and temperature, the distribution of rainfall within a particular season plays a critical role in crop growth. Dry spells relate directly to agricultural impacts since their distribution and duration indicate availability of soil moisture thus the degree of water stress plants are exposed to *(Usman and Reason, 2004)*. Crop sowing dates, length of the growing season and the behaviour of characteristics such as evapotranspiration are equally important to small scale farmers. Knowledge about these characteristics helps farmers in pre-season farming decision making, for instance in choosing the type of cultivar. In this study, knowing how these climate characteristics have changed in the past is useful as it helps to better understand the impacts of future crop model simulations discussed in chapter 5. The following sections give an overview of the baseline dry spell distribution and crop sowing date climate characteristics over the region.

3.2.2 Dry spell distribution

During the period 1979 to 1999, dry spells occurred most often over the semi-desert areas of the southwest parts of the study region (Namibia, Botswana and western South Africa) (Figure 2.5). In general, this region experiences above 8 dry spells during the DJF season with maximum durations of about 14 days. On average 5 dry spells occurred over central Zimbabwe, southern Zambia and the Limpopo region of South Africa with maximum durations ranging between to 9 days around the southern tip of Zambia to 12 days over Limpopo. During the summer season, regions close to the position of the ITCZ that stretches across northern Mozambique, Zambia and Malawi experience the least number of dry spells (~2).

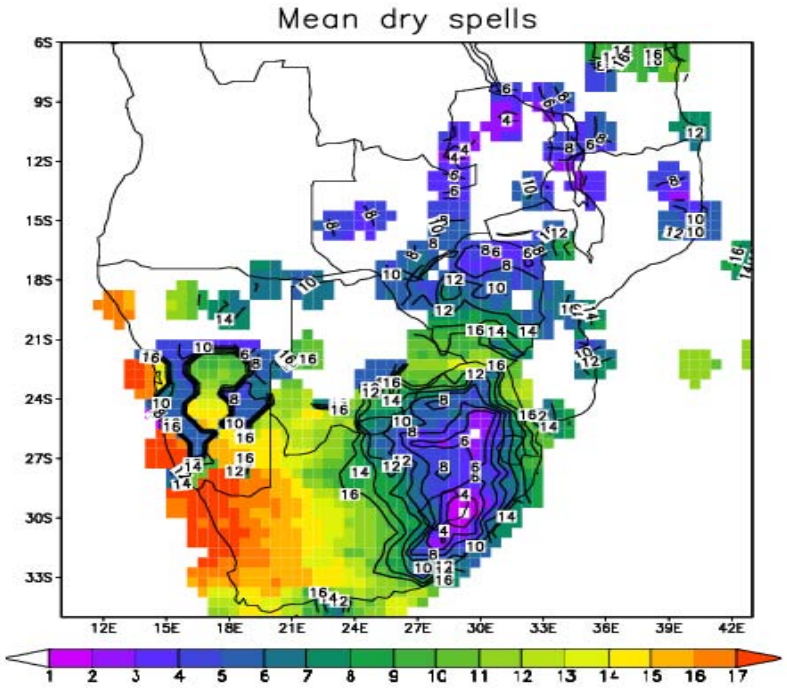

Figure 3.2: *Mean number of dry spells during DJF (shaded) and duration (contours in days) during the peak DJF summer season using gridded observation station data averaged for the period 1979 to 1999*

The number of dry spells greatly varies over the region from year to year. This variation has previously been associated with shifts in the location of TTT over much of southern Africa (*Usman et al., 2004*). In addition, some studies have linked El-Niño (La-Niña) to high (low) number of dry spells over the region (e.g. *Hachigonta and Reason, 2006*). *Usman and Reason (2004)* showed that there is a very close relationship between dry spell frequency and ENSO over southern Africa (Figure 3.3). It should be noted that in some instances, moderate number of dry spells within a season with short durations (1 to 2 days) could be beneficial to crop development in seasons with normal rainfall.

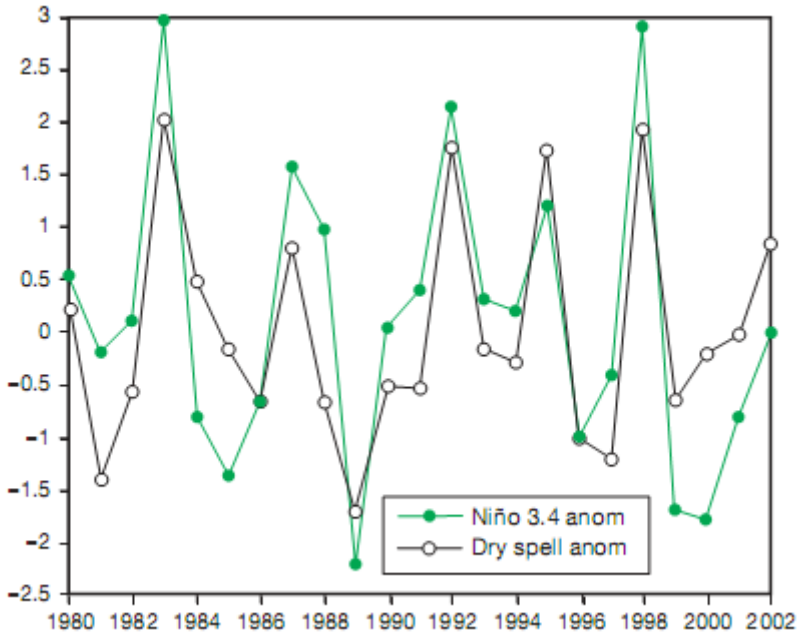

Figure 3.3: *Standardized time series anomalies in dry spell frequency and Niño 3.4 Sea Surface Temperature for the 1979 to 2001 summer period. Area averaged for southern Africa. (Source: Usman and Reason, 2004)*

3.2.3 Crop sowing dates

Figure 3.4a shows the sowing date's derived using observation data averaged for the period 1979 to 1999. The earliest sowing dates are attained over the central and eastern parts of South Africa between October to November while late sowing dates (January to February) are observed in the dry south-western regions of Namibia and northern Mozambique. The rest of the sub-region is characterised by a broad band of mean sowing dates in late November and December. Despite having early sowing dates, the central and eastern parts of South Africa are prone to high interannual variability (Figure 3.4b.). Other regions showing high variability in sowing dates include northern Zimbabwe and central Zambia. The early rains in this region could be as a result of the Angola low, which develops during this period and influences the westerly moisture feed from the tropical southeast Atlantic Ocean (*Cook et al. 2004*).

In a recent study, *Tadross et al. (2010)* observed a weak trend for later planting and earlier cessation dates in the northern parts of southern Africa, leading to shorter rainfall seasons. The duration of the rainfall season over southern Zambia was shown to often be close to critical thresholds, which forces farmers to plant as early possible.

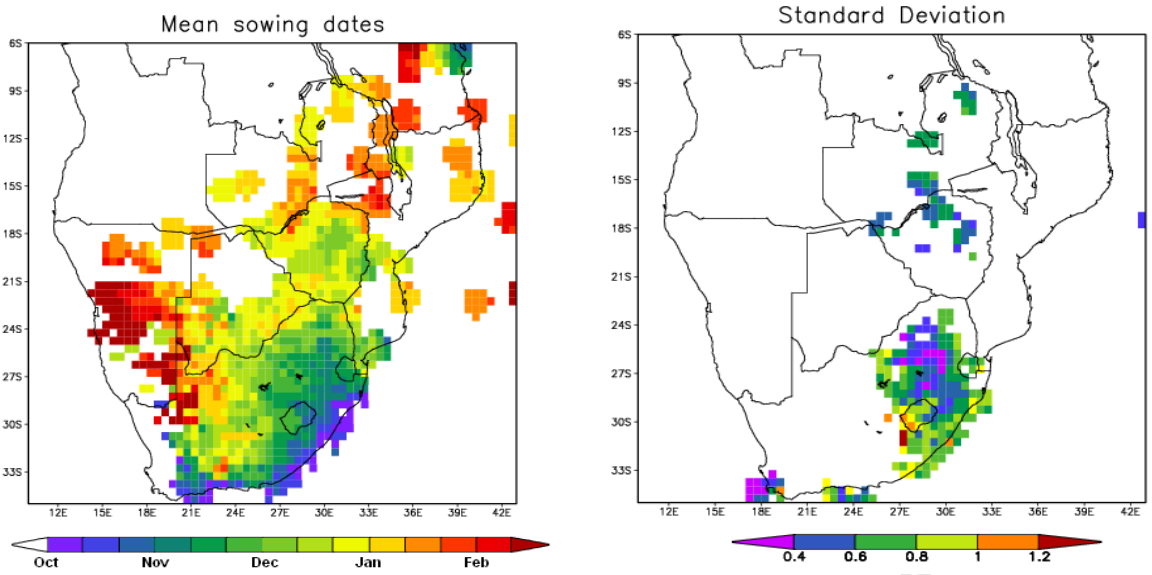

(a) (b)

Figure 3.4: *(a) Mean sowing dates (1979-1999) over southern Africa based on observational rainfall thresholds. (b) Mean sowing date standard deviation for the1979-1999*

3.2.4 Summary on baseline climate characteristics

By using past climate data and literature from previous studies it has been shown that no significant increasing trends in precipitation are evident over the region during the past decades. However the region is subjected to high rainfall variability in both space and time. Studies have also observed a weak trend for later sowing dates and earlier cessation dates in the northern parts of southern Africa, leading to shorter rainfall seasons during the last 30 years. Unlike precipitation, considerable increases in temperatures have been observed over the region and are linked to the effect of global anthropogenic climate change. In most instances, higher temperature over the region or surrounding oceans typically translates into extreme regional precipitation because evapotranspiration (which is a function of temperature) is an integral component of rainfall feedback. Thus, although no significant trends in precipitation are observed, the number of regional extreme events has been on a rise.

3.3 Biases in downscaled GCM output

Downscaled precipitation and temperature forced by NCEP reanalysis atmospheric fields (referred in this study as NCEP-DS) is used in this study to evaluate the downscaled GCMs variables (referred here as GCM-DS) during the control period. In this context, comparing GCM-DS control data with NCEP-DS gives as an indication of how well the GCM simulates the control climate. In a study over South Africa, Hewitson and Crane (2006) demonstrated that downscaled NCEP rainfall captured the observed season rainfall patterns and spatial gradients across the region including the high orographic rainfall region of the Drakensberg Mountains. It was also shown that downscaling NCEP outputs capture the summer convective systems in the interior plateau, as well as the winter frontal rainfall over the south-west of South Africa. As the downscaled variables (i.e. precipitation and temperature) are at a station level, the GCM-DS and NCEP-DS data are interpolated to a common 0.5 degree grid. The period of interest in this evaluation is the summer rainfall season as this is the main crop growing season for the region.

3.3.1 Regional biases between GCM-DS and NCEP-DS

Figure 3.5a compares the daily precipitation climatology (1979 to 1999) between five GCM-DS with NCEP-DS (black line) averaged over the entire southern Africa (12ºE-40ºE; 35ºS-8ºS) to evaluate the ability of the GCMs to reproduce the regional season cycle. This time series is an average of 20 year precipitation amounts for each calendar day (from the 1st of January to the 31st of December). The five GCMs-DS (Figure 3.5a) individually capture the NCEP-DS reanalysis precipitation annual cycle and the same follows for the GCM-DS ensemble mean shown in Figure 3.5b. The overall picture from the area averaged time series indicates that the highest values (in the GCM-DS data) are representative of the summer rainfall season (see section 3.2.1), whereby the highest daily rainfall is observed in December, January and February declining towards winter (June). The beginning of summer is evident from the increased rainfall in October/November. In general, all the five GCM-DS simulations are close to the NCEP-DS seasonal cycle. This demonstrates that the region's seasonal cycle is well reproduced by the climate models.

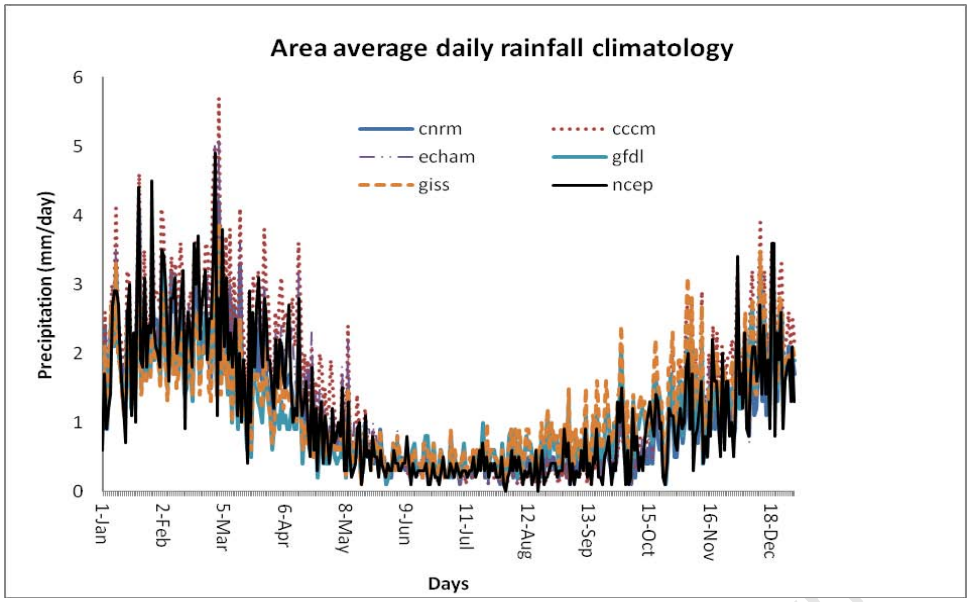

Figure 3.5a:*Daily climatology (1979-1999) precipitation annual cycle averaged over southern Africa (12◦E-40◦E; 35◦S-8◦S). Control period of five downscaled GCMs against NCEP-DS data (black)*

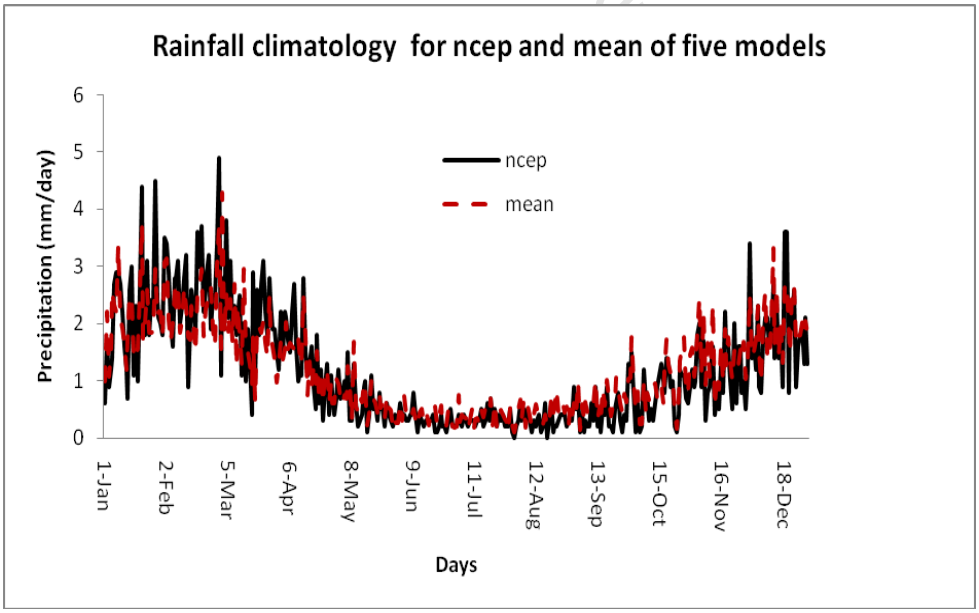

Figure 3.5b: *Climatology (1979-1999) precipitation annual cycle averaged over southern Africa (12◦E-40◦E; 35◦S-8◦S). Mean of the five downscaled GCMs (red) and NCEP-DS data*

The close matching of the GCM-DS (precipitation) with NCEP-DS values implies that the confidence exists to use GCM-DS precipitation for future climate projections, as is the aim of this investigation. However, demonstrating area-averaged temporal representation alone is not sufficient for the purposes of this investigation as it gives a broad picture of the regional changes as opposed to capturing the small scale spatial variation required in climate change impact assessment studies. In this regard, a more detailed spatial comparison is performed to

evaluate the downscaled GCM precipitation. The evaluation is done for the early summer (September, October, November: refered as SON), peak summer (December, January, February refered as: DJF) and late summer (March, April, May refered as: MAM) summer.

3.3.2 Station level biases between GCM-DS and NCEP-DS

Figure 3.6 depicts the difference between precipitation composites of NCEP-DS reanalysis and those from the mean of five member GCM-DS ensemble for the period 1979 to 1999. For each seasonal precipitation map presented, values between -5 and 5 mm/month (white colour) are considered to have minimal changes or are close to zero. Red indicates regions where the model ensemble overestimates rainfall (positive bias) and blue where the models underestimate rainfall (negative bias).

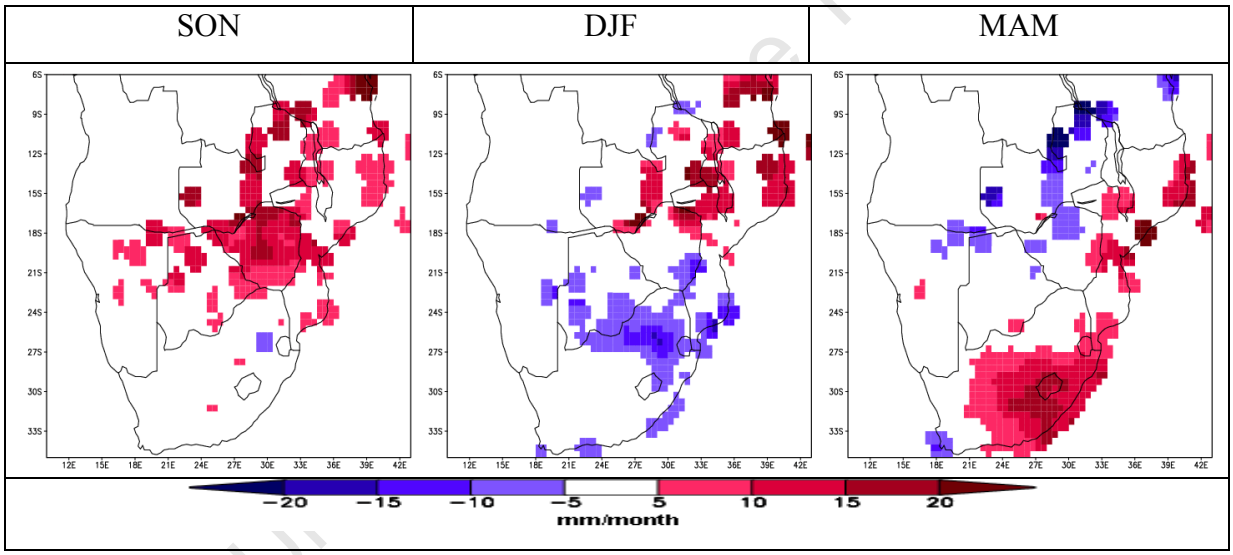

Figure 3.6: *Spatial climatology precipitation maps (1979 to 1999 averages) showing the difference between GCM-DS ensemble and NCEP-DS reanalysis (i.e. GCM-DS minus NCEP-DS) during early, peak and late summer season*

Countries to the north of the study region (Zambia, Zimbabwe, Malawi and most parts of Mozambique) show a positive rainfall bias of about 10 to 15 mm/month during the early summer season (SON) (Figure 3.6). During the peak summer season (DJF), the GCM-DS ensemble mean shows slight underestimation of precipitation of about 10 mm/month over parts of north eastern South Africa and a positive bias over parts of Zambia and Malawi. The late summer season (MAM) shows a positive bias of approximately 12 mm/month, mostly

over the south eastern parts of South Africa, parts of Mozambique and the southern tip of Malawi.

The comparison of individual GCM-DS simulations with NCEP-DS during the peak summer season (DJF) is shown in Figure 3.7. The GFDL and CNRM depict opposite signals of negative and positive bias respectively for southern Zimbabwe and the central eastern parts of South Africa, meanwhile the ECHAM model shows the least precipitation bias over study domain when compared to NCEP-DS.

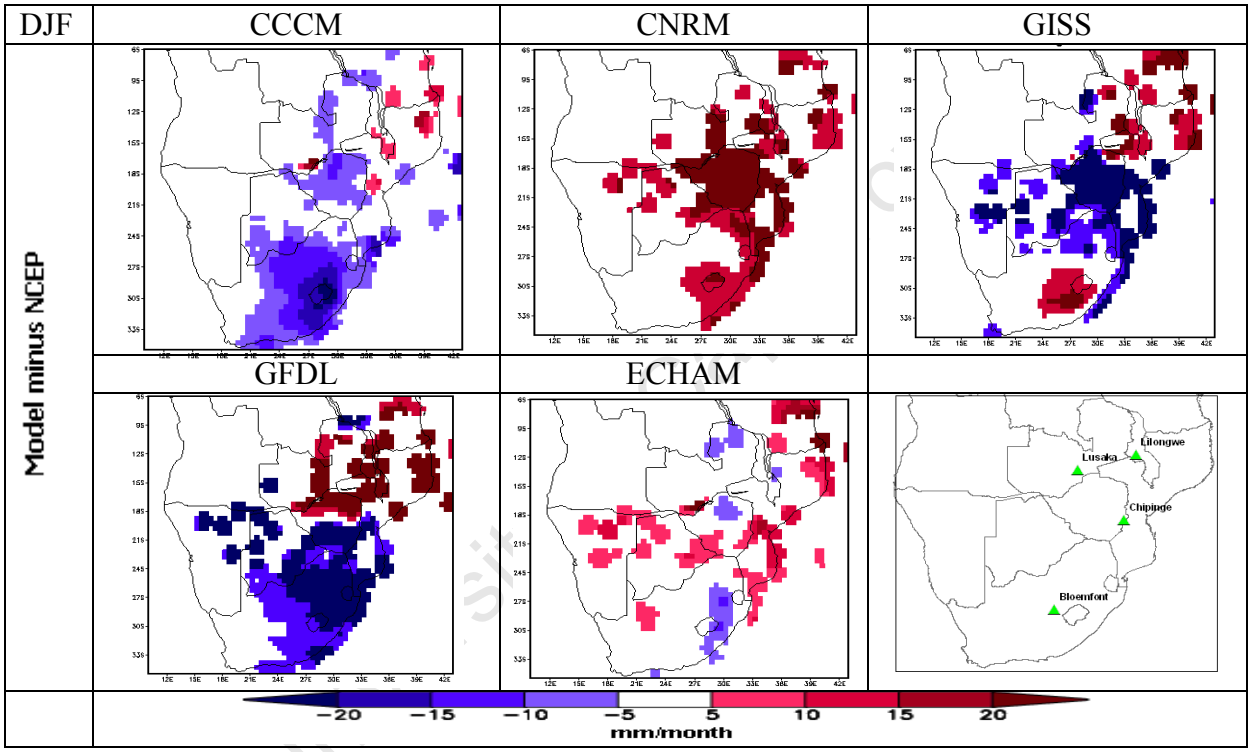

Figure 3.7 *Difference between individual GCM-DS and NCEP-DS during peak (DJF) summer season (mm/month). Bottom right picture shows stations picked for daily time series analysis in Figure 3.8*

To have an insight of how local scale biases in GCM-DS precipitation distributions perform when compared to NCEP-DS for the entire year, four stations (see bottom right of Figure 3.7) were further evaluated. The selected stations represent the areas with the highest GCM-DS bias values relative to NCEP-DS. A simple time series comparison between the five GCMs-DS and NCEP-DS at the four stations was performed (Figure 3.8).

Chipinge station located over the eastern parts of Zimbabwe illustrates the tendency of CNRM overestimating NCEP-DS throughout the summer rainfall season (October to March)

by about 2mm/day while the anomalies for GISS and GFDL are highly negative, about 3 mm/day, during the later summer season. ECHAM and CCCM show the best fit with the NCEP-DS reanalysis throughout the year.

Lilongwe station lies in Malawi's central region near the border of Mozambique and Zambia. On a daily basis, all the GCMs with the exception of GFDL show a good relationship with NCEP-DS. GFDL slightly overestimates NCEP-DS by about 1mm/day during the summer season.

Bloemfontein station located in central parts of South Africa shows CNRM to have the highest positive bias with maximum peak difference of about 2 mm/day during late summer season while the GFDL GCM-DS underestimates NCEP-DS reanalysis, by about 0.8 mm/day, during the same period. The pattern of the five models is very close to NCEP-DS during the early summer season at this station.

Lusaka station located in the southern part of Zambia shows that most GCMs are able to capture NCEP reanalysis, although GFDL and CNRM have a positive bias, of approximately 1 mm/day, during the summer season. The GISS model also shows a tendency to under estimate precipitation by approximately 1.2 mm/day during the later summer season.

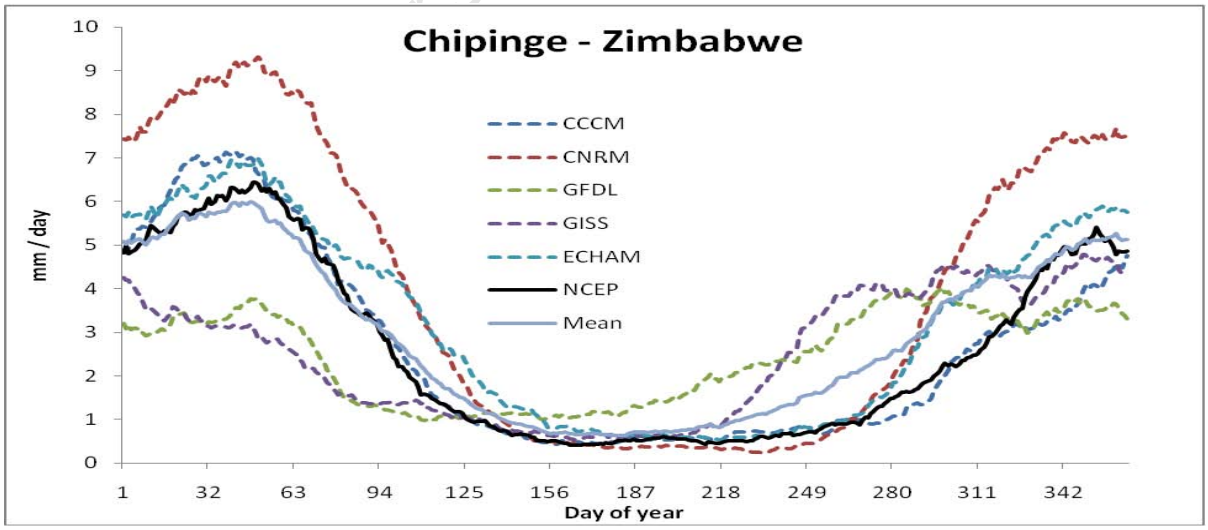

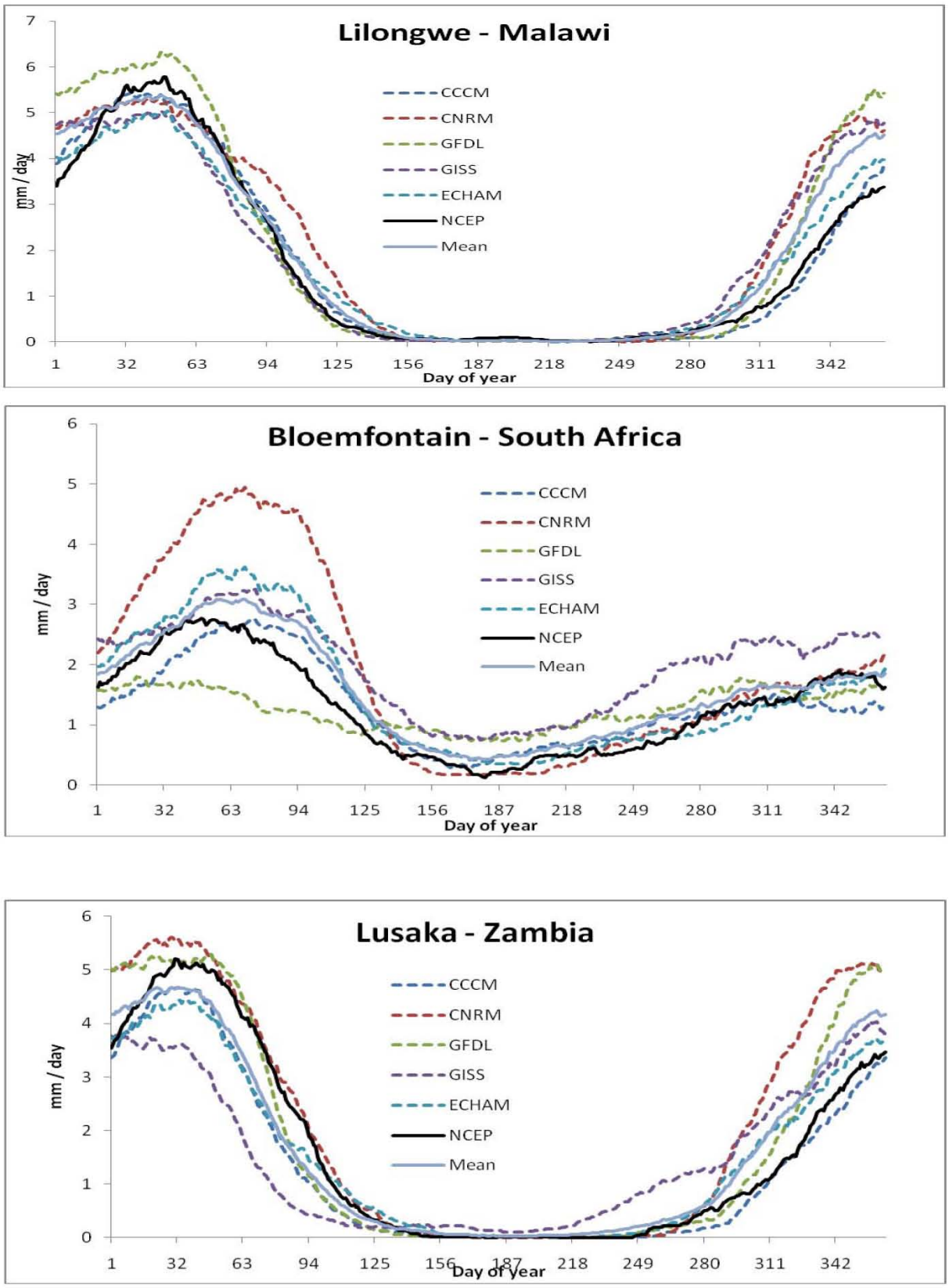

Figure 3.8: *Precipitation time series (mm/day) of five GCM-DS and NCEP-DS reanalysis at four selected stations*

Unlike precipitation, which is a product of complex interactions on scales not resolved by the GCMs, downscaled GCM temperature compares very well with NCEP-DS temperature (Figure 3.9). This implies that higher confidence should be placed on the GCM ability to simulate temperature and the related functions (e.g. evapotranspiration) as compared to precipitation. In a similar study, *Gleckler et al. (2008)* compares the errors in modeling precipitation and surface air temperature in the GCMs. They found that the models simulate temperature better than precipitation. Another interesting feature noted in this study is that, regions (along central South Africa) showing high negative bias in precipitation (Figure 3.6) are associated with negative bias in temperature during the same period (Figure 3.9).

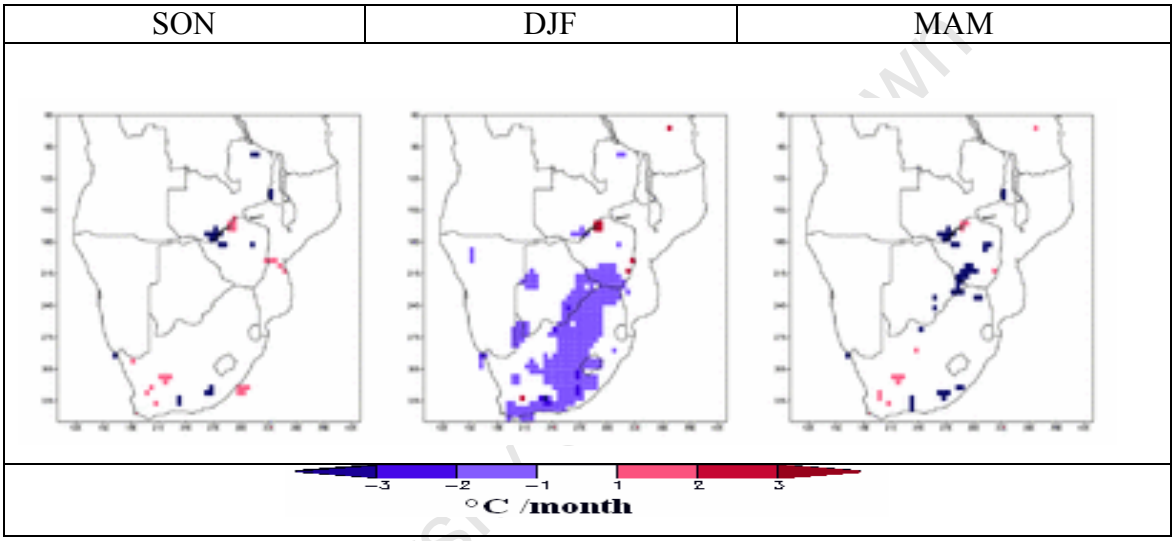

Figure 3.9: *Spatial climatology of mean Temperature maps (1979 to 1999 averages) showing the difference between GCM-DS ensemble and NCEP-DS during early (SON,DJF and MAM) summer season*

Given the large precipitation biases in the results noted in the previous sections, it is necessary to investigate and attempt to quantify them. Misrepresentation of local and large-scale atmospheric dynamics by the GCMs can lead to biases in precipitation output and some biases could be directly linked to the inability of models to correctly simulate precipitation over topographically complex regions (e.g. on high-altitude landscape). A number of model inter-comparison studies have shown that different variables are simulated with varying degrees of success by different models and that no particular model is best for all variables and/or all regions (*Gleckler et al., 2008; Johnston and Sharma, 2009*). The following section attempts to assess if the large precipitation biases noted in some GCM-DS outputs could be

associated with large-scale atmospheric dynamics within individual GCMs using specific humidity as an indicator.

3.3.3 Influence of specific humidity to GCM precipitation bias

Figure 3.10 shows 800 hPa specific humidity fields for the five GCMs and NCEP reanalysis (bottom right) over the region. Specific humidity was used as input in the downscaling process and plays an important role in the dynamics of regional precipitation. The missing low level specific humidity fields (shown as white blocks in Figure 3.10) over central and eastern South Africa (in GFDL and GISS) and southern Angola (GISS) could possibly be linked to high precipitation biases. The missing specific humidity appears to be more related with the presence of high topography that the GCMs cannot resolve, particularly over the escarpments of central and eastern South Africa. Some of the biases in the GCMs could be due to different parameterization schemes used by the respective models that influence the circulation dynamics. In a similar study, *Cavasos and Hewitson (2005)* showed specific humidity (at 700 hPa) to be an important predictor for downscaling precipitation.

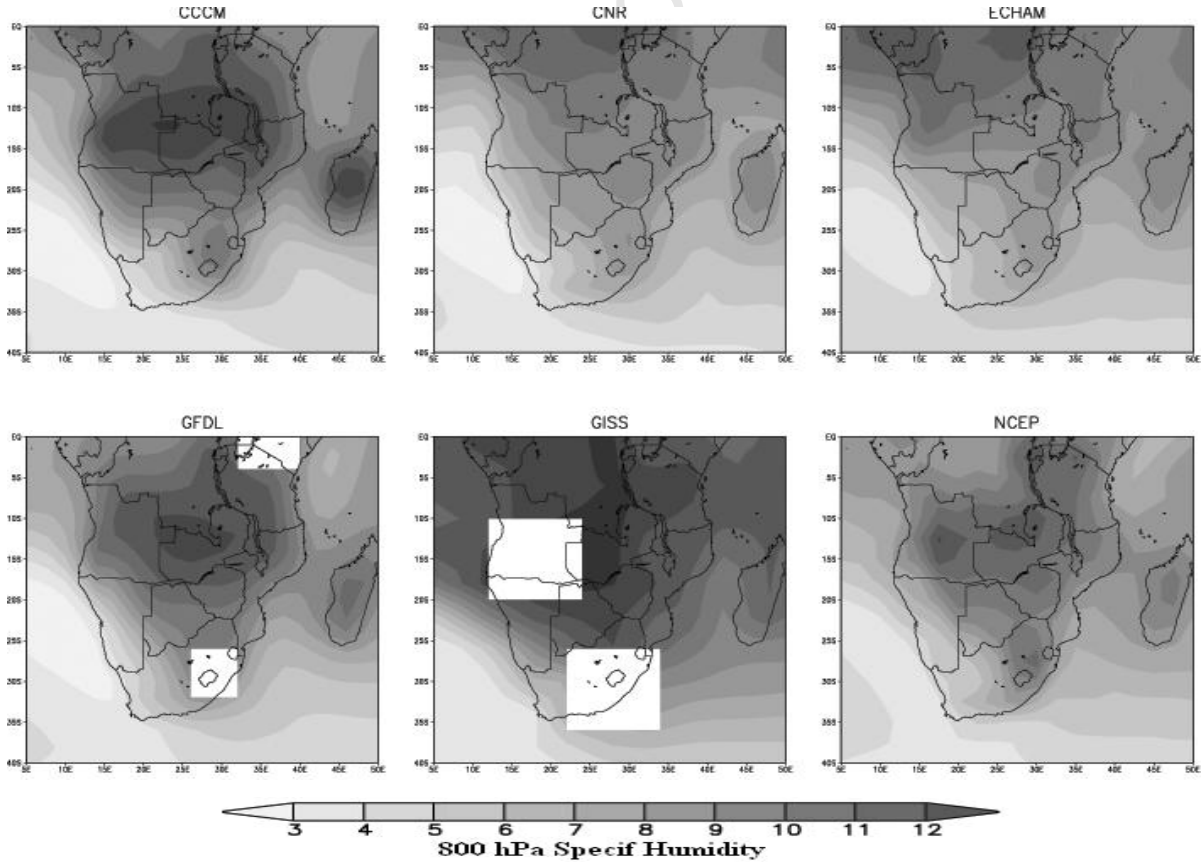

Figure 3.10: *DJF low level specific humidity field for five GCMs (Not downscaled) and NCEP reanalysis (surface composite)*

3.3.4 Summary on GCM evaluation

The spatial and temporal comparisons in this chapter illustrate biases associated with GCM-DS when simulating NCEP-DS precipitation. The downscaled control simulations from the five GCMs have shown the ability to capture the "observed" NCEP-DS seasonal precipitation cycle over most of the region as well as spatial patterns although some regions show disparities. Some notable biases that reflect in the downscaled GCM control precipitation simulation are as a result of surface synoptic systems in individual GCMs (such as missing specific humidity), that are used as input in the downscaling process. The magnitudes of the anomalies reflect a 15 to 20% bias in peak summer precipitation relative to NCEP-DS. Notable is the difference between the CNRM and GFDL, which show opposite biases in precipitation over central Zimbabwe. Using three GCMs, *Hewitson and Crane (2006)* indicated that the use of downscaling techniques show notable coherency when forced by several different GCMs and the spatial pattern of the future change is largely in agreement for South Africa.

3.4 Evaluation of estimated solar radiation against CRU solar radiation

The Hargreaves and Samani (HS) solar radiation method is adopted from *Ball et al., 2004* (see section 2.4.1 of chapter 2 for the literature). This method requires minimum temperature, maximum temperature and altitude as input data sets. CRU monthly data was used to calculate solar radiation coefficients (refer to chapter 2) instead of the fixed literature values of 0.17 (inland) and 0.20 (coastal). Figure 3.11 illustrates DJF spatial distribution of coefficients needed for estimating solar radiation using the HS technique. The coefficient varies with time, location and environment. Values ranging between 0.19 and 0.20 are observed along the coastline and parts of the arid regions (south west of the study) while the interior regions have values ranging from 0.14 to 0.17.

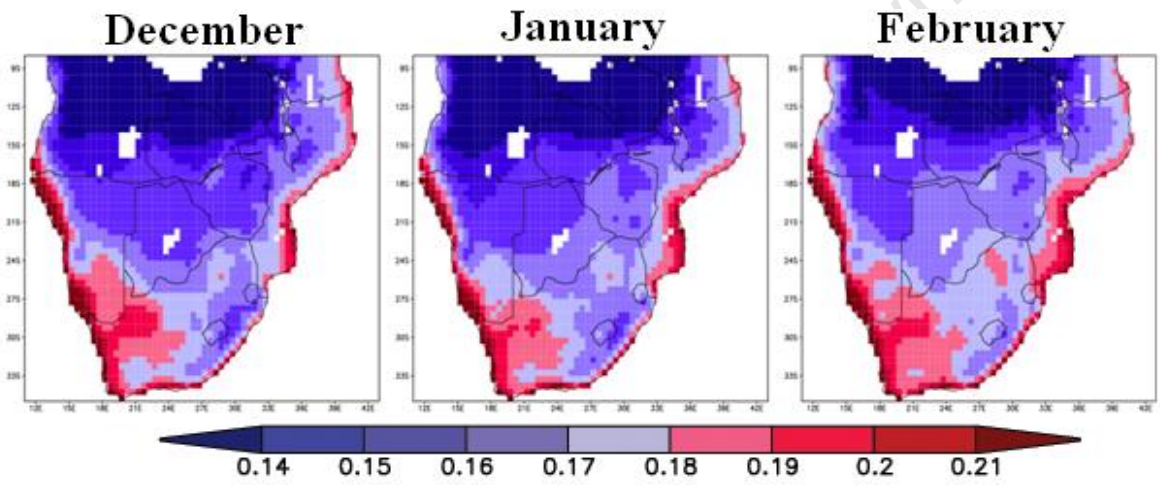

Figure 3.11: *Solar radiation coefficient values K_s (calculation based on method adapted from Ball et al. 2004) for December, January and February*

Figure 3.12 shows the estimated spatial DJF distribution for solar radiation. High values are observed over the arid western region (area bordering Namibia and South Africa) while the northern part of the study region (Zambia and Malawi) show lower values (18 MJ m^{-2} d^{-1}).

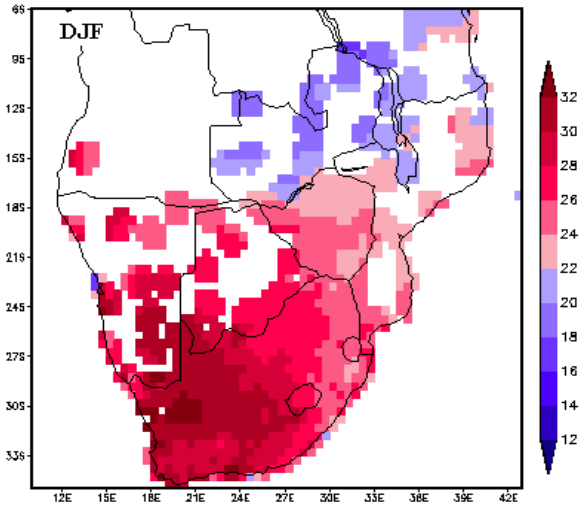

Figure 3.12: *Mean spatial distribution of solar radiation (MJ m^{-2} d^{-1}) during DJF season*

Figure 3.13 compares estimated solar radiation (computed using daily observation data and gridded to 0.5 resolution) with those obtained from CRU at 170 station points (corresponding to stations marked in Figure 2.1) averaged for the period 1979 to 1999. We use the coefficient of determination value (R^2: see Appendix A) to determine how estimated solar radiation outputs at all the stations conform to data obtained from CRU. R^2 values range from 0 to 1, with 1 representing a perfect fit between the data and the line drawn through them, and 0 representing no statistical relationship between the data and a line. Calculated R^2 values between the calculated and CRU solar radiation values were above 0.9 during most of the peak summer December and January while in February the R^2 was 0.86. In general, the HS model has a tendency to slightly underestimate radiation over parts of the humid regions of northern Zambia (not shown) relative to CRU solar radiation values.

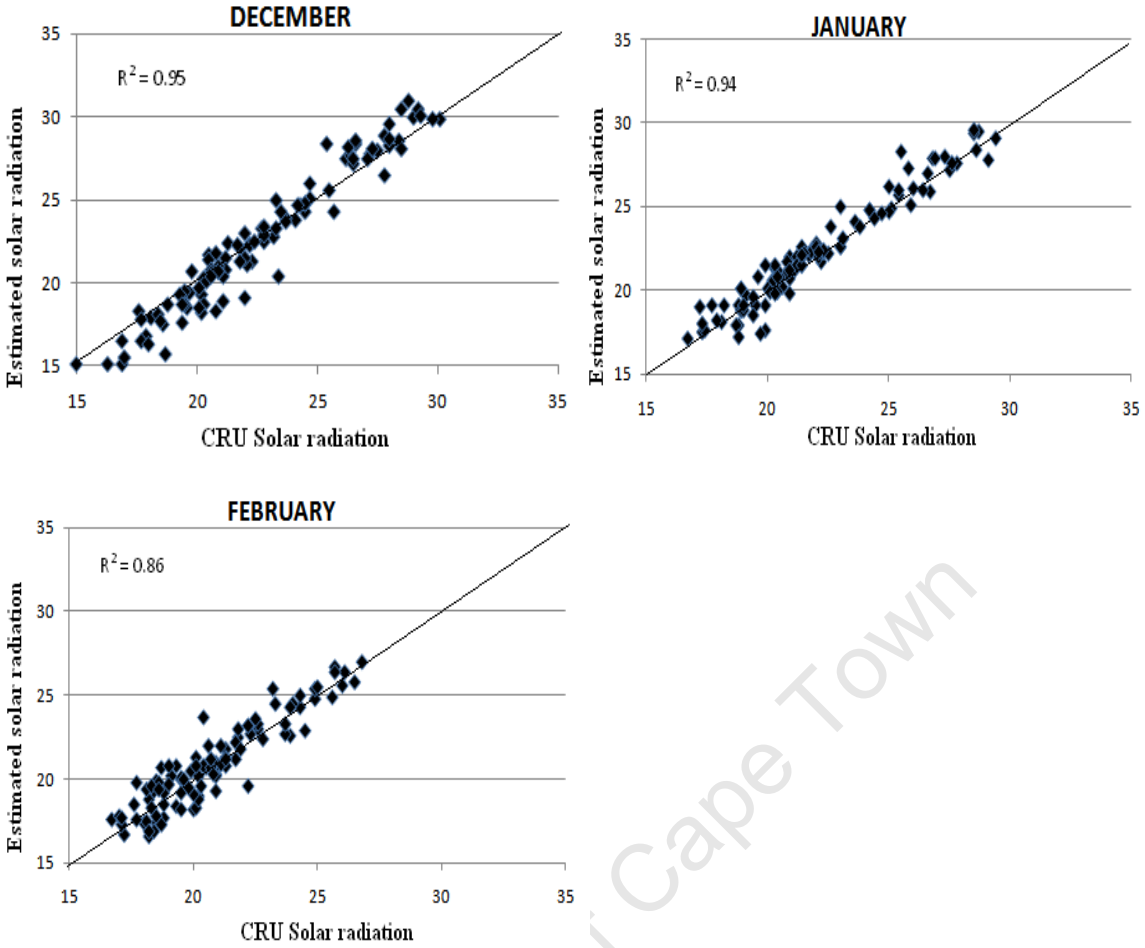

Figure 3.13: *Estimated solar radiation (average 1979-1990) vs. CRU solar radiation (MJ m^{-2} d^{-1}). Each dot represents a station and closer the dots are to the diagonal line the higher the R^2 value*

The HS model performed well when estimating solar radiation relative to the CRU monthly values. The calculation of solar radiation is feasible using a simple equation that is a linear function of a combination of basic weather variables. The modified HS model can therefore be used to estimate solar radiation, using variables present in the GCMs (minimum and maximum surface temperature). The daily evapotranspiration values used later in the study to drive the crop growth model are computed using daily station values of temperature (at 2 m) and solar radiation calculated using the HS model.

3.5 Comparison between Penman-Monteith, Priestly-Taylor and Hargreaves evapotranspiration methods

Three equations are used to evaluate evapotranspiration using the monthly CRU data. Outputs from the Priestly-Taylor (PT) and Hargreaves (HG) methods are compared to those obtained using FAO-56 Penman-Montieth reference (PM_o) evapotranspiration method. The PM_o was used as a benchmark equation because of its detailed theoretical base and high correlation with observed data as noted by previous studies (*Samani, 2000; Allen et al., 1998*). The literature for the three above mentioned evapotranspiration methods is discussed in chapter 2, section 2.4.2, 2.4.3 and 2.4.4.

3.5.1 Region distribution of reference evapotranspiration

The first step involved the computation of the PM_o equation based on the FAO-56 equation (see equation 2.7 of Chapter 2). Only average monthly values for estimated ET are shown in all the figures below, as they are derived from monthly CRU data. Mean monthly PT values are statistically compared to PM_o outputs using the index of agreement (d), relative root mean square error (RMSE) and the coefficient of determination (see Appendix A). The square boxes (Figure 3.14) represent ET classification based on amount of DJF values (i.e. from lowest (level 1) to highest (level 4).

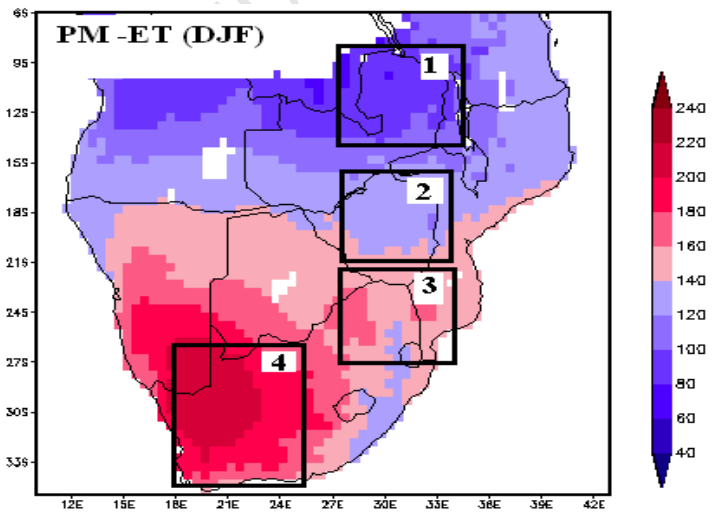

Figure 3.14: *DJF spatial distribution of the PM_o -ET (mm/month) calculated using CRU data*

Regionally, the highest ET values (computed using PM_o) are observed in the south western parts of the study region, particularly around the area bordering Namibia and South Africa during the peak summer rainfall season (Figure 3.14). The south western region has average

monthly accumulated values of up to 240 (MJ m^{-2} $month^{-1}$). Lowest values of ET (100 MJ m^{-2} $month^{-1}$) are observed north of the study region while regions 2 and 3 have ET values of between 120 and 160 (MJ m^{-2} $month^{-1}$). Region 1 is located over northern Zambia is classified as humid, Regions 2 and 3 are classified as semi arid while region 4 is classified as arid. The spatial PM_o evapotranspiration pattern closely resembles that of solar radiation (a function of temperature) presented in section 3.4 suggesting that this variable is a major factor when estimating evapotranspiration over the region.

Studies conducted around the globe (*Jensen, 1985; Naoum and Tsanis, 2003)* have shown that temperature and solar radiation account for most of the variation in evapotranspiration. The following section is intended to verify whether this notion holds for southern Africa. This is important in identifying which input variables play a major role in evapotranspiration estimation over a particular region and at a particular time period. In addition, results derived from this experiment are useful in choosing an alternative evapotranspiration equation that uses less data and thus could be easily implemented with climate change models as compared to the PM_o.

3.5.2 Sensitivity of PM Evapotranspiration to input data

A simple evaluation of the sensitivity of PM method to three climate variables (wind speed at 2m height, mean air temperatures and net solar radiation) is shown in Figure 3.15. The PM sensitivity test involved constant increments in one of the climate variables (e.g. wind speed) while keeping the other variables (e.g. temperature and solar radiation) constant. This procedure is repeated for all climate variables at 10% and 20% at the four regions shown in Figure 3.14. The solid lines in Figure 3.15 represent the sensitivity of PM to a 10% increase in temperature, wind and net solar radiation while the dotted lines show the PM response to a 20% increase in the climate variables. Generally, PM is more sensitive to temperature in all regions while wind speed is the least sensitive variable in all regions and throughout the year. Net solar radiation was found to be the most dominant variable in the humid region (Region 1) during the DJF season.

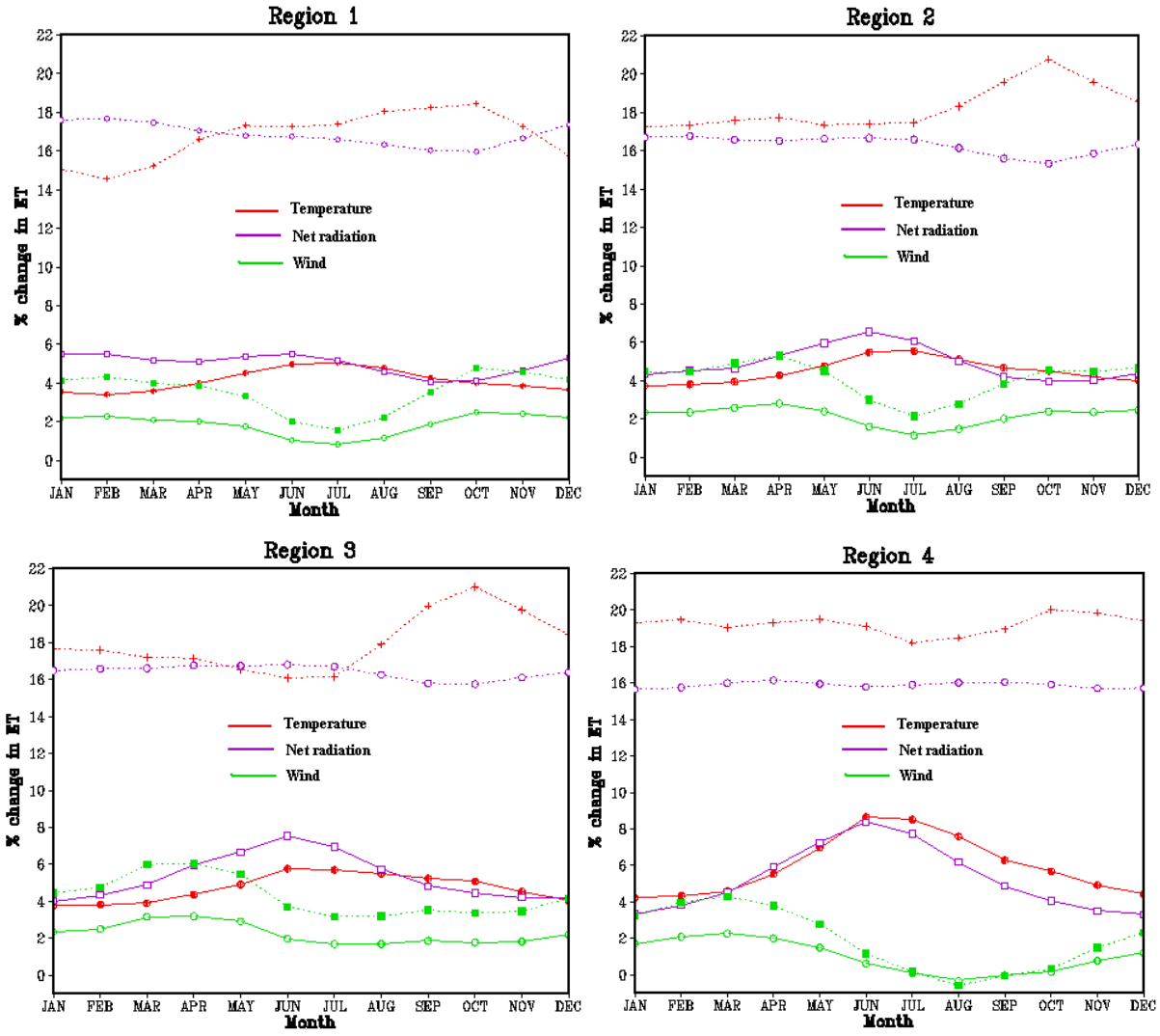

Figure 3.15: *Sensitivity of PM to temperature, net radiation and wind at four regions highlighted in Figure 3.14 (solid lines correspond to response of PM-ET$_o$ to 10% change and the dashed lines correspond to PM-ET$_o$ response to a 20% change)*

Changes in mean temperature and net solar radiation produce similar responses in PM during most of the year. On average, a 10% and 20% change in temperature and net solar radiation result in about 5% and 15% increase in PM respectively while the same change in wind speed result in a 2% and 4% change in PM respectively. Mean temperature has most influence on PM in Region 1 with the exception of the peak summer season. The sensitivity of PM to wind speed is higher during the summer months and lower during the winter over most regions. The high sensitivity of PM to mean temperature and net solar radiation implies that the PT evapotranspiration method (which only requires these two variables) could perform well over the region although slight biases might be anticipated in Region 4 as a result of the regions high PM sensitivity response to large changes in wind speed. It should be noted here that

change in evapotranspiration is not linear (i.e. a 10% Temperature increase results in a 5% increase in evapotranspiration) thus in a global warming context regions that experience greater warming will have even greater evapotranspiration.

3.5.3 Comparison between PM_o, PT and HG methods

Figure 3.16 shows the relationship between PM_o and PT evapotranspiration methods during the peak summer season. Comparison of the PM_o and PT monthly values indicates that the two methods agree well over the region. Slight underestimations are observed in the humid regions while small overestimations are noticed around the central and southwestern parts of the region (not shown). On the other hand, values derived using the HG method overestimate PM_o over the study region (Figure 3.17), especially during January and February.

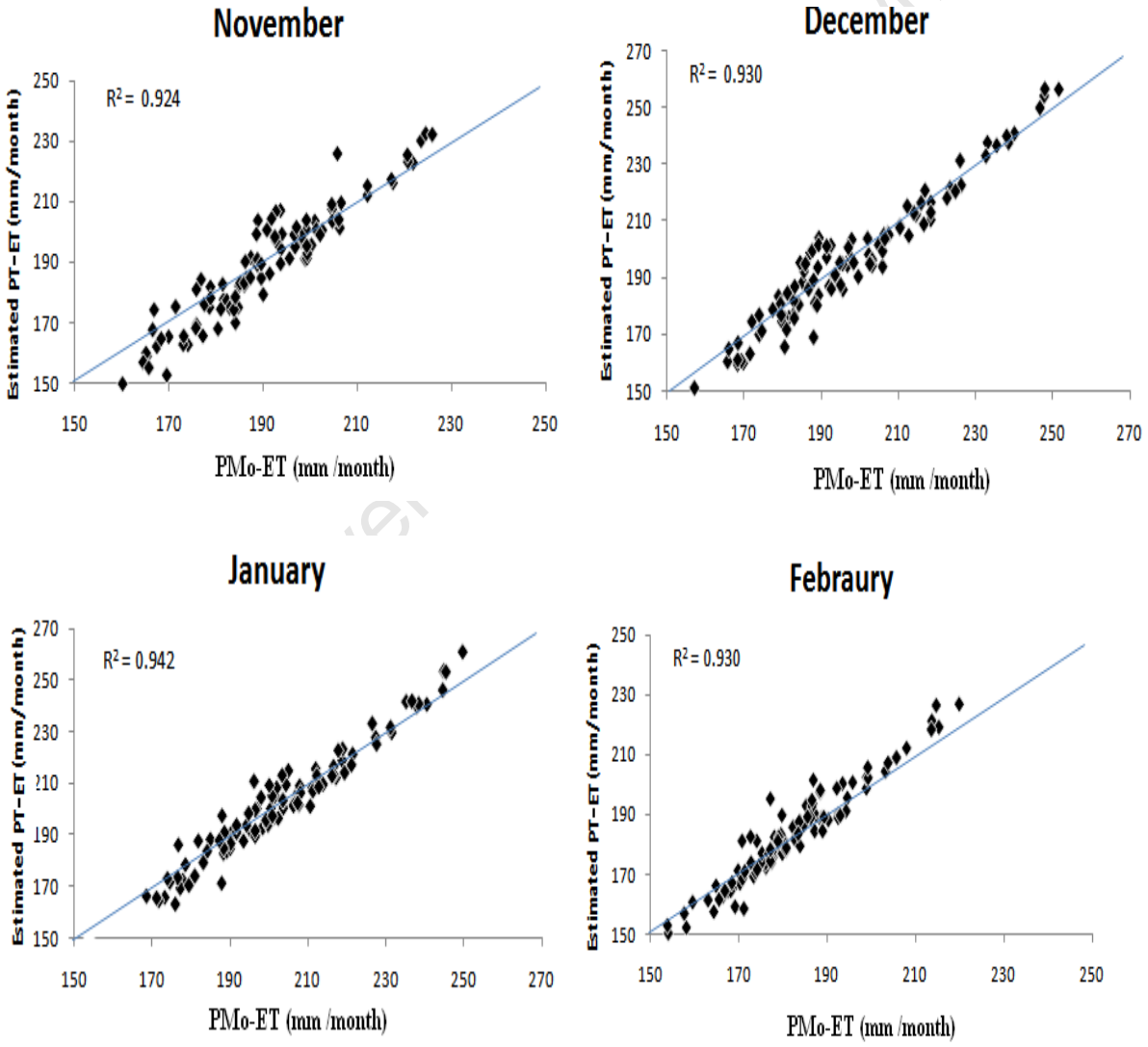

Figure 3.16: *Relation between PM_o and PT evapotranspiration (mm/month) at 176 station locations (Observed ET is the reference ET calculated using CRU data with the PM_o method)*

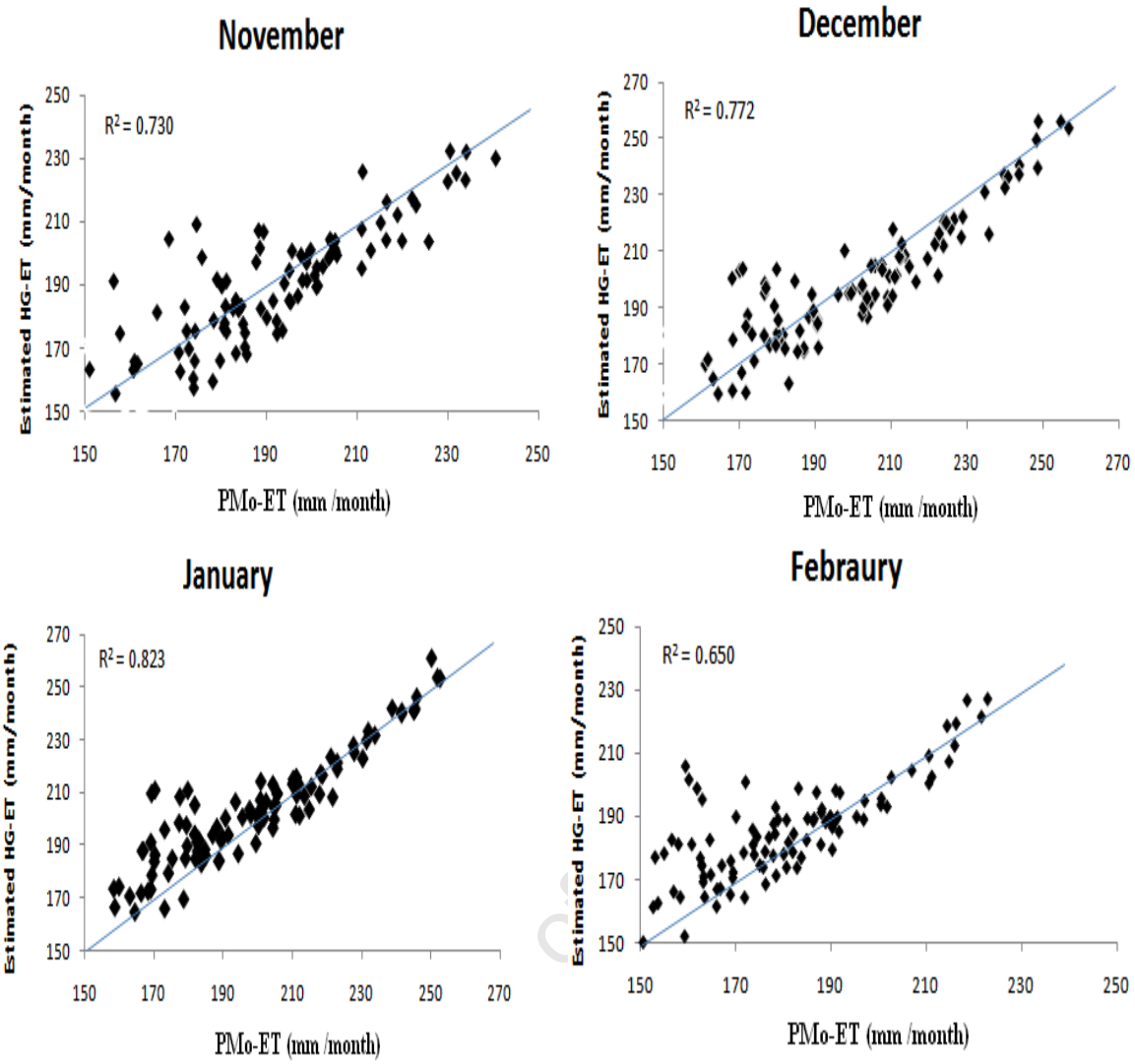

Figure 3.17: *Relation between PM_o and HG evapotranspiration (mm/month) at all sites (Observed ET is the reference ET calculated using CRU data with the PM method)*

Table 3.1 presents a summary of results for all the 170 stations, averaged over the region. All the R^2 monthly values between PT and PM_o methods from November to February are above 0.94. The PT method offers the best performance with R^2 values below 0.2 and an index of agreement (d) of above 0.95. On the other hand, the HG method performs poorly during the peak summer months as compared to the PT method. Low d values (below 0.95) combined with low R^2 values particularly in the early part of the peak summer season are observed.

Table 3.1: *Comparison of PM_o, PT and HG methods at 170 locations*

November	R^2	D	RMSE
PT	0.924	0.967	0.038
HG	0.730	0.918	0.069
December			
PT	0.930	0.979	0.032
HG	0.772	0.928	0.066
January			
PT	0.942	0.981	0.0280
HG	0.823	0.928	0.0643
February			
PT	0.930	0.972	0.028
HG	0.650	0.869	0.074

3.5.4 Summary on evapotranspiration method evaluation

Generally, recommended literature constant values involved in each empirical equation work relatively well for the study region, except that the recommended value of α= 1.26 in Priestley-Taylor was too high for the region. After adjustments, the best PT constant value for most regions was about 1.09 (i.e. relative to PM_o outputs). The Priestly-Taylor method compares more closely to the FAO-56 Penman–Monteith method than Hargreaves method. This suggests that it is practical to use the Priestly-Taylor method with the downscaled GCM data, since it requires fewer parameters (solar radiation, maximum, minimum and mean air temperatures) available in the GCM-DS. Some of the differences noted between the PM_o and two methods might be due to biases originating from the solar radiation estimates. Based on the above comparison, daily evapotranspiration values calculated using the PT method are used as input for the crop modeling discussed in the next section as well as to evaluate the future changes in projected crop yields over the region.

3.6 Crop model evaluation

Figure 3.18 illustrates the gridded WRSI obtained using daily observation data averaged for the period 1979 to 1999. According to the Food and Agriculture Organization WRSI classification, a WRSI of above 90 indicates good crop yield while WRSI of below 50 indicates crop failure (see Table 2.4 of chapter 2). As expected the WRSI trend is high over the northern parts of the study region and gradually decreases as one approaches the arid southwestern parts of the region in agreement with water availability (refer to Figure 3.1b).

The region can be split into approximately three sub-areas with regard to summer distribution of WRSI. The first region covers Zambia, Malawi, northern Zimbabwe and northern Mozambique and has a high mean WRSI (about 80%), which relates to average to above average yields (Table 2.4). The second region covers a wide strip from the northern Namibia to the north eastern parts of South Africa, through northern Botswana and parts of southern Zimbabwe, southern Mozambique, Swaziland and Lesotho; here the mean WRSI is between 50-60% suggesting poor yields. The third region is classified as having WRSI below 50, which indicates complete crop failure and unsuitability for growing maize. This region covers parts of southern Namibia, southwest Botswana and western South Africa.

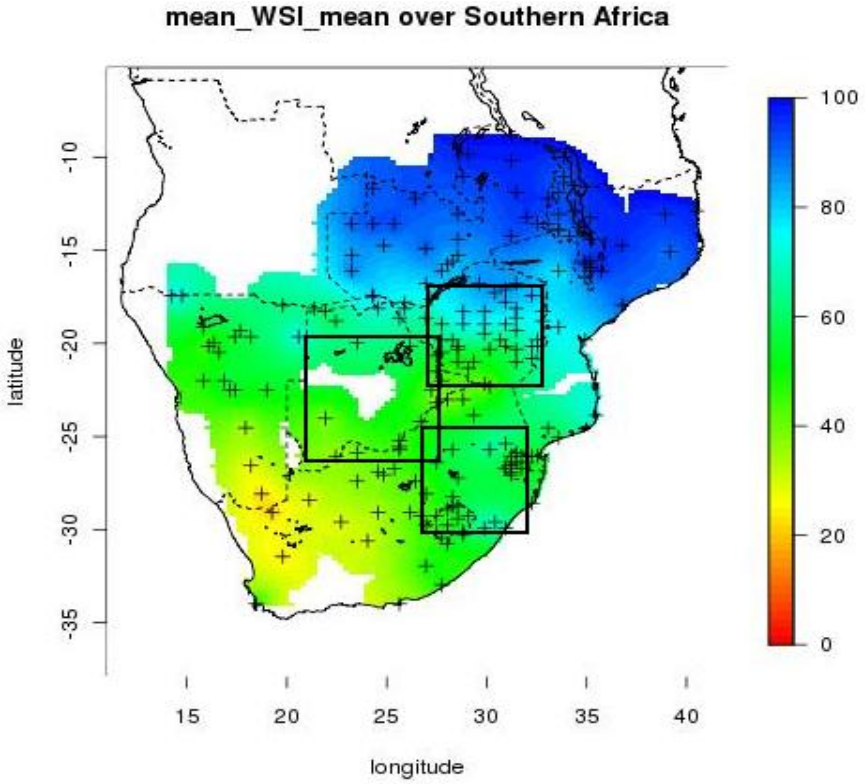

Figure 3.18: *Mean WRSI simulated from station observed climate between 1979 and 1999. Square boxes show the regions (area average) used for evaluating the crop model and they represent Zimbabwe, Botswana and central and eastern South Africa*

Figure 3.19 shows total cereal production (production in metric tonnes) over selected regions. The crop data (source: FAO database: http://faostat.fao.org/) were mapped in order to categorize the crop growing regions. This data is based on the period 1979 to1999 thus might not reflect the current or recent crop patterns in some regions. For instance, land reforms in Zimbabwe during the last 10 years have seen drastic reduction in crop production. Some

countries (Zambia and Mozambique) are not spatially mapped due to lack of data at the time of the study. Figure 3.19 indicates that the highest crop production areas for maize are located in the central province of South Africa followed by western Zimbabwe while the least maize growing region are located in Namibia and Botswana.

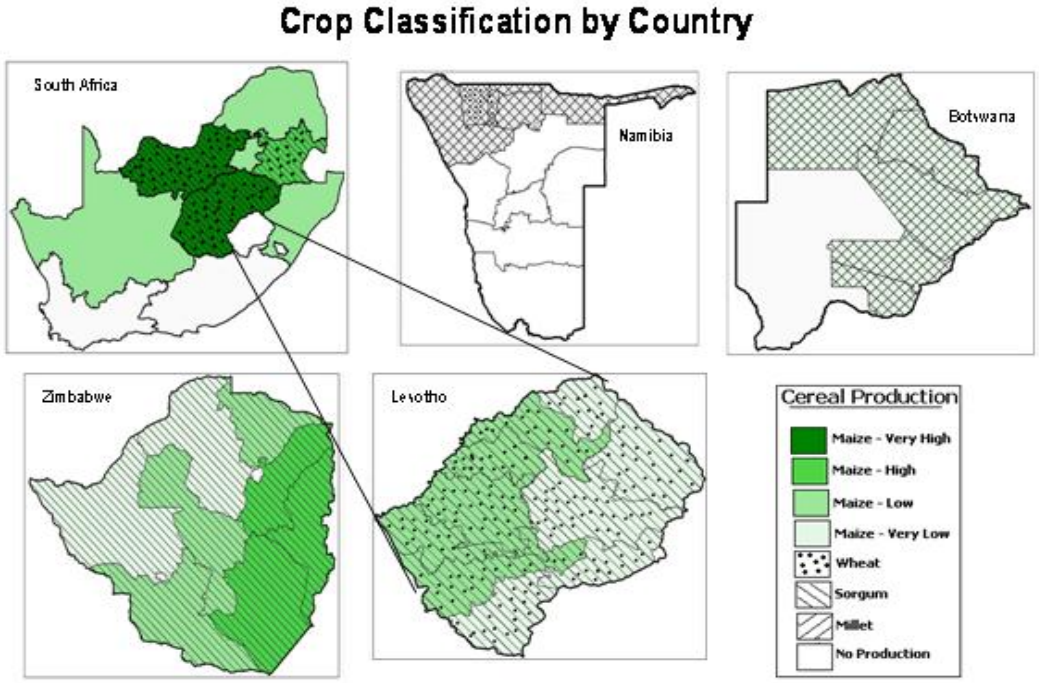

Figure 3.19: *Total cereal production (production in metric tonnes) over selected regions (Very High >1000000, High: 100000-500000, Low: 10000-50000, Very Low<10000).* Data *source: FAO database: http://faostat.fao.org/*

The evaluation of the Agrometshell crop model outputs involved the averaging of stations within Botswana (25°S-20°S, 20°E-27°E), Zimbabwe (22°S-17°S, 28°E-32°E) and central and eastern South Africa (30°S-25°S, 26°E-32°E). The standardized (anomaly from the mean of the time series divided by the standard deviation) WRSI values are then compared to standardized historically maize yields over the selected regions for the period 1979 to 1999. Worth noting is the fact that there has been no noticeable increased linear trend in maize production (pink line in Figure 3.20) over the selected regions during 1979 to 1999. Due to data limitations, crop model evaluation is performed on three selected regions (shown in Figure 3.18).

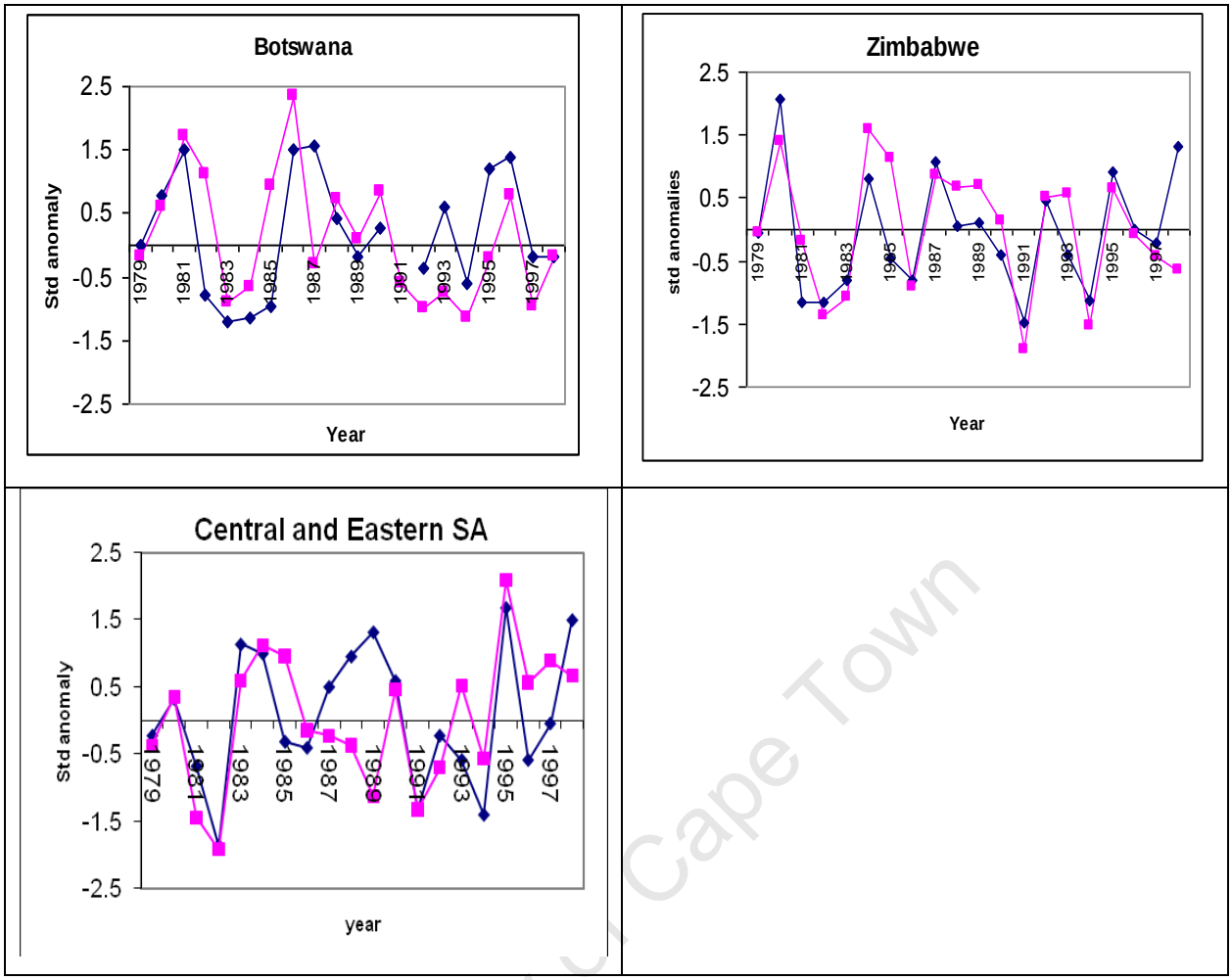

Figure 3.20: *Example of relationship between standardized agrometshell WRSI anomalies (blue) and observed maize (pink) yield anomalies (Botswana: correlation= 0.55, Zimbabwe: correlation =0.69, central and eastern South Africa: correlation =0.58)*

Agrometshell reasonably detects inter-annual variations in maize production considering that other factors that contribute to the variability in crop production are not taken into account (e.g. technological and socio-economic factors). During the period from 1979 to 1999, the correlation between standardized historical record and maize WRSI is 0.58 for the central and eastern South Africa, 0.55 for Botswana and 0.69 for Zimbabwe. Figure 3.21 shows spatial relationship between maize WRSI and historical maize yield for the 1994 season. Due to limitation on provincial data, only spatial map for Zimbabwe is shown as an example to demonstrate how Agrometshell can capture spatial patterns. The WRSI is able to capture most of the spatial variation across Zimbabwe (Figure 3.21).

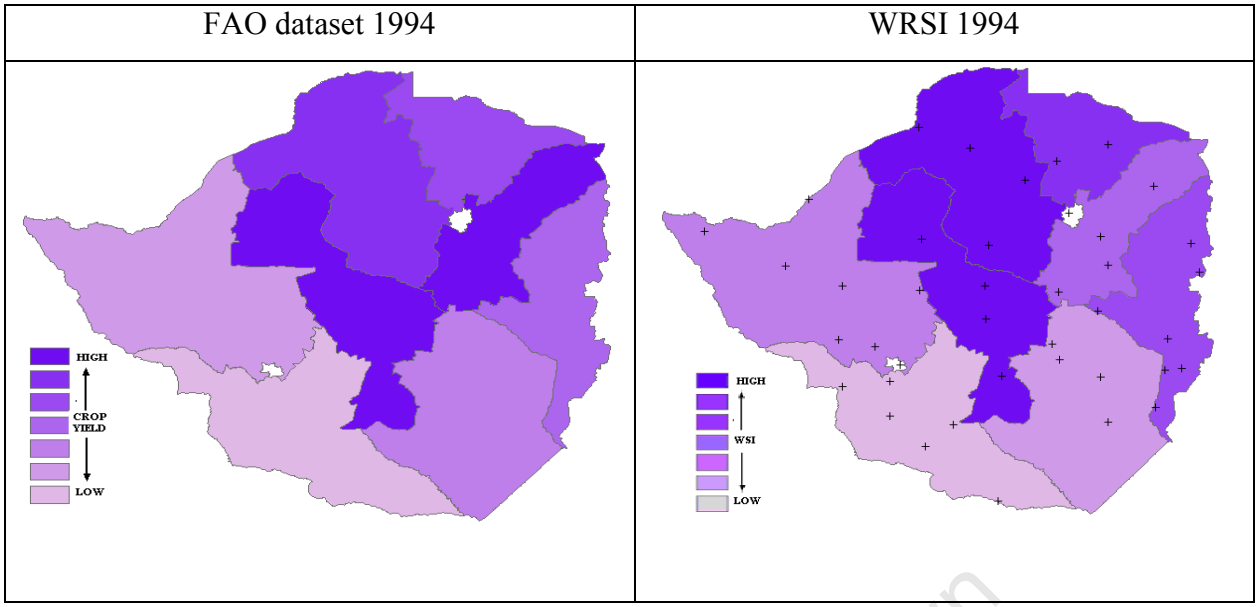

***Figure 3.21**: Example of WRSI distribution when compared to FAO data (http://faostat.fao.org) over Zimbabwe during the 1994 season. Each province is represented by the average of the stations (black points). Deep blue colours show regions with highest yield and WRSI during 1994*

3.7 Summary

This chapter evaluated downscaled climate variables as well as data derived from various empirical methods. The source of uncertainties associated with downscaled GCM outputs during the control period as well as tools used for crop modeling assessments is presented. The summary for the chapter can be outlined as below:

- The downscaled GCMs precipitation is able to reproduce downscaled NCEP reanalysis precipitation annual seasonal cycle. During the peak summer season, model ensemble shows underestimation of precipitation over parts of north eastern South Africa and a positive bias over parts of Zambia and Malawi;
- Some large biases in the downscaled GCM precipitation outputs (GFDL and GISS) could be attributed to missing GCM surface atmospheric fields used in the downscaling process;
- The Hargreaves and Samani solar radiation method is highly correlated to the CRU monthly radiation values thus can be used in all the radiation estimations using GCM data;
- The Priestly-Taylor method compares favorably to the FAO-56 Penman–Monteith method which suggests that it is practical to use this method for downscaled GCM data since it requires fewer parameters (radiation, maximum, minimum and mean air temperatures);

- The Agrometshell crop model simulates crop yield over selected regions reasonably well despite its fewer data requirements thus it is justifiable to use this model for future projections.

In the chapters that follow, methods recommended in this chapter are used to calculate evapotranspiration and downscaled climate change data is investigated.

Chapter 4

Projected changes in climate characteristics

4.1 Introduction

The previous two chapters presented the background on baseline climate during the recent past (1979 to 1999) as well as how downscaled GCM variables (GCM-DS) are able to represent downscaled NCEP reanalysis. This chapter addresses the second research question posed in chapter 1 (section 1.4), which is to investigate changes (between future [2046 to 2065] and recent past [1979 to 1999]) in climate characteristics using multiple downscaled climate datasets, to identify regions and periods where the GCM-DS show consistent changes and to investigate how changes in large-scale atmospheric circulations are related to changes in precipitation characteristics.

The downscaled GCM variables are at a daily time scale and it was thus possible to calculate climate characteristics that directly impact crop growth over the region. These climate characteristics are represented by crop sowing dates, number and duration of dry spells, total rainfall and evapotranspiration during the summer season. Daily evapotranspiration are derived from temperature and solar radiation, using the Priestley Taylor equation (see section 2.7) while the number of dry spells and crop sowing dates are calculated according to the formula presented in section 2.6.2 and 2.6.3 respectively.

A number of previous studies (*Tebaldi et al., 2006; Cooper et al., 2008; Shongwe et al., 2009)* have used GCM data to evaluate changes in future climate (2050's and 2100's) both regionally and globally. Unlike most studies, that utilized climate data directly obtained from GCMs, this study uses an ensemble of five state-of-the-art downscaled GCM projections to investigate changes in precipitation characteristics and evapotranspiration over southern Africa. The advantage of using downscaled GCM precipitation is that hot spots where GCMs agree on the change can be found for smaller, climatically homogeneous regions. Additionally, downscaling precipitation used in this study is able to more reasonably simulate regional rainfall as was revealed in chapter 2. Regional atmospheric systems are also investigated because GCMs are known to be more

robust in simulating these systems, which are characterised by prognostic variables, as compared to how well they produce localized variables (for instance precipitation), which are diagnostic variables.

4.2 Mean changes in summer season precipitation

Figure 4.1 shows spatial changes in precipitation for each of the five GCMs-DS during early (SON), peak (DJF) and late (MAM) summer seasons. One feature observed in Figure 4.1 is that changes in precipitation vary across the GCMs despite some convergence expected when using downscaled outputs. For instance, two of the five GCMs (CNRM and GISS) show a decrease over some parts of the sub continent particularly over central Zimbabwe and Zambia during SON while CCCM shows an increase over the same domain. Similar inconsistent patterns are noted during DJF and MAM. However, consistency among GCM-DS is evident over central and eastern South Africa where the five GCMS-DS project increased rainfall during early summer season. This implies that there is high confidence in projecting rainfall changes over this region which encompasses the "maize region" of South Africa, geographically delimited by the towns of Bloemfontein, Christiana, Zeerust, Warmbad, Machadadorp, Piet Retief and Ladysmith (*Johnston, 2008*). Model consistency and uncertainty is further investigated in section 4.2.1.

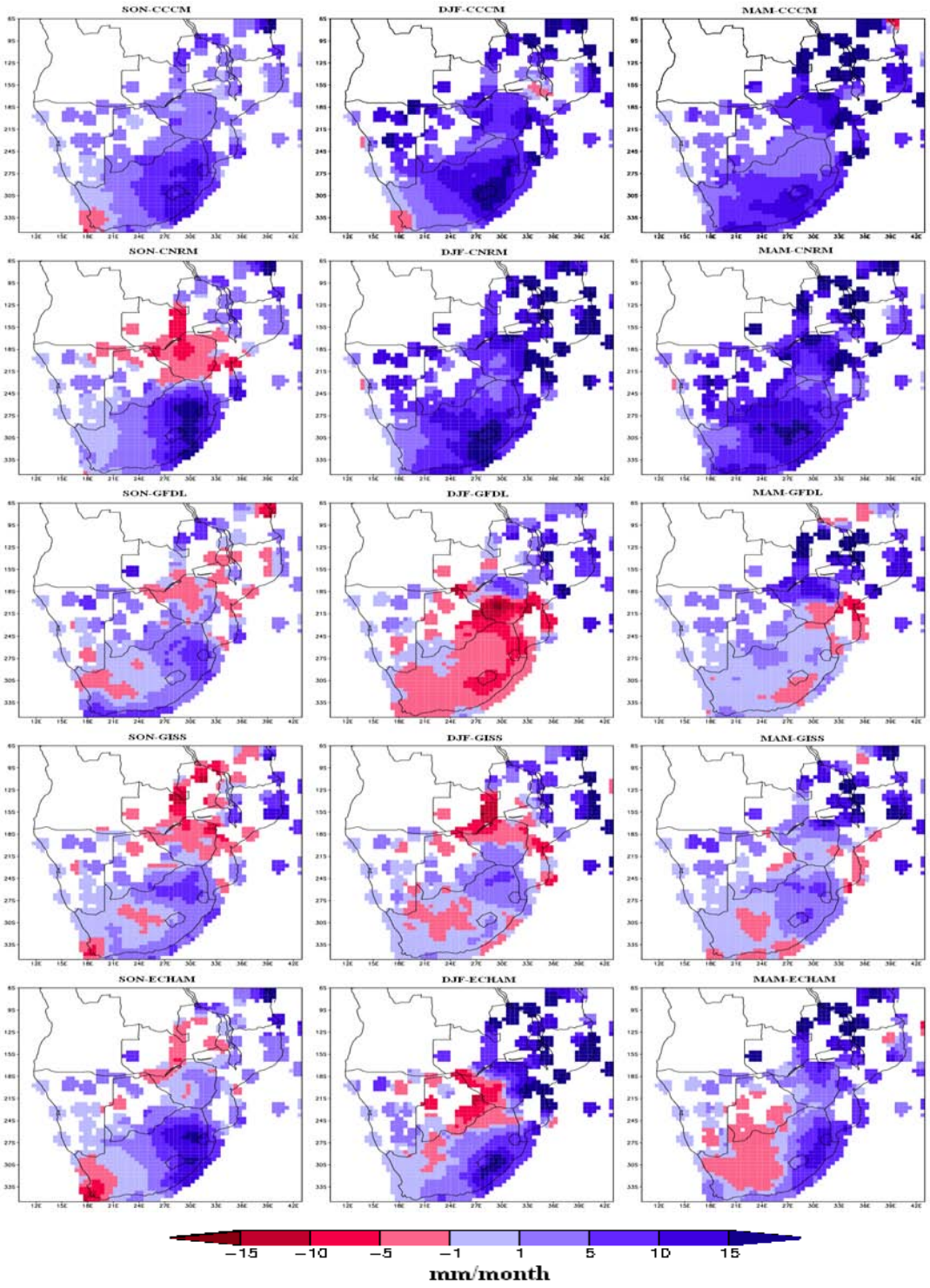

Figure 4.1: *Projected change (2050s-recent past) in precipitation (mm/month) for the individual downscaled GCMs. Order of GCM-DS from top to bottom is CCCM, CNRM, GFDL, GISS and ECHAM. The first column represents SON, second column is for DJF and third column is for MAM*

The latter part of the second research question is aimed at investigating the link between mean rainfall changes and regional atmospheric systems. The following section investigates whether the observed changes in mean rainfall by 2050 for each GCM-DS is associated with typical regional atmospheric circulation patterns. Due to data limitation at the time of the study, only moisture influx at 800 hPa (represented by wind vectors and specific humidity) and near surface geopotential height (Appendix B) are used to represent the behaviour of circulation patterns over sub continent. This is a reasonable representation as the convergence and divergence of moisture flux is physically linked to rainfall patterns. It is further assumed that shifts in atmospheric circulation patterns linked to increased (or reduced) precipitation in the future will resemble those responsible for present and past rainfall anomalies.

Mean seasonal changes for 800 hPa wind (a) and specific humidity (b) are shown in Figure 4.2. During SON, the central and eastern South Africa is characterised by increased specific humidity as well as anticyclonic wind anomalies centred along the border between South Africa and Mozambique. The increased moisture influx could be explained by an enhanced encroachment of the ridge from the Indian and Atlantic Ocean high pressure system onto the sub-continent in the future. These features have previously been associated with early start of the rainfall season over Zimbabwe and parts of South Africa (*Tadross et al., 2005; Reason et al., 2005*) and could possibly be linked with increased GCM rainfall in the future over central and eastern South Africa projected by 2050.

A reduction in specific humidity over the region bordering southern Angola and northern Namibia is observed in the models (CNRM, GFDL and GISS) showing reduced precipitation (Figure 4.2b). A poorly developed surface low over Angola (Figure 4.2) reduces mid-latitude westerly waves passing south of Africa, resulting in poor formation of extra-tropical cloud bands. This has previously been associated with reduced rainfall over Zambia and parts of South Africa. In a study over southern Africa, *Mulenga (1998)* observed that the position of the inland low pressure system plays a role in modulating convergence of moist air over the subcontinent.

The atmospheric circulation patterns observed in the GCM outputs are similar to those noted in previous studies using observation data (*Mulenga, 1998; Tadross et al., 2005; Reason et al., 2005*). The results described above suggest that, moisture influx within individual GCMs supports the changes in precipitation over the region. The models capture the regional moisture influx reasonably well when compared to present day atmospheric state. However, it should be noted here that, systems other than those noted in this study play a significant role in summer rainfall behavior over the region.

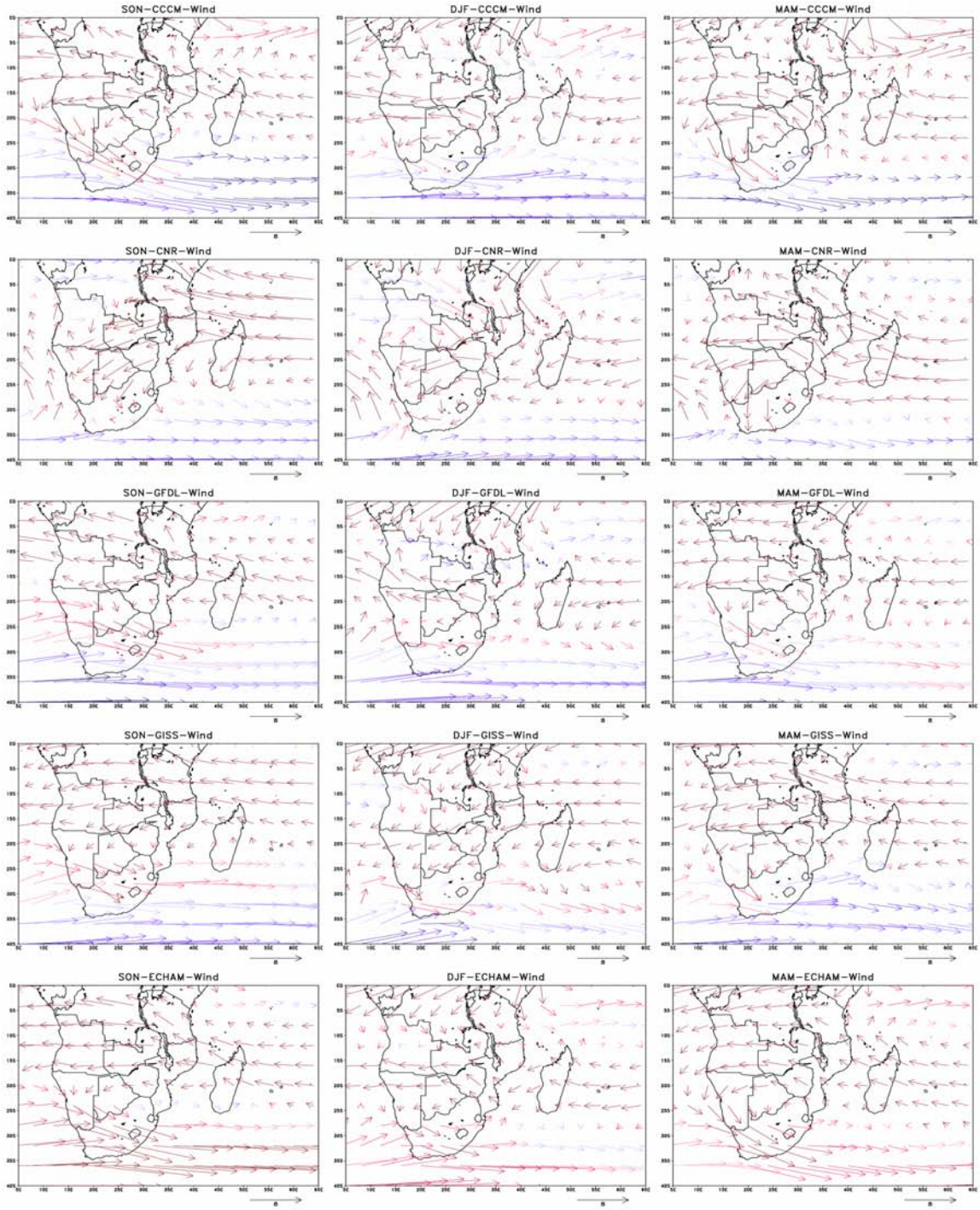

Figure 4.2a: *Changes (2046-2065 minus 1979-1999) in 800 hPa wind (vectors) magnitude scale showing red (high) and blue (low) strength. First column displays change in SON composites, Second column displays DJF composites and third column shows the MAM period*

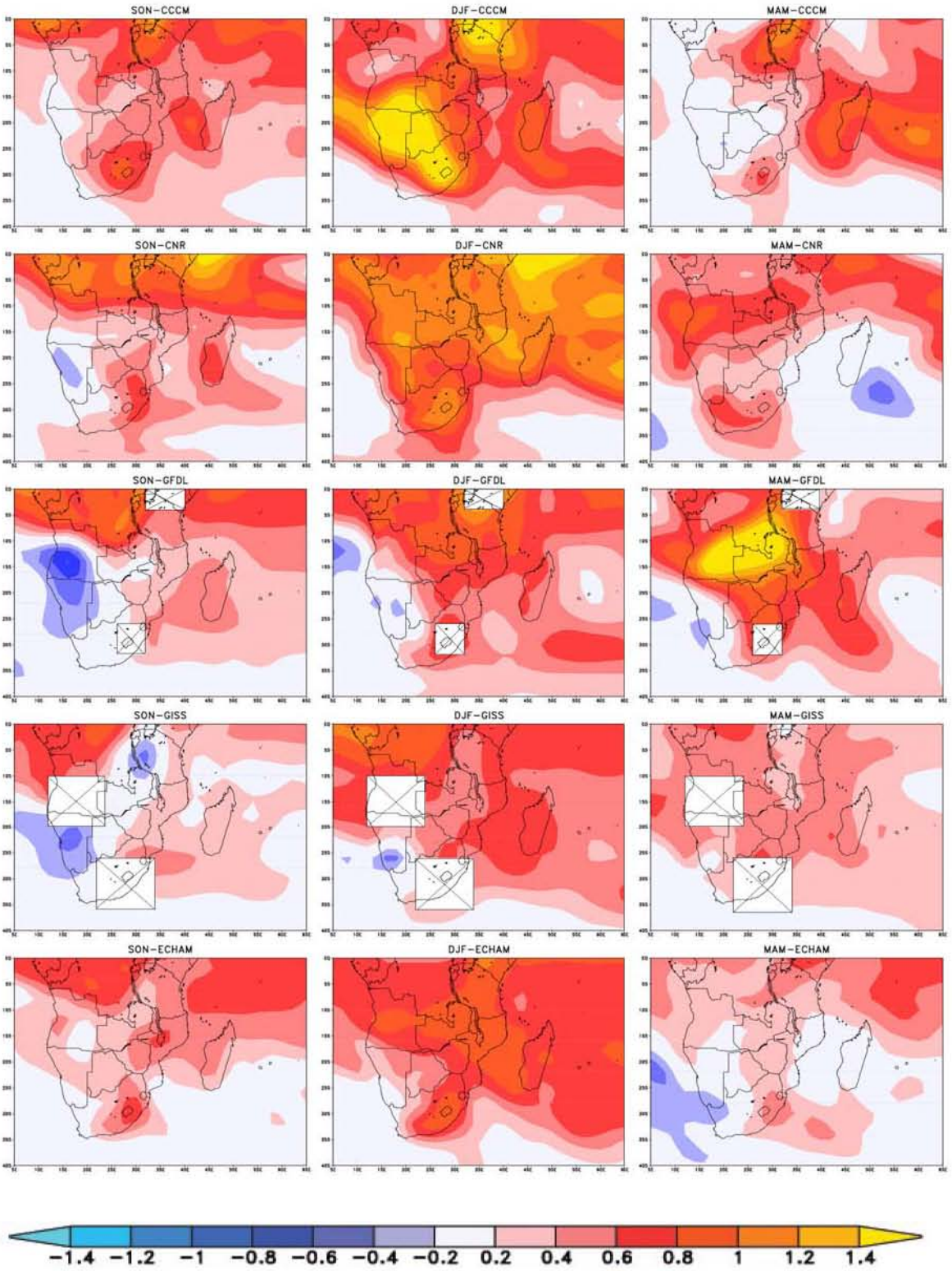

Figure 4.2b: *Changes in 800 hPa specific humidity anomaly fields. First column displays change (1979-1999 and 2046-2065) in SON composites, Second column displays DJF composites and third column shows the MAM period. Cross boxes show undefined specific humidity values*

4.2.1 Median, 20th and 80th percentile change

A clear picture emerging from this work is that, simulated precipitation values are not always consistent among GCMs-DS. This introduces uncertainty when interpreting the expected changes. In order to address uncertainties associated with using multi model ensembles, a number of studies have concluded that a multi-model ensemble mean should be used to obtain a reliable impression of change and the uncertainty surrounding these impacts (*Lambert and Boer, 2001; Murphy et al., 2004; Tebaldi and Knutti, 2007). Wiley and Palmer (2008)* showed that a suite of GCMs can be used to develop "uncertainty boundaries" that reflect the degree of agreement between the GCMs and thus provides a "most likely" scenario based on the consensus results of the GCMs.

In this study, the median, 80th and 20th percentile are used to represent the changes in seasonal precipitation. The 20th and 80th percentiles are total precipitation values simulated by 20% (i.e. at least one of the five GCMs-DS) and 80% (i.e. at least four of the five GCMs-DS) of the GCMs-DS respectively. *Tang et al. (2008)* noted that when the spread of predictions around the median is small, then the model convergence is good and we have confidence that the predictions are reasonably insensitive to the choice of model. However when the model convergence is poor, then the predictions that we get using a particular model could vary markedly from those of a second model (*Johnston and Sharma, 2009*).

The results presented in Figure 4.3 provide an insight on the expected changes in regional precipitation by 2050 using the GCM-DS ensemble median. The changes are positive over most of the region. The highest precipitation increase (~ +15 mm/month) is attained over central and eastern South Africa during early summer (SON). However, northern Zimbabwe, central and eastern Zambia as well as parts of central Mozambique project a reduction in SON rainfall (~ -10 mm/month). Insignificant (less than 1mm/month) changes in precipitation are noted during DJF over Zambia, central and northern Zimbabwe and most of Botswana while the rest of the region depicts increased precipitation. During late summer season (MAM), the entire region shows an increase in

summer precipitation, implying an extension of the summer rainfall season over most regions.

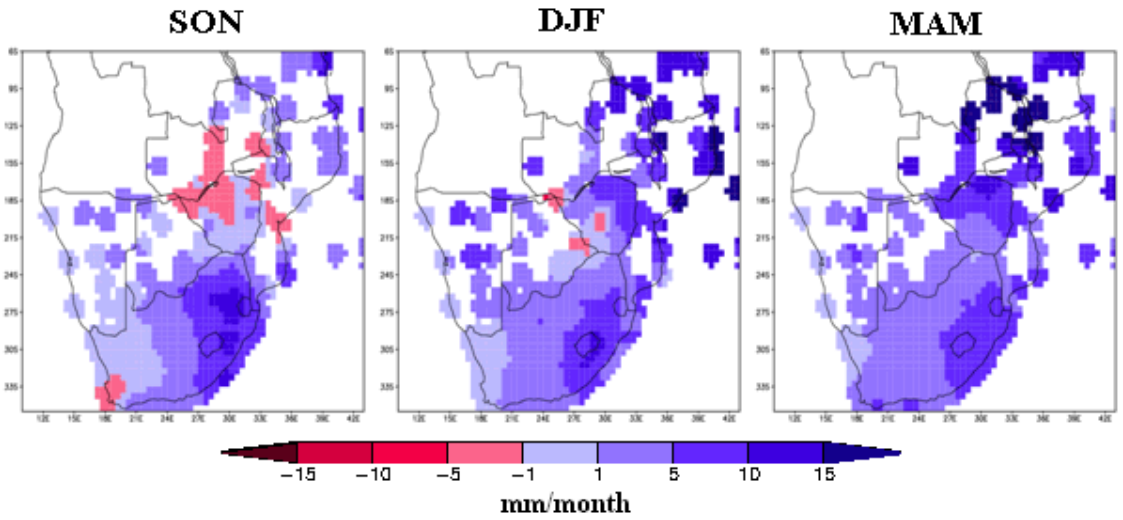

Figure 4.3: *Changes in precipitation during SON, DJF and MAM (GCM-DS ensemble median)*

In Figure 4.4, changes in spread (80th minus 20th percentile) between the GCMs-DS are investigated. Examining early season (SON) reveals that GCMs-DS rainfall spread over most of the region is less in the future when compared to the recent past. Lower spread implies that, there is higher consistency (lower uncertainty) in projecting reduced early summer precipitation over most parts of the region in the future. The DJF period depicts a slight increase in GCMs-DS rainfall spread over most of the region (with the exception of northern Zambia). The increase spread implies that GCMs-DS are more inconsistent in projecting future DJF precipitation changes over the region as compared to SON. A similar pattern applies for the late summer season over the region with the exception of south west Botswana, northern South Africa and Namibia (which indicates reduced spread in the future). These results indicate that GCM-DS ensemble is more uncertain in projecting regional precipitation during DJF and MAM as compared to SON, especially for the central-eastern regions.

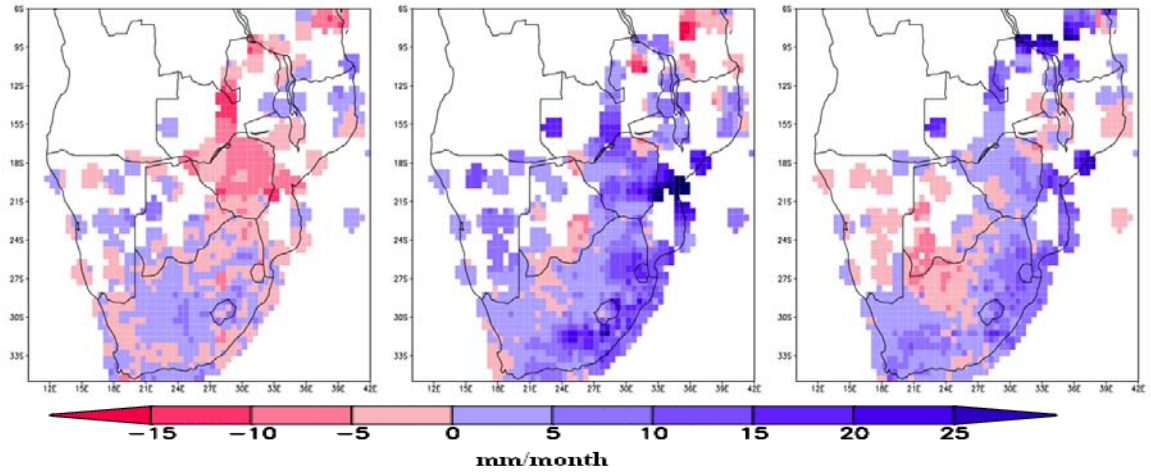

Figure 4.4: *Showing changes (future minus control) of GCM envelope (spread) during SON, DJF and MAM summer season*

4.2.2 Mean changes in seasonal rainfall variability

Besides long-term change discussed in the previous sections, year-to-year variability information is crucial to farm management decisions over southern Arica. Whilst a number of studies have been done on the regional inter-annual climate variability and on events such as the El-Niño Southern Oscillation (ENSO) and Antarctic Oscillation (AAO), (*e.g. Mason, 1995; Hulme et al., 2001; Reason & Rouault, 2006*), relatively fewer studies have investigated how inter-annual rainfall variability will unfold in the future. Although investigating inter-annual variability in the future is problematic in that it is difficult to associate individual years with extreme precipitation, knowledge on the frequency of these events in the future could possibly help explain regional climate change impacts.

To explore changes in inter-annual variability, the standard deviation (SD) (Equation 2.12) for each of the two time slots (2046-2065 and 1979-1999) is calculated. SD is a measure of variation from the mean. In this case, it serves as a proxy for inter-annual variability and therefore changes can be used to identify regions showing increase or decrease in inter-annual precipitation variability. The blue shading in Figure 4.5 corresponds to regions with reduced inter-annual variability and red are regions with increased inter-annual variability in total seasonal rainfall by 2050.

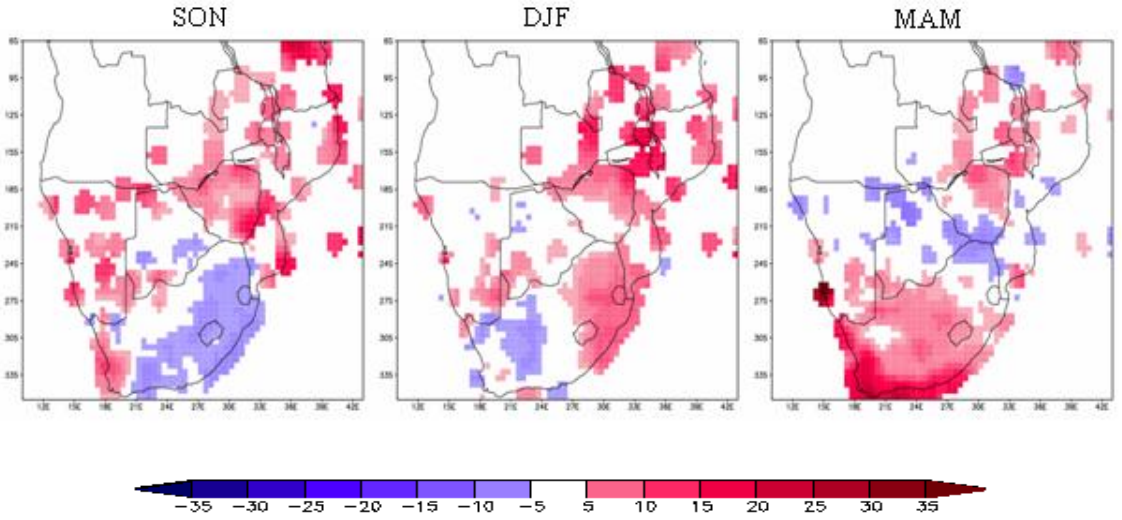

Figure 4.5: *Changes (future-control) in inter-annual rainfall variability during SON, DJF and MAM (GCM-DS ensemble median)*

With the exception of central and eastern South Africa, most of the study domain could have increased inter-annual rainfall variability during SON by 2050. Regions showing reduced interannual rainfall variability during early summer roughly coincide with those indicating increased SON precipitation. This further highlights the view that central and eastern South Africa could have favorable rainfall condition in the future during SON. The early and peak summer seasons are marked by increased rainfall variability across Namibia, Zimbabwe with a northward extension into Zambia and Malawi suggesting that these regions could experience reduced rainfall conditions relative to the present.

4.3 Crop sowing dates

Considering the importance of early rains for small scale agriculture and given the changes noted in SON precipitation over central Zambia and northern Zimbabwe, we further investigate the behavior of crop sowing dates (i.e. assumed here to be the dekad (10 day period) suitable for planting maize) over the region. As noted earlier, reduced SON precipitation has implications for seasonal crop sowing dates in southern Africa. The sowing dates are calculated according to the definition given in section 2.6.3. The

threshold rainfall amount after 1st of August was set to: 25mm in the first dekad concurrently followed by at least 20 mm in the next two dekads.

4.3.1 Mean changes in sowing dates

Figure 4.6 displays projected mean changes in sowing dates over the region from five GCMs-DS and the ensemble mean (bottom right). A later sowing date is consistently simulated across GCMs-DS over southern Zambia and northern Zimbabwe. Two GCMs-DS (GFDL and GISS) indicate an extension of late sowing dates towards Botswana and the Limpopo region of South Africa. Meanwhile three GCMs-DS (CCCM, CNRM and ECHAM) project an earlier start to future sowing dates (~ 10 days relative to the control) over parts of central and eastern South Africa. Changes in sowing date variability (see appendix) suggests that models showing an earlier start of sowing dates do not demonstrate increased variability in the future. On the other hand, GCMs-DS showing a later start in sowing dates over parts of the region (southern Zambia and northern Zimbabwe) also show increased variability. This implies that events, such as ENSO, known to influence the inter annual variability in rainfall season onset over the region (*Usman & Reason, 2004; Reason et al., 2005; Hachigonta et al., 2007*) could be enhanced in the future. It also suggests that increased total seasonal rainfall does not necessarily mean earlier sowing dates (see Figure 4.3). This thesis provides no solid evidence to support the statement that ENSO influence will likely be enhanced in the future. However, this is the avenue for future research.

It is was also found that GCMs-DS projecting anomalously late sowing dates (GISS and GFDL) over southern Zambia and parts of central Zimbabwe are characterised by reduced (SON and DJF) specific humidity (Figure 4.2b) over the south western parts of the study region. These models show a weaker Angola low during SON (Figure 4.2a), which typically starts to develop over this part of southern Africa in the austral spring. A weakening of trade winds is also evident in GISS and GFDL over the southwest Indian Ocean together with some ridging south of South Africa. These features could be linked to the later sowing dates being projected in these two GCMs-DS by 2050 over central Zambia and northern Zimbabwe. On the other hand, the central and eastern South Africa,

projecting a shift towards early sowing dates in the future, shows increased specific humidity (Figure 4.2b). In addition regions indicating early sowing dates are associated with an anticyclonic anomaly pattern to the southeast of South Africa during SON. Increase in moisture flux anomalies at 800 hPa, together with the anticyclonic anomaly around east of South Africa implies relative moisture convergence over eastern South Africa during the start of the season, favourable for early sowing dates. *Reason et al. (2005)* found a similar pattern to be associated with early rainfall north of South Africa. They linked the development of a low pressure over this region to a Rossby wave train (see *Randel, 1988*) that extends from the tropical central Pacific across the South East Pacific and mid-latitude South Atlantic Oceans and into the South West Indian Ocean, and are reminiscent of the Pacific South America (PSA) pattern associated with ENSO.

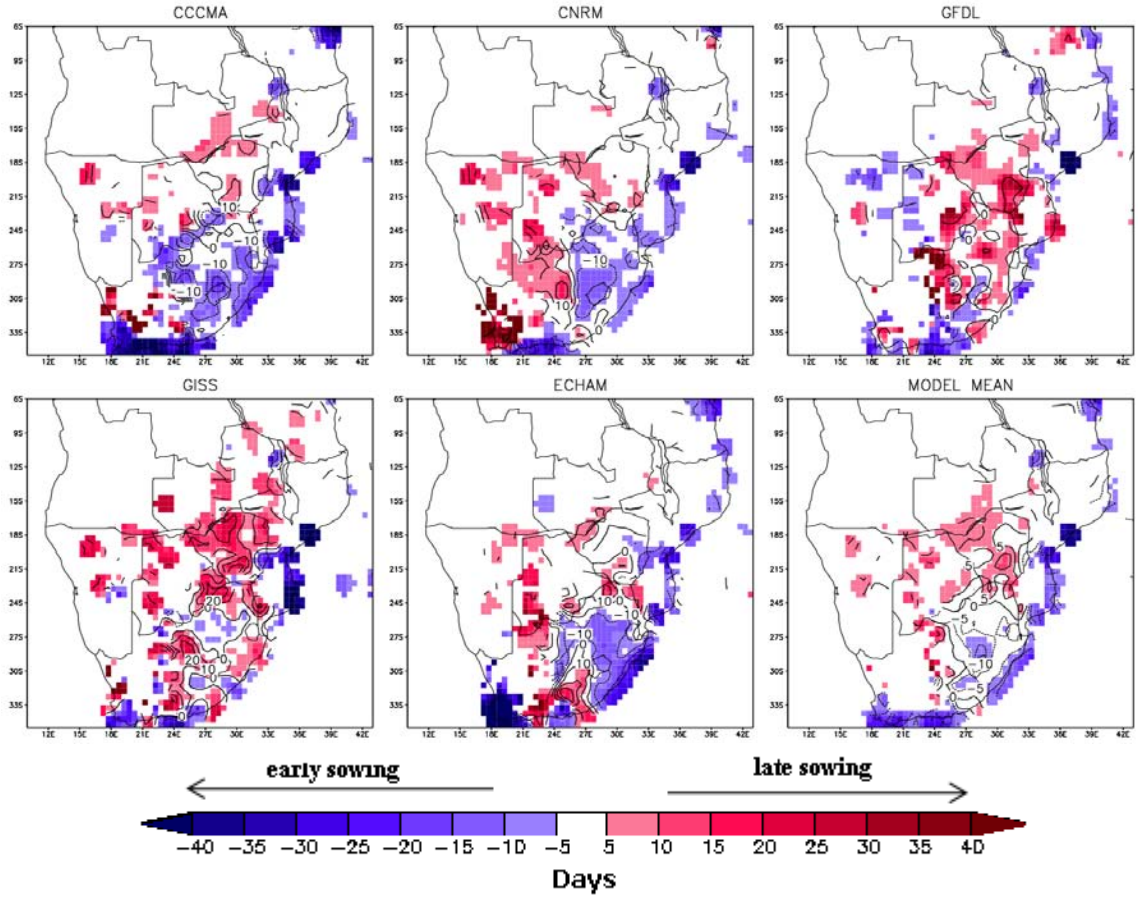

Figure 4.6: *Projected change in sowing dates. Sowing date defined as at least 25 mm rainfall falls in the first 10 days and at least 20 mm falls in the following 20 days after 1st of august (Red (Blue) colour shows regions with later (early) sowing dates in future*

The GCM-DS ensemble mean indicates a late sowing date (~ -10days) over Botswana, Zimbabwe, central parts of Zambia, the Limpopo region of South Africa and the region bordering Mozambique and South Africa. On the other hand, patches of central and eastern parts of South Africa project early sowing dates (~ +10days) by 2050. Further comparison of sowing dates (i.e. GCM-DS mean) with seasonal SON precipitation (section 4.2), reveals that that regions with increased (reduced) rainfall totals during the early part of the season are associated with earlier (later) sowing dates. This is expected given the mean seasonal increase in precipitation over this region, as noted in section 4.2. However, this is not always the case for individual GCMs-DS. For instance, while the CCCM model projects increased precipitation over central Zambia during SON, sowing dates are projected to shift later by about 10 days in the future. This shows that cumulative rainfall does not fully explain impacts on agriculture and increased rainfall may lead to a false impression that a growing season is good. This suggests that it is preferable to consider other measures such as calculating sowing date on a daily time scale other than using seasonal rainfall totals to explain the impacts on agriculture.

4.4 Dry spells during peak summer season

The overall message from the previous sections suggests reduction in SON rainfall over central Zimbabwe and parts of Zambia while increase in precipitation is projected during DJF and MAM over most of the region (with exception of the region bordering Zimbabwe, Botswana and South Africa). This section, investigates changes in number of dry spells and mean dry spell duration during DJF over the region. A dry spell is defined as a pentad (5 day period) with less than 5 mm of rainfall (see chapter 2). Dry spell duration is calculated as the average length of a dry spell during DJF. The DJF season is investigated in this study because of its relevance as the peak of the growing season within the major cropping areas and because this is typically when ENSO impacts over southern Africa reaches their maximum strength (*Nicholson and Selato, 2000*).

4.4.1 Mean changes in number and duration of dry spells

Figure 4.7a displays changes in number of dry spells during DJF as represented by the five GCMs-DS. The bottom right map in Figure 4.8a displays the GCM-DS ensemble mean change. All the GCMs-DS show a decrease (~ 2) in dry spells over the central and eastern parts of South Africa. This further serves to highlight that consistent responses may be better detected in sub-seasonal rainfall characteristics, as opposed to changes in the seasonal or monthly means. Contrary to the number of dry spells a general increase in mean dry spell duration is projected over most of region (Figure 4.7b). This may be as a result of increased interannual rainfall variability projected by 2050 over most of the study domain, which could lead to longer dry or wet periods. A second possibility is that, the winter dry season is longer and extends later in the future and therefore contributes to an increase in the mean dry spell duration.

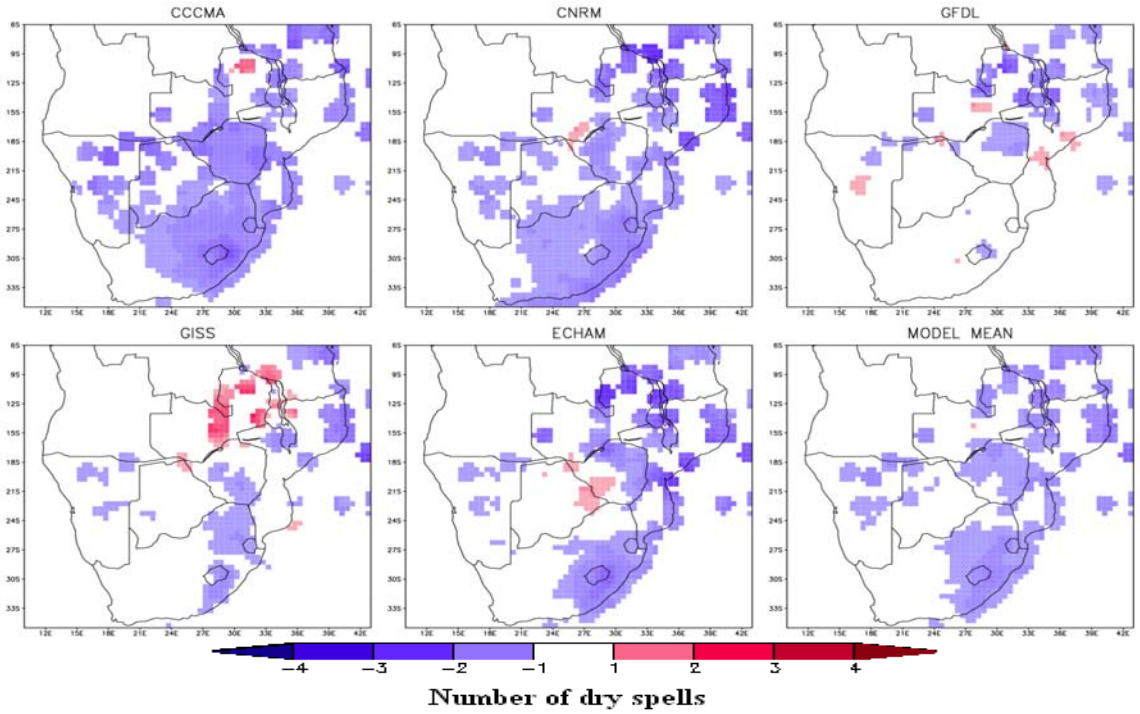

Figure 4.7a: *Projected changes in number of dry spells during the peak DJF summer season. White space represents zero change in dry spells by 2050*

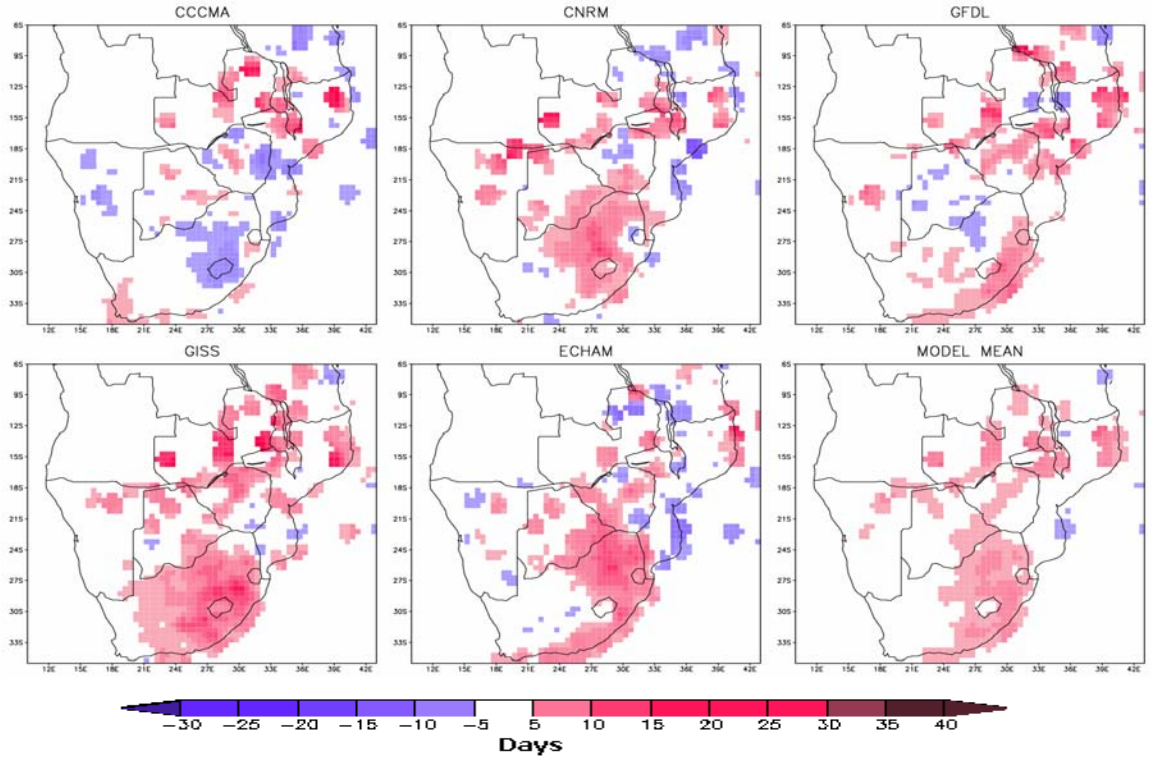

Figure 4.7b: *Projected changes in mean dry spell duration during the peak DJF summer season. Contours depict the actual change in days*

It was observed that during DJF, an anticyclonic anomaly pattern is present over South Africa (Figure 4.2a) suggesting a weaker low level monsoonal westerlies by 2050. As a result, less moisture from the northeast monsoon is advected away from East Africa by these westerlies implying more low level moisture present over tropical southern Africa and thus a reduction in number of dry spells. The GISS model reveals an increase in north easterly low level moisture influx implying reduced moisture penetration over Zambia from the Angola low and less moisture convergence. These features are in line with observation by *Hachigonta and Reason (2006)* and could thus explain increased length dry spells being projected over central Zambia by 2050.

The relationship between change in number of dry spells and the change in dry spell variability during DJF is not linear (not shown). The GCM-DS ensemble mean depicts an increase in dry spell variability over the eastern parts of South Africa bordering Mozambique, parts of central Botswana, central and eastern Zambia extending towards

Malawi. The western parts of the region (with the exception of Western Cape) project a decrease in dry spell variability while no significant changes are projected over the central parts of Zimbabwe. An increase in dry spell variability could have either a positive or a negative effect on crop development depending on changes in mean seasonal rainfall totals. For instance, crops in regions showing an increase in extreme wet episodes (central South Africa) could benefit from an increase but evenly distributed dry spells variability that are not too long to reduce soil moisture content during crop development. However, crops in regions consistently projecting increase in DJF dry spell variability and later sowing dates (e.g. southern Zimbabwe and the Limpopo province of South Africa) could have a negative impact as the length of the growing season could be reduced.

4.5 Mean changes in evapotranspiration

Evapotranspiration is closely linked to soil moisture content and the behavior of crops during the growing season. In this study, only the mean values (Figure 4.8) are shown due to the high model consistency between the GCMs-DS (not shown). An increase in evapotranspiration is projected over the entire region during the summer season. This could largely be attributed to increased temperatures and solar radiation projected over the region as they are used as input for the evapotranspiration method. Highest increases (~9 mm/month) in evapotranspiration are projected in the northern parts of the region (Zambia) during SON. However, this region shows little (less than 2 mm/month) change during the late (MAM) summer season over central Zambia. The lower increase in late summer season (MAM) evapotranspiration could due to the increased precipitation noted during this time of the season that might be having a cooling effect over much of the region. This shows that rainfall characteristics, soil moisture content and evapotranspiration are closely linked over the region.

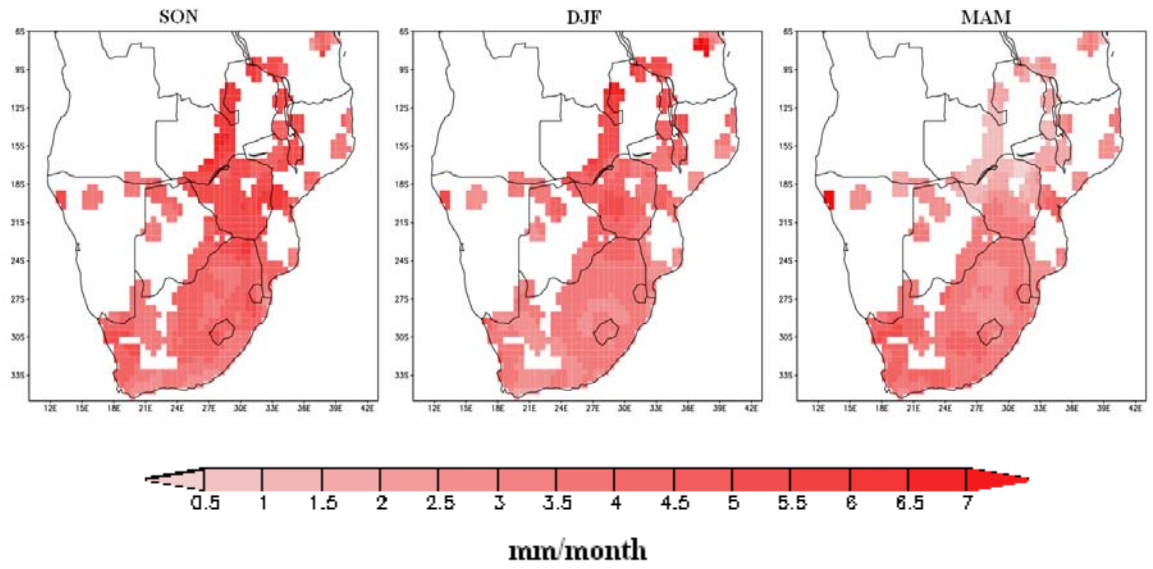

Figure 4.8 *Model ensemble mean showing projected changes in evapotranspiration during SON, DJF and MAM*

4.7 Summary

This chapter investigated changes (2046-2065 and 1979-1999) in climate characteristics over southern Africa using five downscaled GCMs-DS. The goals of this chapter were to: 1) Understand mean changes in climate characteristics, 2) Identify regions where GCMs-DS are consistent with the sign of change and 3) identify if changes in precipitation could be supported by large scale atmospheric systems.

A common signal was extracted from the GCMs-DS by looking at the ensemble median as well as the change in GCMs-DS spread. It was found that GCMs-DS are more consistent in simulating increased rainfall, an early start of the season and reduced rainfall variability over the central and eastern parts of South Africa in the future. This implies more favourable future conditions for crop production over these regions. The increase in precipitation over central and eastern parts of South Africa is in agreement with *Hewitson and Crane (2006)*. A consistent pattern was also prominent from across the GCMs-DS in projecting late sowing dates (~10 days relative to the control) over Botswana, Zimbabwe, central parts of Zambia, the Limpopo region of South Africa and the region bordering Mozambique and South Africa. Despite the reduction in the number

of dry spells during DJF, increased mean dry spell duration is apparent over most of the region during DJF. The increased dry spell duration may be linked to increased interannual rainfall variability, which could lead to longer dry or wet periods over the region.

In view of the second objective, it was shown that changes in number of dry spells and shifts in sowing dates, which often are of greater relevance to agriculture than changes in the mean, are more consistent in the future than mean seasonal changes. Regions showing reduced precipitation in the future are associated with low specific humidity over the region bordering southern Angola and northern Namibia. The increase in precipitation observed over central and eastern South Africa may be linked with increased specific humidity over this region as well as anticyclonic wind anomalies centred along the border between South Africa and Mozambique. GCMs-DS projecting late sowing dates in the future over southern Zambia and parts of central Zimbabwe are characterised by reduced specific humidity over the region bordering Namibia and Angola. Early sowing dates over central and eastern parts of South Africa are associated with increased specific humidity over this region and an anticyclonic anomaly pattern to the southeast of South Africa during SON. The main findings of the chapter can be summarised as below:

- GCMs-DS are more consistent when simulating dry spells and sowing dates than rainfall totals. This suggests that consistent responses may be better detected in sub-seasonal rainfall characteristics, as opposed to changes in the seasonal or monthly means.
- Despite the reduction in the number of dry spells, the mean dry spell duration is projected to increase over most of the region. This might be linked to increased interannual rainfall variability, which could lead to longer dry or wet periods over the region.
- Increase in precipitation over central and eastern South Africa are associated with increased specific humidity over this region as well as anticyclonic wind anomalies south east of the study region.

- Later sowing dates (~10 days relative to the control) are projected over Botswana, Zimbabwe, central parts of Zambia, the Limpopo region of South Africa and the region bordering Mozambique and South Africa while early sowing over the central and eastern parts of South Africa (~10 days) in the future.
- Late sowing dates in the future over southern Zambia and parts of central Zimbabwe are characterised by reduced specific humidity over the region bordering Namibia and Angola.

In the next chapter, downscaled GCM outputs discussed here are used to drive a crop model in order to investigate which of these climate characteristics may have more influence on crop development in rain fed agriculture systems and how farming basic decisions may be adapted to respond to such changes.

Chapter 5

Projected changes in maize water requirements

5.1 Introduction

This chapter investigates the response of maize water requirement satisfaction index to changes in rainfall and evapotranspiration over southern Africa by the mid 21st century. This is achieved by forcing a crop model with downscaled data from an ensemble of five GCMs. As outlined in section 1.5, the objectives of this chapter are to (i) asses the response maize water requirement to changes in downscaled GCM variables; (ii) resolve how changes in the sowing date decision rule (changes in maize planting dates) could be used to mitigate negative climate change impacts.

The results presented below are based on the average of 1000 Agrometshell simulations (using different sowing date combinations) for each year of the control (20 years) and future (20 years) climates of each of the five downscaled GCMs and for each of the 170 stations available across southern Africa (see Figure 2.1 in chapter 2). Daily evapotranspiration values used to drive the crop model are derived using the Priestley-Taylor method (refer to section 2.7.2 of chapter 2). Throughout this chapter, maize WRSI is referred to as WRSI. A table on how to interpret the WRSI in relation to crop yield is given in chapter 2 (Table 2.4)

5.2 Distribution of WRSI based on GCM control data

Figure 5.1 shows spatial WRSI ensemble mean forced by data from the five GCMs-DS during the control period. The WRSI calculated using GCM-DS climates for the control period produce good estimates when compared to simulations from observed WRSI values (1979 to 1999) over the region. Higher values are observed over the northern parts of the study region (~ 90), suggesting above average soil moisture and crop yield (refer to Table 2.4). Average to poor conditions prevail over most parts of Botswana, Lesotho, Namibia and South Africa.

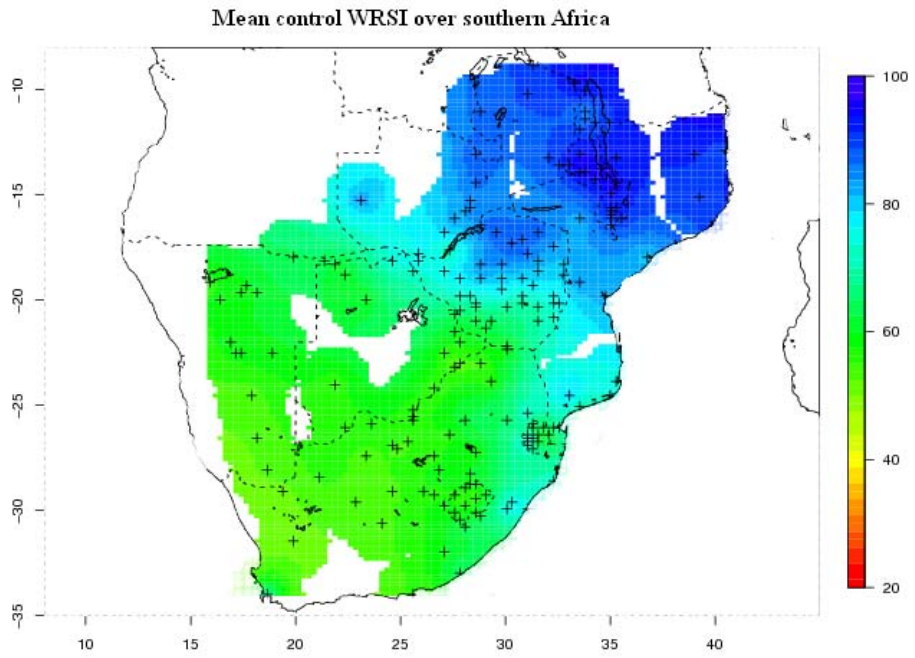

Figure 5.1: *Mean WRSI of five GCMs averaged for the period 1979 to 1999*

Agrometshell returns a missing value of WRSI if the defined sowing dekad is not met within a specified set time window. For instance, the time window for sowing dekad calculation was set to be from 1st August to end of March in the following year. Not surprisingly, the dry arid regions to the southwest most often simulate high crop simulation failures. Figure 5.2 shows that of the 1000 simulations over the southwest parts of the study domain, there are above 700 crop simulation failures. The large number of crop failures over this region suggests that crop model simulations in this region could not be achieved. This is because of the unfulfilled sowing date decision rule or due to simulated WRSI being lower than 50 (refer to Table 2.4 in chapter 2). Whilst maize is not cropped over the arid parts of southern Namibia and western South Africa at present, this is not to say that these regions may be more viable in a future climate. Thus, simulating regions or conditions that do not currently grow maize is necessary to deal with potentially new climatic conditions in the future.

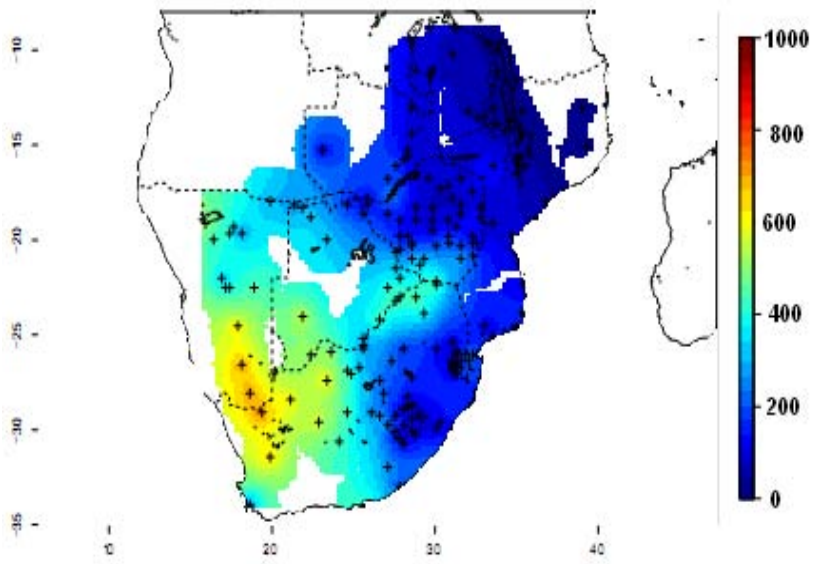

Figure 5.2: *Mean crop failures (as defined WRSI simulation below 50) from the 1000 simulations. White patch show interpolated regions that are outside the radius of influence*

5.3 Change in simulated maize WRSI based on downscaled GCM data

This section investigates mean regional changes in WRSI between the future (2046 to 2065) and control (1979 to1999) climate scenarios. The area averaged (mean for 170 stations) change in WRSI which gives a general overview of regional changes in WRSI is shown in Figure 5.3. The CCCM and CNRM simulation shows an increase in future WRSI while two models (GISS and ECHAM) show a reduction of about 4% relative to the control. Slight changes are observed in the GFDL WRSI despite GFDL showing significant reduction in precipitation values during peak summer as was observed in Chapter 4. However, a generalization overview over a wide landmass as southern Africa has some caveats. For example, spatial variations in WRSI from station to station could well average out at the regional level thus could conceal important details for policy purposes.

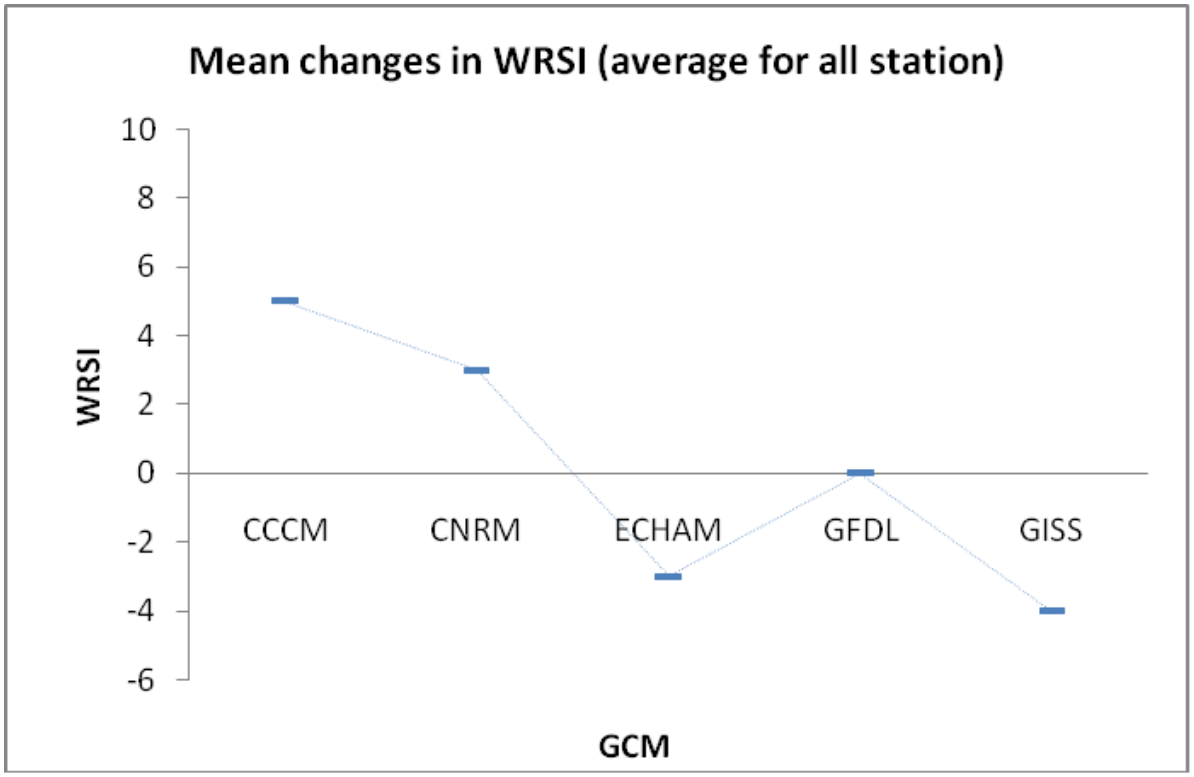

***Figure 5.3**: Mean change (between future and control) in WSRI (average for 170 stations) over the region. Refer to Table 2.4 on how to interpret WRSI*

To have an insight of the spatial changes in WRSI at a local scale, maize simulation driven by the five GCMs-DS are analysed individually as depicted in Figure 5.4. Blue colours in the figures indicate reduction in WRSI while yellow to red indicate an increase. All the GCMs-DS exhibit an increase in WRSI over the central and eastern parts of South Africa. Four GCMs-DS (with the exception of CNRM) show a reduction in WRSI over the central and northern part of Zimbabwe. The decrease (about 4%) is more pronounced in the GFDL and GISS GCMs-DS. However, the GISS model does not show any significant future decrease in precipitation meaning that factors other than precipitation totals influence the reduction in WRSI. One parameter likely to be contributing to the reduction in GISS WRSI is the sowing date which is projected to start later in the future over this region. Later sowing date and increase in evapotranspiration could translate into reduced WRSI because of the crop having to grow through less suitable temperatures. For instance, higher temperatures during the first days of sowing results in more evapotranspiration which could further affects the soil moisture leading to crops failure.

The WRSI ensemble mean broadly indicates an increase in WRSI over most of the study region (bottom right in Figure 5.4). The highest WRSI increase by 2050 is observed over the eastern South Africa, northern Namibia and northern Zambia. These regions project an increase in WRSI of approximately 8%. Over northern Zambia, WRSI in the current climate is already high thus the future changes would improve the already existing good conditions. The eastern parts of South Africa, has much lower WRSI values in the current climate implying that an increase in WRSI could be beneficial. On the other hand, the central and southern parts of Zimbabwe are projected to have a reduction in WRSI, which is potentially problematic as these regions which are clearly on the threshold of crop failure (see Figure 5.1). In this regard, while policy markers should be looking at ways of achieving high productivity by investments in modern farming technologies, the developed and implemented of simple adaptation strategies based on climate indices as discussed in the section below has the potential of improving crop yield.

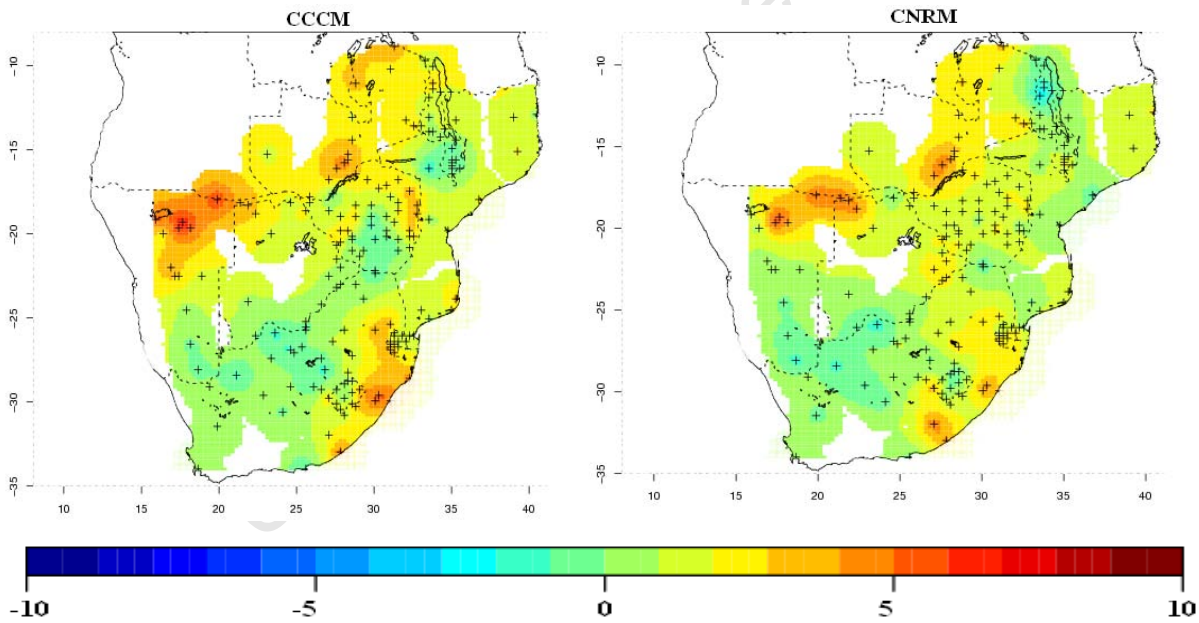

Figure 5.4: *Simulated mean change in WSRI forced by climate data from the five GCMs-DS.*
Continued on next page……

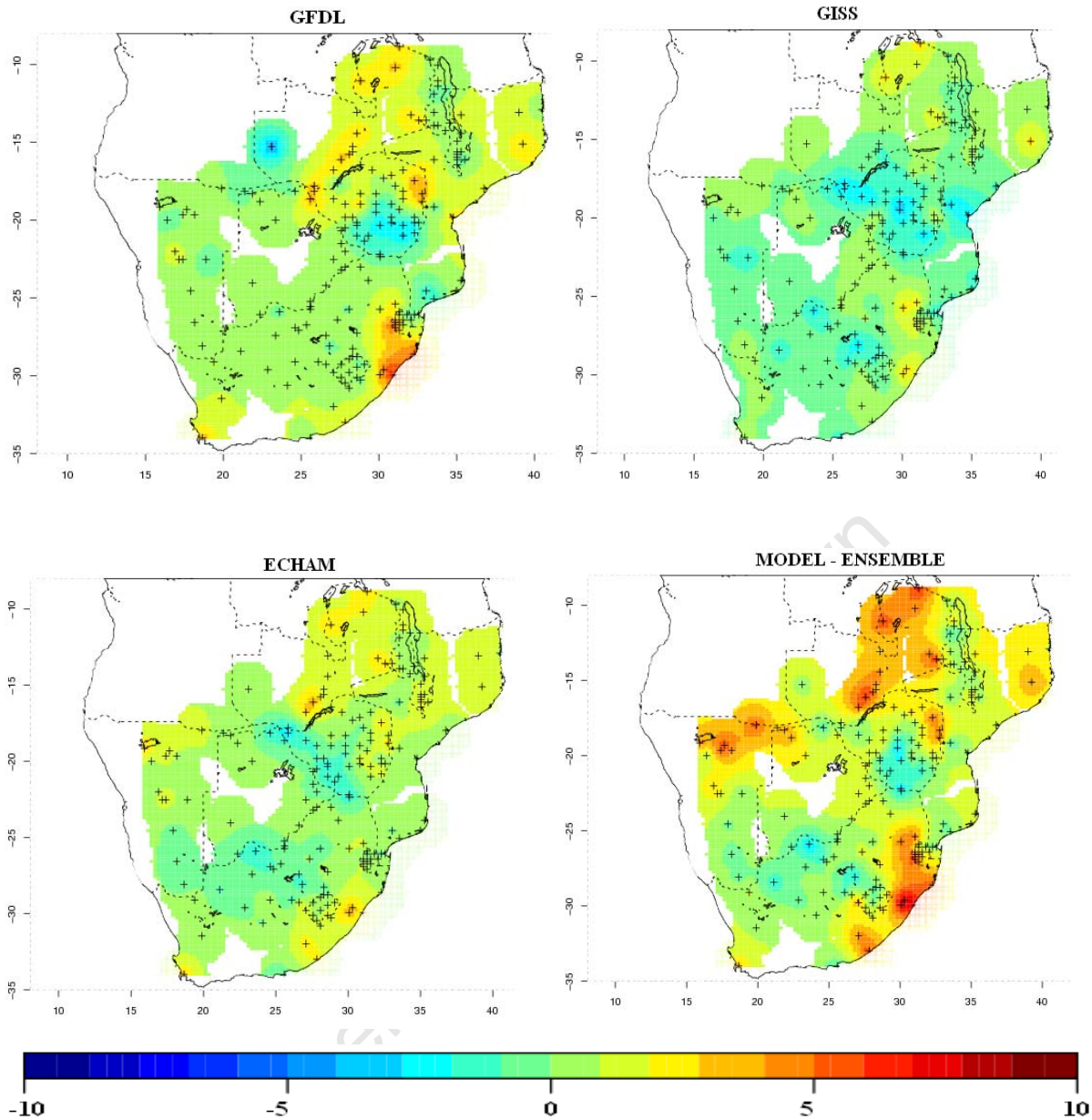

Figure 5.4: *Simulated mean change in WSRI forced by climate data from the five GCMs-DS and (bottom right) average WRSI (five GCMs-DS)*

Figure 5.5a shows the number of GCMs-DS which agree on the sign (+/−) of change in WRSI. Except for a few stations where the models disagree on the sign of change, nearly all of the GCMs-DS agree on the positive impacts in Zambia and eastern South Africa, while 4 GCMs-DS or more agree on the negative impact expected in the central region of Zimbabwe. Interesting to note is that, while GCM-DS model prediction of mean summer precipitation characteristics by 2050s is inconsistent over parts of the study domain as shown in chapter 4 the projected change in WRSI is very consistent among the GCMs (Figure 5.5a). This

demonstrates that the projection of the impact is more robust to climate model than the climate change itself.

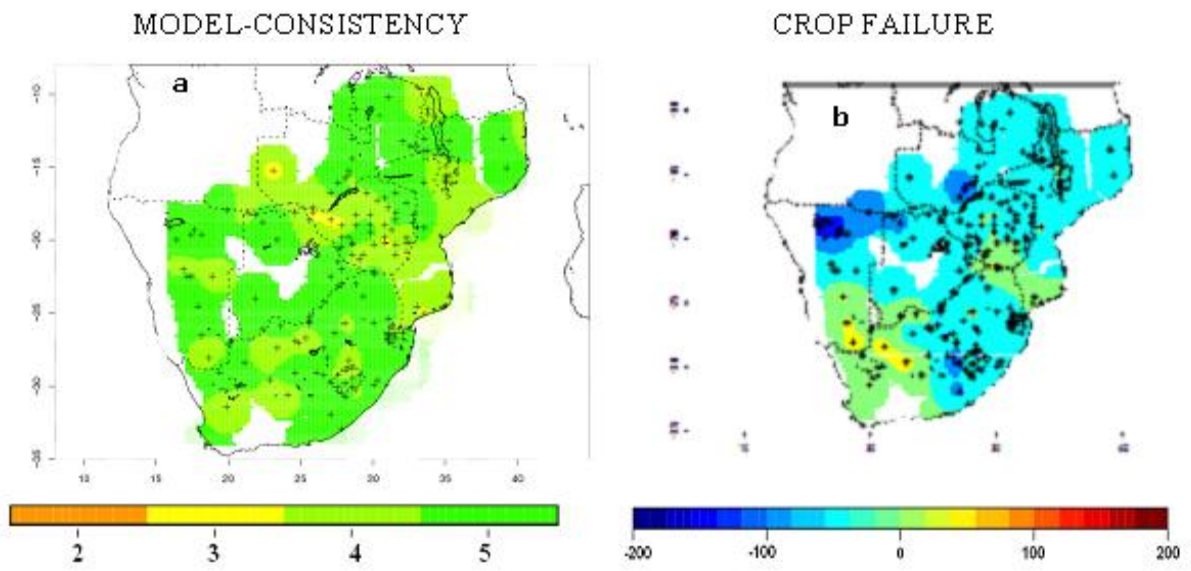

Figure 5.5: *(a) Model agreement on the sign according to the WRSI mean change. (b) Mean change in crop failures (as defined WRSI simulation below 50)*

Figure 5.5b depicts the mean change in crop failures (from the 1000 simulations) between the control and future periods for the five GCMs. Most of parts of southern Africa indicate less frequent crop failures in the future although there is a consistent increase over the arid area of southern Namibia and western South Africa, as well as over southern Mozambique and Zimbabwe (around the Limpopo valley). Whilst the mean increase in WRSI over eastern South Africa is associated with more frequent crop opportunities, the decrease in mean WRSI over south Zimbabwe is not necessarily associated with more cropping failures.

5.4 WRSI sensitivity to sowing date based on GCM control data

Despite the uncertainties in future climate scenarios, an assessment of how the regions agricultural production under varying climate conditions is important for formulating response strategies, which should be practical, affordable and acceptable to farmers (*Mall et al., 2006*). The following sections present results of an approach that could be used to mitigate negative climate change impacts. This approach computes the sensitivity of WRSI to sowing date decision rule. For the description of sensitivity approach, refer to section 2.5.3 of chapter 2.

Figures 5.6a and 5.6b show the mean contribution of rainfall during the first dekad (*x1*) and the following two dekads (*x2*) to simulated WRSI computed using modeled control climate between 1979 and 1999. In general, WRSI variability is most sensitive to *x1* which contributed up to 40% in eastern South Africa, some parts of Zimbabwe and northern Namibia.

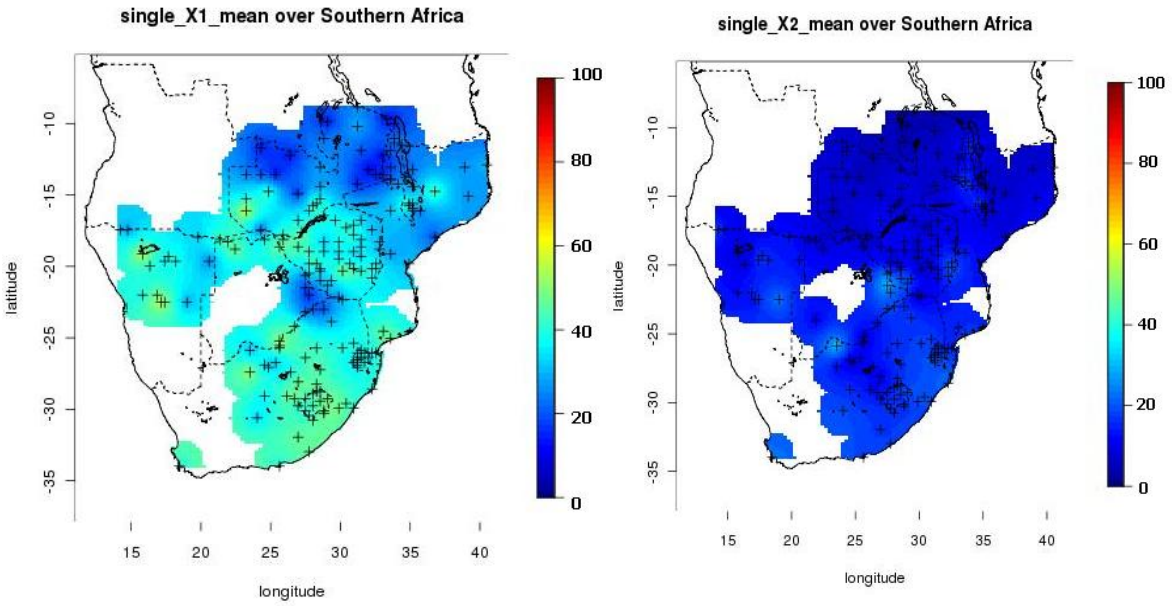

(a) (b)

Figure 5.6: *(a) Mean contribution of x1 (%) to WRSI variance using GCM control data and (b) mean x2 contribution (%) to WRSI variance*

The relationship between *x1* and WRSI is more evident compared to WRSI and *x2*. The contribution of *x2* to the WRSI variability barely rises above 20% in most parts of southern Africa. However, in some parts of Malawi and northern Zambia where *x1* and *x2* contributions are low, the combined total of *x1* and *x2* considerably contributes to the overall changes in WRSI. In general, slight variability in rainfall amounts during the first dekad will considerably affect WRSI (by about 40%) over most parts of southern Africa as compared to variability rainfall amounts in the following 20 days.

5.5 Simulated changes in sensitivity of maize WRSI to the definition of sowing date

Figure 5.7a, depicts the mean change (future minus control) in *x1* contribution to WRSI variability across the five climate models while Figure 5.7b shows the corresponding *x2* contribution. Using control climate data (Figure 5.6), it was earlier shown that the contribution of *x1* is high over central Zimbabwe and eastern parts South Africa, with lower contributions to the west while that of *x2* has less influence everywhere.

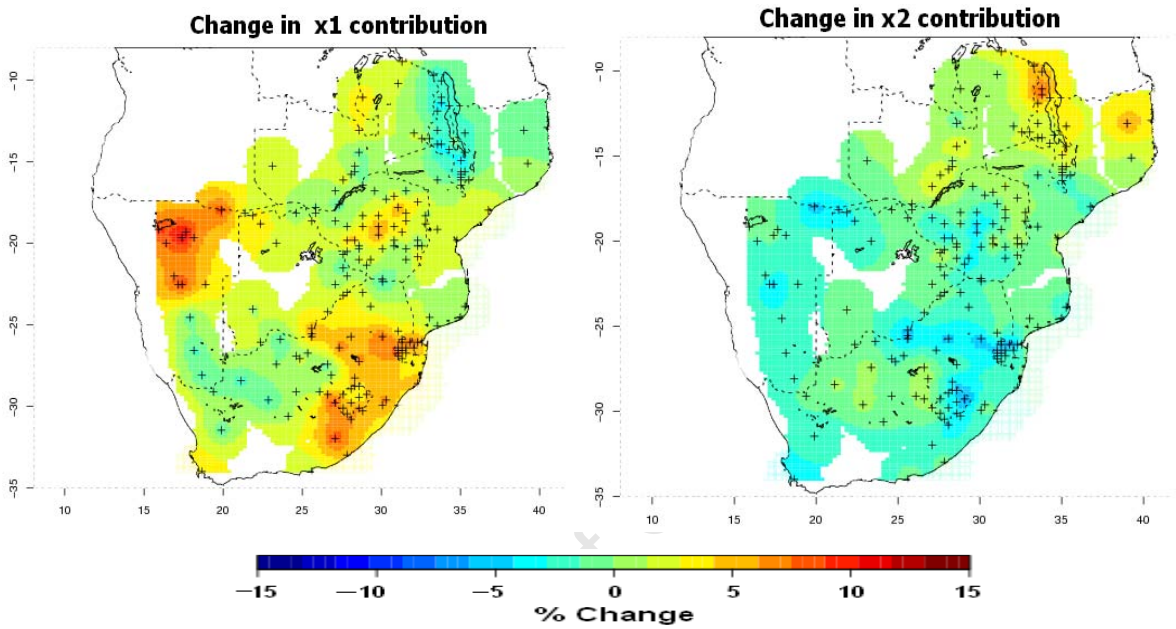

Figure 5.7:*(a) Mean % change in x1 contribution (fraction) to WRSI variance and (b) mean % change in of x2 contributing (fraction) to WRSI variance*

By 2050, most of the region could have increased WRSI variability with the choice of *x1* contributing more to the variability in WRSI. However over the southern part of Zambia (region bordering Zimbabwe) an increase in future WRSI of about 8% is projected while the contribution of *x1* to WRSI remains unchanged. On the other hand, most GCMs show a reduction in future WRSI in the central region of Zimbabwe (Figure 5.4) while showing an increase in the *x1* contribution to WRSI variability (Figure 5.7). In addition, this region (central Zimbabwe) shows a shift toward later sowing dates in the future relative to the control (chapter 4) and a high sensitivity of WRSI to the choice of *x1* in the observed climate. This implies that farmers in central Zimbabwe can significantly influence their WRSI (and hence yields) by changing sowing dates (particularly the first 10 days of sowing) in the future. This is therefore a potential adaptation option, which is expected to be more effective in the future than at present. It should also be noted that the influence of *x1* remains strong

across the rest of the region, suggesting that it remains the most important aspect when defining the sowing date. However, the sowing date adaptation strategy can only be achieved by either having accurate weekly and monthly rainfall forecast before the sowing date or replanting seeds when the conditions have not been met in the first days on sowing.

5.6 Summary

Regional climate policy requires a better understanding of climate change impacts. This chapter outlines how changes in climate are reflected in a crop model. In addition, results of a sensitivity method for assessing agricultural adaptation decisions under uncertain climatic conditions are presented. The study shows that impact models can provide useful indices for understanding future projections as compared to monthly climate variables. It was found that the expected WRSI calculated from the five models mostly produce consistent projections as compared to GCM-DS climate variables.

One of the factors found to have influence on maize WRSI is the sowing date during the rainfall season. It is shown that, currently the water amount required during the first dekad of the decision process (*x1*) contributes more to yield variation than the water amount required during the following 2 dekads (*x2*) over most of southern Africa. From a practical point of view, this means that current and future WRSI can be improved simply by changing the sowing date, particularly during the first dekad of sowing.

In the future (2050s), contribution of the *x1* decision parameter to WRSI variability was shown to increase over Zimbabwe and eastern South Africa. It was also shown that the eastern parts of South Africa project an increase in WRSI indicating that, despite this increase, the region remains susceptible to the definition of *x1*. Other regions that project considerable increase (about 8%) in WRSI are the northern parts of Namibia and Zambia. A reduction in WRSI was observed over most of Zimbabwe, with an increase in the contribution of *x1*. This implies that adaptation will be necessary over Zimbabwe and that *x1* is a potentially efficient adaptation tool both now and in the future. Even though a beneficial increase in WRSI is simulated over eastern South Africa, the need for adaptation will depend on the farming system (e.g. irrigated, non-irrigated) and how close these systems are to critical thresholds of climate. If new opportunities become available (for instance, new

farming regions), they may be close to these critical thresholds and in either case adapting *x1* is suggested as a potentially useful adaptation measure.

In Malawi little change in WRSI is projected by 2050s. However, *x2* is projected to contribute more to the WRSI variability than *x1* in the future, compared to the situation under current climate conditions. This provides the decision maker with the caution that (1) an efficient current adaptation decision might not be efficient for a long time, and (2) that the decision process by itself, even if no production decrease is to be expected, is likely to change from current 'optimal' decisions. This clearly demonstrates that seeking adaptation options in the current climate e.g. to current climate variability, is not necessarily the most effective way for the future impacts.

Chapter 6
Summary and Conclusion

The goal of this thesis as set out in chapter 1, section 1.5 was to determine the response of maize water requirement satisfaction index to climate change given the imperfect climate data. To accomplish this goal, a crop model (Agrometshell) was forced with downscaled data from an ensemble of five GCMs. In addition, a new sensitivity approach, which evaluates how the sowing date decisions will evolve under a changed climate, was presented to determine the robustness of using GCMs in developing crop adaptation options. The following sections present a summary of the main findings and the extent to which the research questions posed in chapter 1 were addressed.

6.1 Determining solar radiation and evapotranspiration values

The first research question of the thesis was aimed at exploring evapotranspiration estimations. The Penman-Montieth reference evapotranspiration technique was used as standard for the comparison. Given the limited downscaled GCM variables (precipitation, minimum and maximum temperature) over southern Africa as a whole, it was crucial that the estimation technique require fewer input data but perform as well as the Penman-Montieth reference evapotranspiration (PM_o) technique for the southern African region. In order to achieve the above objective, three experiments were performed.

In the first experiment, solar radiation, which serves as input to most evapotranspiration techniques, was estimated using monthly observational temperature data from Climatic Research Unit (CRU). It was found that it is possible to accurately compute solar radiation over the entire study region using minimum and maximum temperature as an input variable. By introducing altitude in the Hargreaves and Samani (HS) solar radiation method, biases between HS and observational CRU solar radiation were significantly reduced. The HS method achieved a good linear relationship (R^2 = 0.98) when compared to CRU solar radiation. As a result the HS method was used to compute solar radiation to drive the evapotranspiration models.

The second experiment involved the computation of the PM_o reference evapotranspiration using CRU data and testing its sensitivity to input variables (minimum and maximum

temperature, wind, specific humidity and net solar radiation). The results show that solar radiation has the greatest impact on PM_o evapotranspiration sensitivity over the humid northern Zambia and Malawi during the DJF season, while wind speed has the least impact. Elsewhere the variation of the PM_o outputs is most sensitive to temperature. Results from the second experiment suggest that temperature and solar radiation based methods can efficiently be used to compute evapotranspiration over most of the region.

In the third experiment, estimates from the Priestly-Taylor (PT) and the Hargreaves evapotranspiration methods were compared to those derived using the PM_o method. The PT estimates were found to have a clear linear relationship with those from PM_o method. However, in order to get values that are close to PM_o outputs, the PT constant had to be adjusted to 1.09 (as compared to the recommended literature value of 1.27). The Hargreaves method performed poorly compared to the PT method and overestimated PM_o outputs. Most high values of overestimation where located over the coastal regions where wind speed is relatively high.

In view of the first objective these findings show that, despite the limited climate data, it is feasible to estimate evapotranspiration over the entire southern African domain using currently available techniques (e.g. Priestley-Taylor) and downscaled climate data. Adjusting the Priestly Taylor constant confirmed the important realization that the models should be calibrated over the region of interest.

6.2 Changes in crop-relevant climate characteristics from the downscaled GCM variables

The second research question posed in section 1.5 was aimed at investigating how climate characteristics relevant to agriculture will change in the future and if these changes are a response to large-scale atmospheric circulation dynamics. The initial step involved comparison of downscaled GCM outputs with observations. It was found that downscaled GCM precipitation captured the observed (downscaled NCEP reanalysis) regional seasonal cycle. The spatial degree of discrepancy between the downscaled precipitation amounts from GCM and NCEP reanalysis varied from region to region. For instance, rainfall is underestimated by most GCMs over parts of north eastern South Africa while it is often overestimated over parts of Zambia and Malawi. This implies that GCMs still had difficulties

in simulating adequately rainfall events in some regions despite using the downscaled outputs. One possible reason for the discrepancies between the models and NCEP reanalysis could be linked to the individual GCM dynamics and choice of predictor variables used in the downscaling process. This might be the case with the GFDL and GISS models which have missing surface specific humidity over high altitude regions and this error might impact the downscaled precipitation. This suggests that, in some models, precipitation is highly sensitive to specific humidity particularly over the mountainous regions. In a similar study, Wilby and Wigley (2000) observed that the choice of the predictor variable and its corresponding domain, in terms of location and spatial extent, may be critical factors affecting the realism and stationarity of downscaled precipitation scenarios. In an attempt to address this bias, CSAG is currently exploring alternatives such as, the use of Principle Component Analysis (PCA) on predictor variables. However, given the confidence in the ability of the five GCMs to represent seasonal precipitation patterns over most of southern Africa, they were used to simulate future maize growth.

Taking the downscaled GCM ensemble median variables as an indication of changes in the future, regions in the central and eastern parts of South Africa indicate increased rainfall during the summer season, an early start to rainfall season as well as a reduction in the number of dry spells. Increased precipitation over south eastern South Africa is characterised by an increase in humidity as well as anticyclonic wind anomalies centred along the border between South Africa and Mozambique during the summer rainfall season. This could be explained by an enhanced encroachment of the ridge from the Indian Ocean high pressure system onto the sub-continent in the future.

An increase in seasonal rainfall totals coupled with the reduction in number of dry spells over eastern South Africa suggests that this region could experience good (relatively to the present) growing conditions for maize. The projected increase in rainfall totals (approximately 20%) in the south eastern parts of South Africa agrees with the finding of *Hewitson and Crane (2006)* and *Shongwe et al. (2009)*. On the other hand, considerable reduction in rainfall is projected further north in central parts of Zimbabwe and Zambia. These regions (central parts of Zimbabwe and Zambia) also indicate highest rainfall variability during the entire summer season. Rainfall variability over these regions has previously been associated with ENSO events. For instance, the El-Nino mode has been

linked to an increase in number of dry spells over the region suggesting that the changes in the future may be due to an increase in the frequency and/or intensity of these events.

Despite the reduction in number of dry spells by 2050, the duration of mean dry spells is projected to increase (approximately 10 days longer) over most of southern Africa. This may be as a result of increased interannual rainfall variability projected by 2050 over most of the study domain, which could lead to longer dry or wet periods and hence largest uncertainty in rainfall characteristics. A second possibility is that the winter dry season is longer in the future and contributes to an increase in the mean dry spell duration. This is consistent with Botswana, Zimbabwe, central parts of Zambia, the Limpopo region of South Africa and the region bordering Mozambique and South Africa projected to have later sowing dates (calculated based on rainfall thresholds) in the future. Reduction in early summer rainfall coupled with later sowing date, increased dry spell duration and increases in evapotranspiration could lead to water scarcity, reduced agricultural productivity, and increased risks of food insecurity and famine over the central parts of Zimbabwe and Zambia.

This study found that moisture influx during high extreme rainfall events in the future show patterns similar to those systems associated with present daily rainfall variability. In attempting to explain the sources of moisture causing high rainfall patterns in the GCM, (e.g. eastern parts of South Africa) as well as low rainfall (over southern Zambia and northern Zimbabwe), it was found that the parameters (wind and humidity, representative of moisture flux) that support enormously high or low rainfall patterns in the GCM were similar to those linked to observed systems. This indicates that although rainfall events by themselves hold high uncertainty, there is high confidence in systems and parameters (e.g. specific humidity) responsible for the changes in the rainfall patterns. For instance, two GCMs (GFDL and GISS) projecting late sowing dates over southern Zambia and parts of central Zimbabwe are characterised by reduced surface humidity during SON over the south western parts of the study region. A later sowing date over Zambia has been previously associated with reduced Angola heat low system. This system is weaker than average in the future for GISS model and could be linked to the significant reduction in precipitation during the early part of the growing season. The increase in dry spells duration over the study domain was associated with south-easterly anomalies in the Mozambique Channel and a strong cyclonic (anticyclonic) anomaly over the subtropical South Indian (central tropical Indian Ocean).

This study found that the GCMs were more consistent in simulating changes in evapotranspiration and dry spells, as compared to mean seasonal rainfall totals. In terms of the second objective, this further highlights the value that consistent responses may be better detected in sub-seasonal rainfall characteristics, as opposed to changes in the seasonal or monthly means.

6.3 Projected changes in maize water requirements and its sensitivity to sowing dates

Based on an ensemble mean from five models, no significant change in Water Requirement Satisfaction Index (WRSI) is simulated over Malawi and Mozambique by 2050s despite increase in rainfall totals. Results over central and northern Zimbabwe indicate slight reductions in WRSI by 2050. This region was also projected to have a later start in sowing date and increase in mean DJF and MAM precipitations. This highlights that mean changes of increased precipitation do not necessarily translate into increased soil moisture required for maize growth over the region. In practical terms, the slightly increased rainfall amounts coupled with the high rainfall variability observed over this region imply more incidences of flash floods and water logging (not simulated in the study) influencing the output of the crop model. Furthermore, the observed increase in evapotranspiration, especially at the end of the dry season could increase water loss particularly over arid or semi arid regions as it is the case with central Zimbabwe, thus leading to reduced soil moisture in the future. In such conditions the best WRSI are simulated when sowing is delayed until more rain falls, thus overcoming the increase in evapotranspiration. On the other hand, increased rainfall and evapotranspiration as well as reduced number of dry spells positively influence maize water requirement outputs over central and eastern South Africa. This region showed a mean increase in WRSI (which relates to maize yield) of approximately 8% in the future.

In view of the fourth research question, it was found that rainfall expected in the first 10 days of sowing (x1) contributed more significantly to the yield variation than rainfall during the following 20 days (x2) in both recent past and future scenarios. From a practical point of view, this implies that there is a better chance of effectively improving WRSI by adapting to x1 as compared to x2. The contribution of x1 to WRSI increases over most of southern Africa by 2050, especially so over northern Namibia and eastern South Africa, whereas the x2 contribution to WRSI variation increases slightly in regions further east, and up to 10% in

northern Malawi. In the case of central Zimbabwe the sum of x1 and x2 contributes close to 50% in WRSI variation. This suggests that we can propose adaptation options over central Zimbabwe based on x1 and x2, in order to mitigate the negative impact expected in these regions. Over Malawi, however, the relative contribution of x1 decreases in the future climate, whereas the contribution of x2 increases implying that the sowing decision will need adapting in the future in order to keep up with the current yields.

The results presented here are applicable for the case of maximising WRSI by shifting sowing dekads. Furthermore, these results are dependent on the accuracy of the crop model, its ability to translate the effect of changing decisions and uncertainty in the climate change scenarios. As a result, this work is limited by a number of assumptions thus several considerations need to be taken into account when interpreting the model outcomes and how they relate to real world situations.

6.4 Summary of findings and Limitations

The main results for the study are:

1. The Hargreaves and Samani solar radiation method is highly correlated to the CRU monthly radiation values and thus can be used in the radiation estimations using GCM data;
2. The Priestly-Taylor method compares favourably to the FAO-56 Penman–Monteith method which suggests that it is practical to use this method for estimating evapotranspiration using downscaled GCM.
3. Increased precipitation over south eastern South Africa by 2050 is characterised by an increase in specific humidity as well as anticyclonic wind anomalies centred along the border between South Africa and Mozambique (promoting onshore advection of moisture) during the summer rainfall season.
4. Later sowing dates are projected over Botswana, Zimbabwe, central parts of Zambia, and the Limpopo region of South Africa and the region bordering Mozambique and South Africa, while earlier sowing dates are projected over the central and eastern parts of South Africa.
5. Maize water requirement satisfaction index simulations across the five GCMs are more consistent (sign of change) in projecting future changes than the rainfall totals

suggesting that consistent responses may be better detected in crop model outputs as opposed to changes in seasonal or monthly rainfall characteristics.

6. In most regions, rainfall in the first sowing dekad, more significantly contributes to variations in yield than rainfall in rainfall in the second dekad and as such is an important consideration for planned future adaptations in maize farming.

The experiments performed in this study provide a step towards understanding and quantifying climate change impacts on maize water requirements over southern Africa using a suit of climate scenarios. The limitations encountered during the course of the study provide sources of uncertainty in the respective research outputs.

Multiple sources of uncertainty are encountered at specific steps in simulating crop growth using downscaled climate change projections. Uncertainties that became evident during the duration of the study could be classified in four main groups as outlined below.

1. Input climate data uncertainty (e.g. GCM data uncertainties, spatial and temporal uncertainties in data).
2. Uncertainty in estimating radiation and evapotranspiration.
3. Crop model uncertainty (e.g. factors not accounted for in the study such as the impacts of future economic, political, social and technological developments).
4. Uncertainty in the downscaling process

These are further discussed in the sections that follow.

The main source of uncertainty was attributed to GCM datasets used in the experiments in particular precipitation. This was evident from the inconsistent downscaled precipitation signal from the five GCMs. In addition, the sparse distribution of stations (e.g. most parts of Zambia and Namibia) meant that data had to be interpolated (upscaled) in order to get a spatial representation for the region. Upscaling to larger areas invariably means a loss in the precision and observation density of data used to parameterize a model thus introducing some uncertainty in the final outputs. The same implies when downscaling GCM outputs to smaller scales. Some notable biases in the downscaled GCM precipitation simulation are as a result of surface synoptic systems in individual GCMs that are used as input in the downscaling process. This

presents uncertainty in the final impact particularly for mountainous regions not well captured by some GCM-DS.

Within Agrometshell crop model, increases in temperature are related to crop growth through increased evapotranspiration which translates into crop water stress particularly if not compensated with increased rainfall. In addition, higher temperature could imply reduction in the length of the growing season which could limit WRSI. Despite reasonably estimating solar radiation and evapotranspiration, the evaluation was only done at a monthly scale thus this presented some uncertainty when the same methods are applied to generate daily values to drive the crop model.

In addition to the direct effects of precipitation and temperature on crop development (e.g. through evapotranspiration), change in temperature and carbon dioxide is directly related to the variation in biophysical processes and development of a crop. For instance, enhanced levels of carbon dioxide concentration in the atmosphere could increase the gradient between the external air and the air spaces inside the leaves thus promoting higher levels of photosynthesis and of biological productivity (*Adejuwon, 2004*). This could lead to less crop water stress resulting in higher WRSI in areas normally considered marginal with respect to precipitation. These processes are not taken into account in this study thus presenting a source of uncertainty.

It must be noted that the results in this study were derived solely by taking into account the changes in climate characteristics. Given the limited time, it was not possible to incorporate all factors that influence small scale farming. However, despite the uncertainties in studying climate change impacts and taking into account some assumptions made during this study, considerable outputs have been achieved that further enhance our understanding on use of climate models for impact assessment in southern Africa.

6.5 Conclusion and future research

This study has highlighted that real-time decision-making strategies can form an effective and robust method of coping and adapting to climate change and variability. For instance, if crop model simulations are to be used as a tool to evaluate real time decisions on sowing dates, the sowing date sensitivity approach used in this paper could be adopted for use with seasonal forecasts. At present, few climate change studies have investigated changes in rainfall

characteristics such as sowing dates and dry spells that are closely tied to practical decisions and the crop growth cycle (e.g. Tadross et al., 2010). Understating the behavior of climate characteristics and managing the consequences of climate variability in the context of other influences on economic, social and natural systems could provide useful adaptation strategies for handling present day and future climate change (Washington et al. 2006). Gadgil et al., 2002 also notes that with targeted climate information, and predictions, it is possible for informed management options relating to parameters such as planting dates to be made.

When this dissertation was written, the goal was to investigate how crops may respond to downscaled climate change data given the uncertainties in these data sets. While this goal has been achieved, further research needs to be done in order to integrate a larger database of climate, soil and crop varieties. For instance, the use of more scenarios will help incorporate a wider range of uncertainties associated with future projections of climate while evaluating a range of crops would help in developing adaptation strategies in regions showing reduced maize growth. Additionally, using a process based crop model that takes into account the effects of nitrogen content on crop yield, irrigation potential and the direct effects of increased temperature and carbon dioxide on crop development could reduce associated uncertainties and increase confidence.

The use of simple adaptation techniques other than the sowing date decision rule in Chapter 5 would be very helpful (e.g. changes in crop varieties). It would also be interesting to investigate the ability of different GCMs to capture the expression of natural variability cycles such as the El Nino Southern Oscillation. This topic should also include the linkage between changes in El Nino Southern Oscillation and regional climate variability by 2050. Also important is to improve downscaling techniques and to ensure the availability of additional adequate and reliable historical climate data, relevant to the localities of the users. For instance, more GCM variables needed in driving crop growth models (e.g. solar radiation) should be downscaled.

References

Adejuwon, J., 2004: Assessing the Suitability of the EPIC Crop Model for Use in the Study of Impacts of Climate Variability and Climate Change in West Africa. *AIACC Working Paper No 5*.

AGRHYMET, 1996: Methodologie de suivi des zones a risque. AGRHYMET FLASH, *Bulletin de Suivi de la Campagne Agricole au Sahel, Centre Regional AGRHYMET*, B.P. 11011, Niamey, Niger. **2**.

Allen, R., 1997: Self-Calibrating Method for Estimating Solar Radiation from Air Temperature. *Journal of Hydrologic Engineering*, **2**: 56-67.

Allen, R., L. Pereira, D. Raes and M. Smith, 1998: Crop evapotranspiration - guidelines for computing crop water requirements. In: FAO Irrigation and drainage paper 56. [Available online from http://www.fao.org/docrep/X0490E/X0490E00.htm.]

Anandhi, A., V. Srinivas, S. Nanjundiah and D. Kumar, 2008: Downscaling precipitation to river basin in India for IPCC SRES scenarios using support vector machine. *International Journal of Climatology*, **28**: 401–420.

Annandale, J., N. Jovanic, N. Benade and R. Allen, 2002: Software for missing data error analysis of penman-monteith reference evapotranspiration. *Irrigation Science,* **21**: 57–67.

Ball, R. A., L. C. Purcell and S. K. Carey, 2004: Evaluation of Solar Radiation Prediction Models in North America. *Agronomy Journal*, **96**: 391-397.

Barron, J., J. Rockström, F. Gichuki and N. Habitu, 2003: Dry spell analysis and maize yields for two semi-arid locations in east Africa. *Agricultural and Forest Meteorology*, **117**: 23-37.

Bartholomeacute, E. and A. Belward, 2005: GLC2000: A new approach to global land cover mapping from Earth observation data. Technical Report. 21020 Ispra (VA), Italy, Institute for Environment and Sustainability, EC Joint Research Centre.

Beaumont, L. J., L. Hughes and A. J. Pitman, 2008: Why is the choice of future climate scenarios for species distribution modelling important? *Ecology Letters*, **11**: 1135–1146.

Benestad, R. E., 2004: Empirical-Statistical Downscaling in Climate Modeling. *American Geophysical Union*, **85**: 417-422.

Boogaard, H. L., C. A. Diepen, R. P. Rötter, J. C. A. Cabrera and H. H. Laar, 1998: User's guide for the WOFOST 7.1 crop growth simulation model and WOFOST control center 1.5. *Technical document* 52. Wageningen, the Netherlands, Winand Staring Centre**:** 144.

Bristow, K. and G. Campbell, 1984: On the relationship between incoming solar radiation and daily maximum and minimum temperature. *Agricultural and Forest Meteorology*, **31**: 159–166.

Brown, M. and C. Funk, 2008: Food security under climate change. *Science*, **319**: 580-581.

Cavazos, T. and B. Hewitson, 2005: Performance of NCEP variables in statistical downscaling of daily precipitation. *Climate Research*, **28**: 95-110.

Cook, C., C. J. C. Reason and B. C. Hewitson, 2004: Wet and dry spells within particularly wet and dry summers in the South African summer rainfall region. *Climate Research*, **26**: 17-31.

Cooper, P. J. M., J. Dimes, K. P. C. Rao, B. Shapiro, B. Shiferaw and S. Twomlow, 2008: Coping better with current climatic variability in the rain-fed farming systems of sub-Saharan Africa: an essential first step in adapting to future climate change. *Agriculture Ecosystems & Environment*, **126** 24–35.

CORDEX, 2010: Regional Climate Modelling and Downscaling. [Available online from http://wcrp.ipsl.jussieu.fr/RCD_CORDEX.html.]

Cressman, G. P. (1959). "An operational objective analysis system Mon." *Monthly Weather Review,* **87**: 367–374

Crimp, S. J., S. C. van den Heever, P. C. D'Abreton, P. D. Tyson and S. J. Mason, 1997: Mesoscale Modelling of Tropical-Temperate Troughs and Associated Systems over Southern Africa. *Technical Report*, Water Research Commision**:** 595.

da Silva, A., A, C. Young and S. Levitus, 1994: Atlas of Surface Marine Data. *NOAA Atlas NESDIS 6*: 83.

Di Stefano, V. and V. Ferro, 1977: Estimation of evapotranspiration by Hargreaves Formula and remotely sensed data in semi-arid Mediterranean areas. *Journal of Agric. Eng. Res*, **68**: 189–199.

Doorenbos, J. and A. Kassam, 1979: Yield response to water. *FAO Irrigation and Drainage Paper 33*.

Eriksen, S., 2005: The role of indigenous plants in household adaptation to climate change: the Kenyan experience. Climate Change and Africa. *Cambridge University Press, Cambridge*: 248-259.

FAO, 1998: Crop and Food Supply Assessment Mission to Zambia. *S. report, Food and Agriculture Organisation.* [Available online from http://www.fao.org/docrep/004/w8885e/w8885e00.htm]

FAO, 2005: FAO/WFP Crop and Food Supply assesement mission to Malawi. [Available online from http://www.fao.org/docrep/008/j5509e/j5509e00.htm.]

Feser, F., 2005: Spatial Scale Separation in Regional Climate Modelling. *Institute for Coastal Research. Geesthacht, Germany, Universität Hamburg*. *PhD Dissertation.*

Fischer, G., H. Velthuizen, M. Shah and F. Nachtergaele, 2002: Global Agro-ecological Assessment for Agriculture in the 21 Century. *IIASA Research Report*. IIASA, Laxenburg

Forest, C., M. Webster and J. Reilly, 2004: Narrowing Uncertainty in Global Climate Change Observations. *American Institute of Physics*: 20-23.

Fox, P. and J. Rockström, 2000: Water harvesting for supplemental irrigation of cereal crops to overcome intra-seasonal dry spells in the Sahel. *Physics and Chemistry of the Earth,* **25**: 289–296.

Gaslikova, L., 2006: High-resolution wave climate analysis in the Helgoland area. *GKSS, International Max Planck Research School. PhD Dissertation*

Gay, J. and D. Hall, 2000: Poverty and livelihoods in Lesotho, 2000: more than a mapping exercise. Sechaba Consultants.

Gbetibouo, G. and R. Hassan, 2005: Economic impact of climate change on major South African field crops: A Ricardian approach.. *Global and Planetary Change*, **47**: 143–152.

GCIS, 2009: South Africa Yearbook 2008/09. [Available online from http://www.gcis.gov.za/resource.]

Giorgi, F. and B. Hewitson, 2001: Regional climate information – evaluation and projections. *In Climate Change 2001: The Scientific Basis. C, Houghton JT, Ding Y, Griggs DJ, Noguer M, van der Linden PJ, Dia X, Maskell K, Johnson CA (eds). Cambridge University Press: Cambridge.*

Giorgi, F. and L. Mearns, 1991: Approaches to the simulation of regional climate change: a review. *Reviews of Geophysics*, **29**: 191-216.

Gleckler, P., K. Taylor and C. M. Doutriaux, 2008: Performance metrics for climate models. *Journal of Geophysical Research-Atmospheres*, **113**.

Gommes, R., 1998: Non-Parametric crop yield forcasting, a didactic case study for Zimbabwe, Environment, Climate Change and Bioenergy Division,FAO. [Available online from http://www.fao.org/NR/climpag/pub/non_parametric_yield_forecasting_FAO.pdf.]

Hachigonta, S. and C. J. C. Reason, 2006: Interannual variability in dry and wet spell characteristics over Zambia. *Climate Research*, **32**: 49-62.

Hachigonta, S., R. Reason and M. Tadross, 2007: An analysis of onset date and rainy season duration over Zambia. *Theoretical and Applied Climatology*, **91**: 229-243, DOI: 10.1007/s00704-007-0306-4.

Hansingo, K., 2008: An Investigation into the Impacts of the Benguela Ni˜no on Rainfall over southern Africa. *Department of Oceanography, University of Cape Town. PhD Dissertation*.

Hargreaves, G. H. and Z. A. Samani, 1982: Estimating potential evapotranspiration. *Journal of Irrigation and drainage Engineering*, **108**: 223-230.

Hargreaves, G. L. and Z. A. Samani, 1985: Reference crop evapotranspiration from temperature. *Applied Engineering in Agriculture*, **21**: 96–99.

Hargurdeep, S. and S. Lalonde, 2003: Injuries to Reproductive Development Under Water Stress and Their Consequences for Crop Productivity. *Journal of Crop Production*, **1**: 223 - 248

Hewitson, B. and R. Crane 1996: Climate downscaling: techniques and application. *Climate Research*, **7**: 85-95.

Hewitson, B. and R. Crane, 2002: Self-organizing maps: applications to synoptic climatology. *Climate Research*, **22**: 1033-1048.

Hewitson, B. and R. Crane, 2006: Consensus between gcm climate change projections with empirical downscaling: precipitation downscaling over south africa. *International Journal of Climatology* **26**: 1315–1337.

Hoogenboom, G., 2001: Weather monitoring formanagement of water resources. *In : [K. J.Hatcher, editor] Proceedings of the 2001 GeorgiaWater Resources Conference. The University ofGeorgia, Athens, Georgia*: 778-781.

Huffman, G. J., R. F. Alder, P. Arkin, A. Chang, R. Ferraro, A. Gruber, J. Janowiak, A. McNab, B. Rulof and S. Schneider, 1997: The global precipitation climatology project (GPCP) combined precipitation dataset. *American Meteorological Society*: 5-20.

Hulme, M., R. Doherty, T. Ngara, M. New and L. D, 2001: African climate change: 1900–2100. *Climate Research*, **17**: 145–168.

IDL-Group, 2002: Trends in the Zambian Agriculture Sector. Technical Report, Department for International Development. [Available online from http://www.odi.org.uk/work/projects/03-food-security-forum/docs/zambia.pdf.]

IPCC, 2001: The Scientific Basis. Contribution of Working Group I to the Third Assessment Report of the Intergovernmental Panel on Climate Change [Houghton, J.T., et al. (eds.)]. *Cambridge University Press, Cambridge, United Kingdom and New York, NY, USA,* : 881.

IPCC, 2007: Impacts, Adaptation and Vulnerability. Contribution of Working Group II to the Fourth Assessment. *Summary for Policymakers*, Report of the Intergovernmental Panel on Climate Change, M.L. Parry, O.F. Canziani, J.P.

Jame, Y., W and H. Cutforth, 1996: Crop growth models for decision support systems. *Plant Science*, **76**: 9-19.

Jensen, M. E, 1985: Personal communication, *ASAE national conference*. Chicago, IL.

Jensen, M., R. Burman and R. Allen, 1990: Evapotranspiraion and Irrigation Water Requirement. ASCE Manuals and Reports on Engineering Practices. *70. 1st Edn., American Society of Civil Engineering (ASCE),* New York, NY, USA: 332-333.

Johnson, F. and A. Sharma, 2009: Measurement of GCM skill in predicting variables relevant for hydroclimatological assessments. *Journal of Climate*, **22**: 4373-4382.

Johnston, P., 2008: The Uptake and Utility of Seasonal Forecasting Products for Commercial Maize Farmers in South Africa*. University of Cape Town. PhD Dissertation.*

Kalnay, E., 2000: The US Reanalysis Program: Climatology for the New Millennium. [Available online from http://www.usclivar.org/Pubs/ReanalysisWorkshop_Rep.html.]

Kalnay, E., M. Kanamitsu, R. Kistler, W. Collins, D. Deaven, L. Gandin, Iredell, S. Saha, G. White, J. Woollen, Y. Zhu, A. Leetmaa, R. Reynolds, M. Chelliah, W. Ebisuzaki, W. Higgins, J. Janowiak, K. Mo, C. Ropelewski, J. Wang, R. Jenne and D. Joseph, 1996: The NCEP/NCAR 40-Year Reanalysis Project. *Bulletin of the American Meteorological Society*, **77**: 437–471.

Kanamitsu, M., W. Ebisuzaki, J. Woollen, S. Yang, J. Hnilo, M. Fiorino and G. Potter, 2002: NCEP-DOE AMIP-II reanalysis. *Bulletin of American Meteorological Society,* **83:** 1631-1643.

Keating, B., P. Carberry, G. Hammer, M. Probert, M. Robertson, D. Holzworth, N. Huth, J. Hargreaves, H. Meinke, Z. Hochman, G. McLean, K. Verburg, V. Snow, J. Dimes, M. Silburn, E. Wang, S. Brown, K. Bristow, S. Asseng, S. Chapman, R. McCown, D. Freebairn and C. Smith, 2003: An overview of apsim, a model designed for farming systems simulation. *European Journal*

of Agronomy, **18**: 267–288.

Kohonen, T., 1995: Self-Organizing Maps. *Series in Information Sciences, Springer, Heidelberg*, **30:** 362.

Kruger, A. C., 2006: Observed trends in daily precipitation indices in South Africa: 1910-2004. *International Journal of Climatology*, **26**: 2275-2285.

Lambert, S. and G. Boer, 2001: CMIP1 evaluation and intercomparison of coupled climate models. *Climate Dynamics*, **17**: 83-106.

Levey, K. M. and M. R. Jury, 1996: Composite intra-seasonal oscillations of convection over Southern Africa. *Journal of Climate*, **9**: 1910-1920.

Linacre, E., 1992 Climate, Data and Resources: A Reference and Guide. *New York, NY: Routledge, Chapman, and Hall, Inc.*

Lobell, D. B., M. B. Burke, C. Tebaldi, M. D. Mastrandrea, W. P. Falcon and R. L. Naylor, 2008: Prioritizing climate change adaptation needs for food security in 2030. *Science*, **319**: 607-610.

Martin, R., R. Washington and T. Downing, 1998: Seasonal Maize Forecasting for South Africa and Zimbabwe Derived from an Agroclimatological Model. *American Meteorological Society* **39**.

Mall, R., R. Singh, A. Gupta, G. Srinivasan and L. Rathore, 2007: Impact of climate change on Indian agriculture: a review. *Climate Change*, **82**: 225-231.

Mason, S. and A. Joubert, 1997: Simulated changes in extreme rainfall over southern Africa. *International Journal of Climatology*, **17**: 291-301.

Mason, S. J., 1995: Sea surface temperature-South African rainfall associations. *International*

Journal of Climatology, **15**: 119–135.

Mason, S. J. and M. R. Jury, 1997: Climate Change and Variability over southern Africa: a reflection on underlying processes. *Progress in Physical Geography*, **21**: 23-50.

Matarira, C. H. and M. R. Jury, 1992: Contrasting meteorological structure of intra-seasonal wet and dry spells in Zimbabwe. *International Journal of climatology*, **12**: 165-176.

Meehl, G. A., T. F. Stocker, W. D. Collins and others, 2007: Global climate projections. In Climate Change 2007: The Physical Science Basis. Contribution of Working Group 1 to the Fourth Assessment Report of the Intergovernmental Panel on Climate Change (Eds S Solomon, D Qin, M Manning, Z Chen, M Marquis, KB Averyt, M Tignor and HLMiller). *Cambridge University Press,Cambridge,* UK and New York.

Mearns, L. O., F. Giorgi, P. Whetton, D. Pabon, M. Hulme and M. Lal 2003: Guidelines for Use of Climate Scenarios Developed from Regional Climate Model Experiments IPCC, TGCIA [Available online from http://www.ipcc-data.org/guidelines/dgm_no1_v1_10-2003.pdf.]

Meinke, H., R. Nelson, P. Kokic, R. Stone, R. Selvaraju and W. Baethgen, 2006: Actionable climate knowledge: from analysis to synthesis. *Climate Research*, **33**: 101–110.

Meza, F. and E. Varas, 2000: Estimation of mean monthly solar global radiation as a function of temperature. *Agricultural and Forest Meteorology*, **100**: 231–241.

Monteith, J. L., 1965: Monteith, Evaporation and environment. *Symp. Soc. Exp. Biol*, **19**: 205–234.

Mukhala, E. and P. Hoefsloot, 2004: AgroMetShell Manual. [Available online from http://www.hoefsloot.com/agrometshell.htm.]

Mulenga, H., 1998: Southern African climatic anomalies, summer rainfall and the Angola low.

Murphy, J., D. Sexton, D. Barnett, G. Jones, M. Webb, M. Collins and D. Stainforth, 2004: Quantification of modelling uncertainties in a large ensemble of climate change simulations. *Nature*, **430**: 768-772.

N.O.A.A, 2002: Climate and the Republic of Zimbabwe: can today's climate Science help over tomorrow's catastrophe?, Office of Global Programs for Africa. [Available online from www.cip.ogp.noaa.gov.]

Nakicenovic, N. and J. Alcamo, et al, 2000: IPCC Special Report on Emissions Scenarios. *Cambridge University Press, Cambridge, U.K*: 599.

Naoum, S. and K. Tsanis, 2003: Hydroinformatics in evapotranspiration estimation. *Environmental Modelling & Software*, **18**: 261-271.

Nelson, G., M. Rosegrant, J. Koo, R. Robertson, T. Sulser, T. Zhu, C. Ringler, S. Msangi, A. Palazzo, M. Batka, M. Magalhaes, R. Valmonte-Santos, M. Ewing and D. Lee, 2009: Impact on Agriculture and Costs of Adaptation. *Technical Report*. Washington, D.C., International Food Policy Research Institute.

New, M., B. Hewitson, D. Stephenson, A. Tsiga, A. Kruger, A. Manhique, B. Gomez, C. Coelho, D. Masisi, E. Kululanga, E. Mbambalala, F. Adesina, H. Saleh, J. Kanyanga, J. Adosi, L. Bulane, L. Fortunata, M. Mdoka and R. Lajoie, 2006: Evidence of trends in daily climate extremes over southern and west Africa. *Journal of Geophysical Research*, **111, D14102**.

New, M., M. Hulme and P. Jones, 1999: Representing Twentieth-Century Space–Time Climate Variability. Part I: Development of a 1961–90 Mean Monthly Terrestrial Climatology. *Journal of Climate*, **12**: 829–856.

Nicholson, S. and J. Selato, 2000: The influence of La Niña on African rainfall. *International*

Journal of Climatology, **20**: 1761-1776.

Omotosho, J. B., A. A. Balogun and K. Ogunjobi, 2000: Predicting monthly and seasonal rainfall, onset and cessation of the rainy season in West Africa using only surface data. *International Journal of climatology*, **20**: 865–880.

Penman, H. L., 1948: Natural evaporation from open water, bare soil, and grass. *Proceedings of the Royal Society of London,* **193**: 120–145.

Persaud , N., G. Hassan, W. D. Joshua and D. Lesolle, 2007: Measures of post-establishment agricultural drought for subsistence sorghum production in eastern Botswana. *International Journal of Agriculture Research*, **2**: 193–210.

Poccard, I., S. Janicot and P. Camberlin, 2000: Comparisong of rainfall structures between NCEP/NCAR reanlyses and observed data over tropical Africa. *Climate Dynamics*, **16**: 897-915.

Pratt, A. and X. Diao (2006). Exploring growth linkages and market opportunities for agriculture in southern Africa. *International Food Policy Research Institute*, **42**.

Priestley, C. and R. Taylor, 1972: On the assessment of surface heat flux and evaporation using large-scale parameters. *Monthly Weather Review*, **100**: 81-82.

Raes, D., A. Sithole, A. Makarau and J. Milford, 2004: valuation of first planting dates recommended by criteria currently used in Zimbabwe *Agricultural and Forest Meteorology*, **125**: 177-185

Randall, D. A., R. Wood, S. Bony, R. Colman, T. Fichefet, J. Fyfe, V. Kattsov, A. Pitman, J. Shukla, J. Srinivasan, R. Stouffer, A. Sumi and K. Taylor, 2007: The Physical Science Basis. Contribution of Working Group I to the Fourth Assessment Report of the Intergovernmental Panel on Climate Change. 589-662.

Randel, W., 1988: The seasonal evolution of planetary waves in the southern hemisphere stratosphere and troposphere. *Meteorology Society*, **114**: 1385–1409.

Reason, C. and M. Rouault, 2006: Sea surface temperature variability in the tropical southeast Atlantic Ocean and West African rainfall. *Geophysical Research Letters*, **33**: L21705 doi:10.1029/2006GL027145.

Reason, C. J. C., S. Hachigonta and R. F. Phaladi, 2005: Interannual variability in rainy season characteristics over the Limpopo region of southern Africa. *International Journal of Climattology*, **25**: 1835-1853.

Reason, C. J. C. and H. Mulenga, 1999: Relationships between South African rainfall and SST anomalies in the south west Indian Ocean. *International Journal of Climatology*, **19**: 1651–1673.

Rosen, S. and L. Scott, 1992: Famine grips Sub-Saharan Africa. *Agricultural Outlook,* **191**: 20-24.

Rosenzweig, C. and D. Hillel, 1995: Potential Impacts of Climate Change on Agriculture and Food Supply. *Consequences*, **1**.

Rukuni, M. and K. Eicher, 1994: Zimbabwe's Agricultural Revolution. *Technical Report*. Harare, University of Zimbabwe**:** 1–50.

Saltelli, A. and S. Tarantola, 1999: A quantitative model-independent method for global sensitivity analysis of model output. *Technometrics,* **41**: 39–56.

Samani, Z., 2000: Estimating solar radiation and evapotranspiration using minimum climatological data. *Journal of Irrigation and drainage Engineering. ASCE*, **126**: 265-267.

Samani, Z., S. Bawazir, M. Bleiweiss, R. Skaggs and V. Tran, 2007: Estimating Daily Net

Radiation over Vegetation Canopy through Remote Sensing and Climatic Data. *Journal of Irrigation and drainage Engineering*, **133**: 291-297.

Schimmelpfennig, D., J. Lewandrowski, J. Reilly, M. Tsigas and I. Parry, 1996: Agricultural adaptation to climate change: issues of longrun sustainability. US Department of Agriculture. *Agricultural Economic Report*. Washington, DC, Economic Research Service**:** 740.

Schulze, R. E. and R. D. Chapman, 2007a: Estimation of solar radiation over South Africa. In: Schulze, R.E. (Ed). 2007. South African Atlas of Climatology and Agrohydrology. *Technical Report*. S. 1489/1/06. Pretoria, R.S.A, Water Research Commission.

Schulze, R. E., M. Maharaj and N. Moult, 2007b: Reference Crop Evaporation by the Penman-Monteith Method. In: Schulze, R.E. (Ed). 2007. South African Atlas of Climatology and Agrohydrology. *Technical Report*. S. 1489/1/06. Pretoria, R.S.A, Water Research Commission.

Semenov, V. and L. Bengtsson, 2002: Secular trends in daily precipitation characteristics: greenhouse gas simulation with a coupled AOGCM. *Climate Dynamics*, **19**: 123–140.

Shah, M. M., G. Fischer and H. van Velthuizen (2008). Food Security and Sustainable Agriculture. The Challenges of Climate Change in Sub-Saharan Africa. *Laxenburg, International Institute for Applied Systems Analysis.*

Shongwe, M. E., G. J. Van oldenborgh and J. J. M. Van den hurk, 2009: Projected Changes in Mean and Extreme Precipitation in Africa under Global Warming. Part I: Southern Africa. *American Meteorological Society*, **22**: 3819-3836.

Sakamoto, C., R. Gommes and P. Hoefsloot, 2006: The principles of crop modelling and their implementation in the CMBox. [Available online from http://80.69.76.153/wiki/index.php?title=Chapter3.]

Supit, I., A. Hooijer and C. van Diepen, 1994: System description of the WOFOST 6.0 crop simulation model implemented in CGMS, vol. 1: Theory and Algorithms. Joint Research Centre, Commission of the European Communities. *EUR 15956 EN, Luxembourg*.

Tadross, M., B. C. Hewitson and M. T. Usman, 2005: The interannual variability of the onset of the maize growing season over South Africa and Zimbabwe. *Journal of Climate*, **18**: 3356-3372.

Tadross, M., P. Suarez, A. Lotsch, S. Hachigonta and others, 2010: Growing-season rainfall and scenarios of future change in southeast Africa: implications for cultivating maize. *Climate Research*, **40**: 147-161.

Tang, Y., H. Lin and A. Moore, 2008: Measuring the potential predictability of ensemble climate predictions. *Journal of Geophysical Research*, **113**.

Tebaldi, C., K. Hayhoe, J. Arblaster and G. Meehl, 2006: Going to the extremes: An intercomparison of model-simulated historical and future changes in extreme events.
Climate Change, **79**: 185-211.

Tebaldi, C. and R. Knutti, 2007: The use of the multimodel ensemble in probabilistic climate projections. *Philosophical Transactions of the Royal Society*.

Thornthwaite, C. W., 1948: An approach toward a rational classification of climate. *Geographical Review*, **38**: 55–94.

Thornton, P., P. Jones, A. Farrow, G. Alagarswamy and J. Andresen, 2008: Crop Yield Response to Climate Change in East Africa: Comparing Highlands and Lowlands. *IHDP*.

Todd, M. and R. Washington, 1999: Circulation anomalies associated with tropical-temperate troughs in southern Africa and the south west Indian Ocean. *Climate Dynamics*, **15**: 937–951.

Usman, M. T. and C. J. C. Reason, 2004: Dry spell frequencies and their variability over southern Africa. *Climate Research*, **26**: 199-211.

Van der Linden, P. and J. Mitchell, 2009: Climate Change and its Impacts: Summary of researchand results from the ENSEMBLES project. *Met Office Hadley Centre, FitzRoy Road, Exeter EX1 3PB, UK*: 160.

Villalobos, F. J., L. Mateos, F. Orgaz and E. Fereres (2002). Fitotecnia. Bases y tecnología de la producción agrícola. Mundi-Prensa. Madrid, Spain.

Walker, N. and R. Schulze, 2008: Climate change impacts on agro-ecosystem sustainability across three climate regions in the maize belt of South Africa. *Agriculture Ecosystems & Environmen*, **124**: 114–124.

Widmann, M. and C. S. Bretherton, 2000: Validation of Mesoscale Precipitation in the NCEP Reanalysis Using a New Grid cell Dataset for the Northwestern United States. *Journal of Climate*, **13**: 1936–1950.

Wiebe, K., 2009: How to Feed the world by 2050. *OECD Global Forum on Agriculture, Insights from an expert meeting at FAO.*

Wilby, R. and T.M. Wigley, 2000: Precipitation predictors for downscaling: observed and general circulation model relationships. *International Journal of Climatology*, **20:** 641-661

Wilby, R. L., S. P. Charles, E. Zorita, B. Timbal, P. Whetton and L. O. Mearns, 2004: Guidelines for Use of Climate Scenarios Developed from Statistical Downscaling Methods. [Available online from http://ipcc-ddc.cru.uea.ac.uk/guidelines/StatDown_Guide.pdf.]

Wilby, R.L. and Fowler, H.J. 2010. Regional climate downscaling. In: Fung, C.F., Lopez, A. and New, M. (Eds.) Modelling the impact of climate change on water resources. *Blackwell Publishing,*

Oxford.

Wilby , R. L. and H. J. Fowler 2007: Regional climate downscaling *Climate Change and Water Resource Modelling - Chapter 4*

Wiley, M. and R. Palmer, 2008: Estimating the Impacts and Uncertainty of Climate Change on a Municipal Water Supply System. *Journal of Water Resource*, **134**.

Williams, L., D. Shaw and R. Mendelohn, 1998: Evaluating GCM Output with Impact Models. *Climate Change*, **39**: 111-133.

Winslow, J. C., E. R. Hunt and S. C. Piper, 2001: A globally applicable model of daily solar irradiance estimated from air temperature and precipitation data. *Ecol. Model*, **143**: 227-243.

Ziervogel, G., 2004: Targetting seasonal climate forecasts for integration into household level decisions: The case of smallholder farmers in Lesotho. *Geographical Journal*, **170**: 6-21.

Ziervogel, G., A. Cartwright, A. Tas, J. Adejuwon, F. Zermoglio, M. Shale and B. Smith, 2008a: Climate change and adaptation in african agriculture. T. Report, Rockefeller Foundation.

Ziervogel, G., A. Taylor, S. Hachigonta and J. Hoffmaister, 2008b: Climate adaptation in southern Africa: Addressing the needs of vulnerable communities. *Stockholm Environment Institute, Commissioned by Oxfam GB*

Appendix A

A.1 Extraterrestrial radiation equation

$$R_a = \frac{12(60)}{\pi} G_{sc} d_r [(\omega_2 - \omega_1)\sin\phi\sin\delta + \cos\phi\cos\delta(\sin(\omega_2) - \sin(\omega_1))]$$

- G_{SC} = *solar constant (0.082 MJ m $^{-2}$ min^{-1})*
- d_r = *inverse relative distance Earth-Sun (correction for eccentricity of Earth's orbit around the sun)*
- ω_1 = *Solar time angle 1/2 hour before ω, that is, at the beginning of period (radians)*
- ω_2 = *Solar time angle 1/2 hour after ω, at end of period (radians)*
- *fe = Station latitude (radians)*
- δ = *Declination of the sun above the celestial equator (radians)*

Where

$$d_r = 1 + 0.033\cos\left[\frac{2\pi}{365} J\right]$$

J = day of year (1-366)

$$\omega_1 = \omega - \left[\frac{1}{2}\right]\left[\frac{\pi}{12}\right] \qquad \omega_2 = \omega + \left[\frac{1}{2}\right]\left[\frac{\pi}{12}\right]$$

Solar time angle ω at midpoint of the hourly period is given by:

$$\omega = \frac{\pi}{12}\left[\left((t - 0.5) - \frac{4}{60}(L_m - L_z) + S_c\right) - 12\right]$$

t = standard clock time (1-24)

L_m = longitude of measurement location (weather station) in degrees

L_z = longitude of the local time meridian (degrees West), 120° for Pacific time zone

$$S_c = 0.1645\sin(2b) - 0.1255\cos(b) - 0.025\sin(b)$$

$$b = \frac{2\pi}{364}(J - 81), \qquad \phi = \frac{\pi Y}{180}, \qquad \delta = 0.409\sin\left[\frac{2\pi}{365} J - 1.39\right]$$

A.2 The coefficient of determination equation R^2 is a measure of how well the least squares equation .

$$\bar{y} = b_0 + b_1 x$$

performs as a predictor of y *(See **http://www.public.iastate.edu/**).*

R^2 is computed as:

$$R^2 = \frac{SS_{yy} - SSE}{SS_{yy}} = \frac{SS_{yy}}{SS_{yy}} - \frac{SSE}{SS_{yy}} = 1 - \frac{SSE}{SS_{yy}}$$

R^2 measures the relative sizes of SSyy and SSE. The smaller SSE, the more reliable the predictions obtained from the model.

- The higher the R^2, the more useful the model.
- R2 takes on values between 0 and 1.
- Essentially, R^2 tells us how much better we can do in predicting y by using the model and computing ˆy than by just using the mean ¯y as a predictor.
- Note that when we use the model and compute ˆy the prediction depends on x because $\bar{y} = b_0 + b_1 x$. Thus, we act as if x contains information about y.
- If we just use ¯y to predict y, then we are saying that x does not contribute information about y and thus our predictions of y do not depend on x.

A.3 Root Mean Square Error (RMSE) was calculated as:

$$RMSE = \left[N^{-1} \sum_{i=1}^{N} (P_i - O_i)^2 \right]^{0.5}$$

where N is the number of observations, P_i are estimated values, and O_i are observed values.

A.4 The index of agreement was computed as:

$$d = 1 - \left[\frac{\sum_{i=1}^{N} (P_i - O_i)^2}{\sum_{i=1}^{N} \left((P_i - O_{\text{avg}}) + (O_i - O_{\text{avg}}) \right)^2} \right], \quad 0 \leq d \leq 1$$

where N is the number of observations, P_i are estimated values, and O_i are observed values.

Appendix B

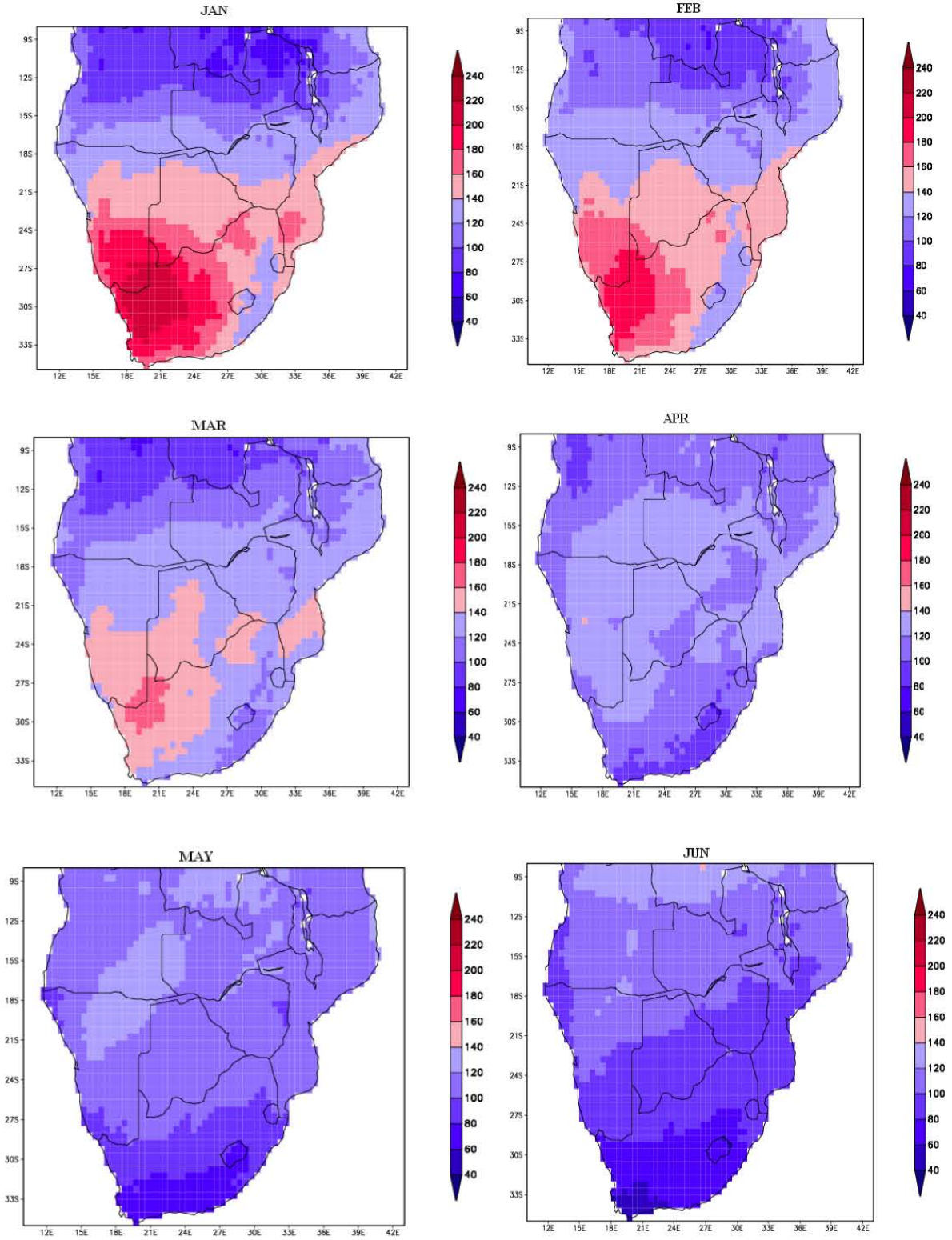

Figure B.1: *Monthly spatial distribution of the PM_o -ET (mm/month) calculated using CRU data. Continued….*

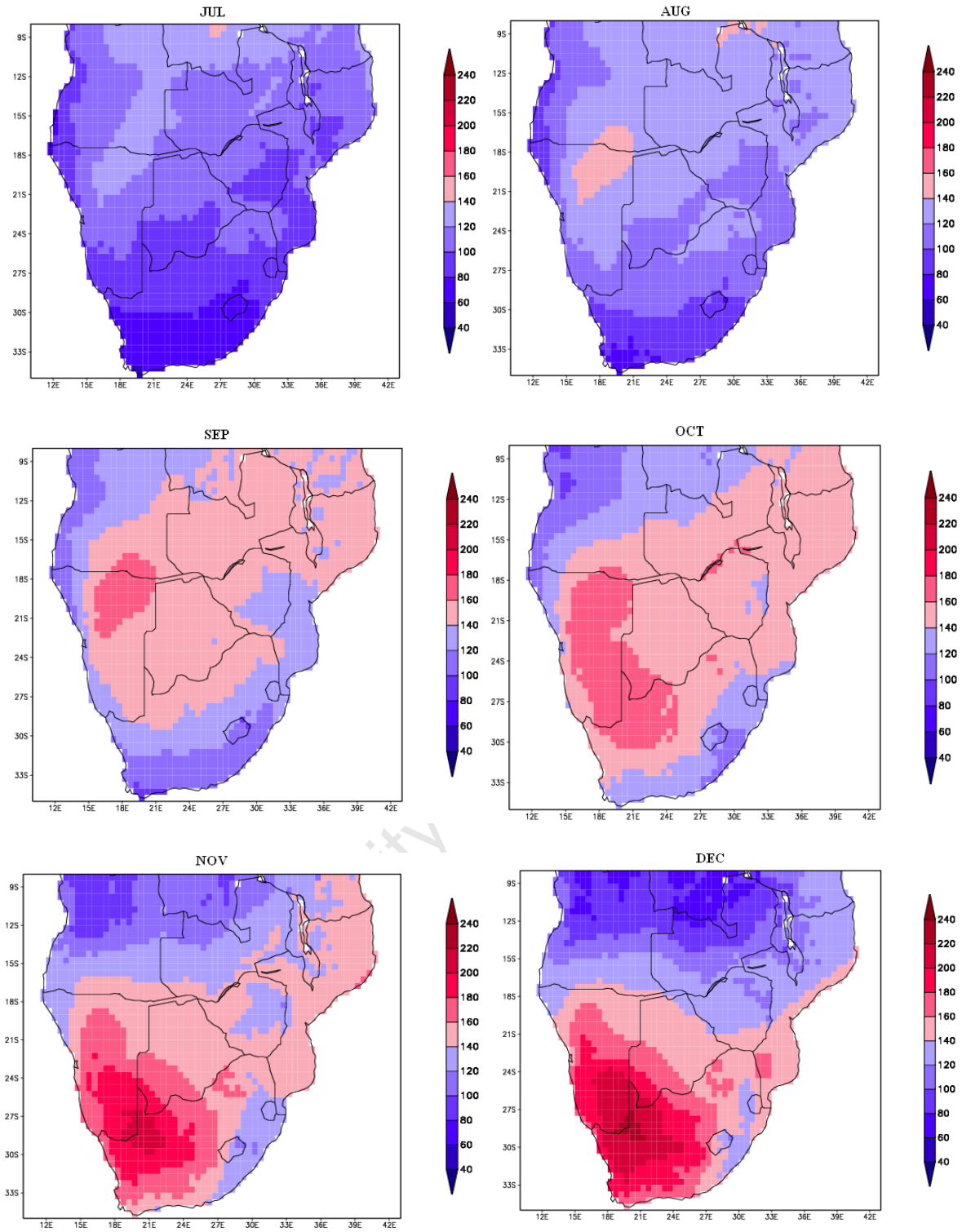

Figure B.1: *Monthly spatial distribution of the PM_o - ET (mm/month) calculated using CRU data.*

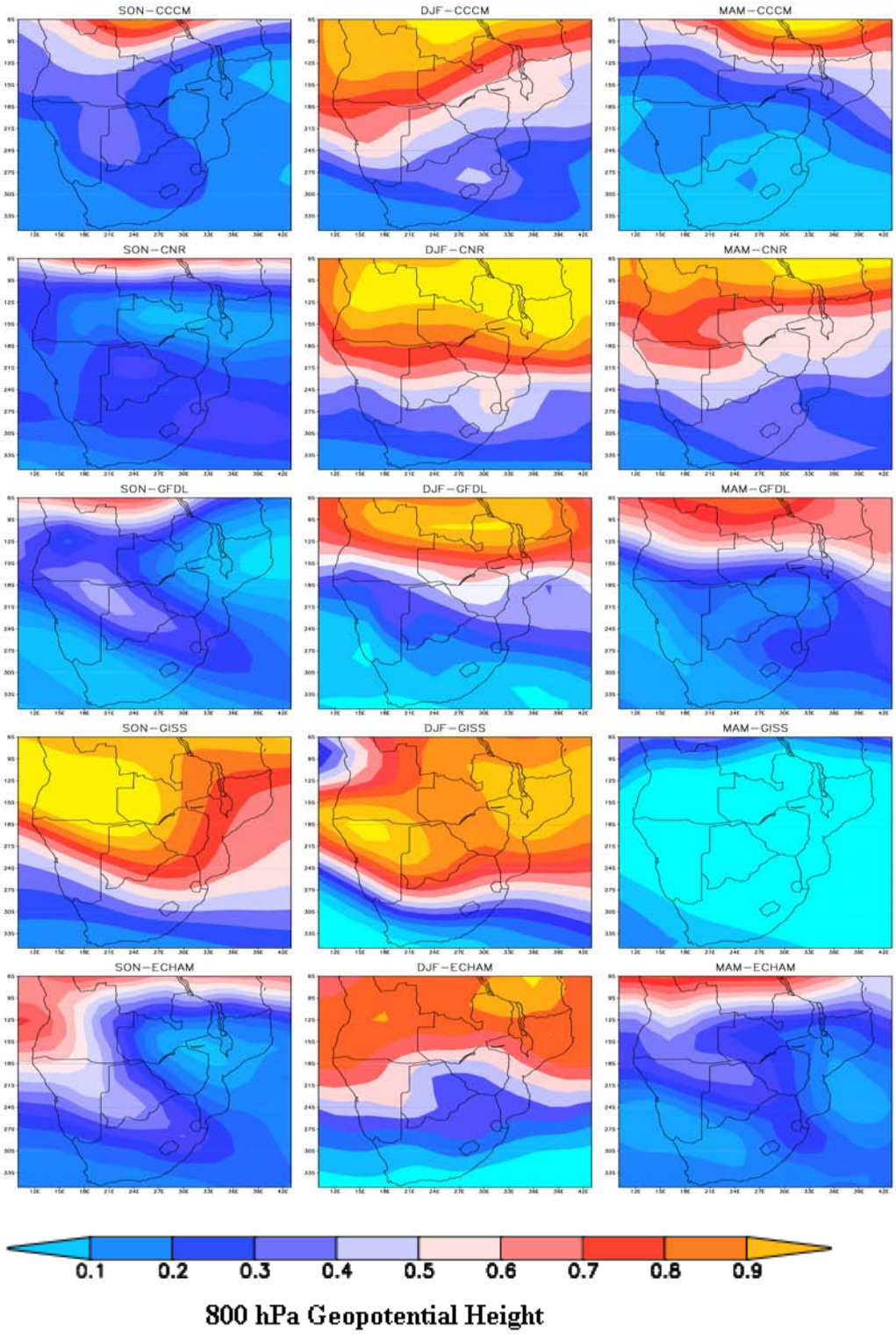

Figure B.2: *Changes in 800 hPa Geopotential height anomaly fields. First column displays change (1979-1999 and 2046-2065) in SON composites, Second column displays DJF composites and third column shows the MAM period. Cross boxes show undefined specific humidity values.*